Monitoring and Targeting Metastasis Through Circulating Tumor Cells: From Molecular Profiling to Natural Killer Cell-Based Therapeutics

by

Zeqi Niu

A dissertation submitted in partial fulfillment
of the requirements for the degree of
Doctor of Philosophy
(Chemical Engineering)
in the University of Michigan
2022

Doctoral Committee:

Professor Sunitha Nagrath, Chair
Professor Mark L. Day
Associate Professor Lana Garmire
Professor James Moon
Associate Professor Greg Thurber
Associate Professor Fei Wen

Zeqi Niu

zeqiniu@umich.edu

ORCID iD: 0000-0002-9025-616X

Dedication

To my parents and my husband, and in memory of my grandmother.

Acknowledgements

I am so fortunate and grateful to have my Ph.D. journey accompanied and supported by many people. They made the thesis work possible.

First, I would like to thank my advisor, professor Sunitha Nagrath, for being constantly inspiring and supportive. She has always allowed and encouraged me to get broad exposures to different disciplines and thrive on my own path. She is a compassionate leader that really cares about the well-being of her students and the clinical impact of our work. Through the collaboration with multiple clinicians, we are constantly reminded of the reasons of our work is not about publications but about solving real-world clinical problems. It has been amazing to have her as my mentor. Thank you.

I would like to thank my committee members, Professor Mark L. Day, Professor Lana Garmire, Professor James Moon, Professor Greg Thurber and Professor Fei Wen for their collaboration, support and suggestions over the last five years. Their diverse expertise has helped me think outside the box, write and publish high quality articles.

This work would also have not been possible without the collaborations within and outside of the Nagrath lab. In the Nagrath lab, I would like to thank Dr. Molly Kozminsky, Dr. Yoon-Tae Kang, Dr. Emma Purcell and Dr. Sarah Owen for their mentorship and support. Their work ethics, guidance and friendship are instrumental in shaping the independent researcher I am today. I would like to thank Professor Mark L. Day, Dr. Phillip L. Palmbos and members of the Day lab, Kathleen C. Day and Luke Broses, for their guidance and help on the bladder CTC project, especially in the early years of the Ph.D. journey. I would like to thank Dr. Aaron Udager and Albert Liu in the

Udager lab for their help on the targeted sequencing projects. I am also grateful to be part of the lung CTC research group and have received mentorship from these amazing clinicians and scientists. Specifically, to Dr. Nithya Ramnath and Professor Venkateshwar Keshamouni, thank you so much for providing invaluable insights on the NK-related projects.

I had the honor to work with some brilliant undergraduate students here at the University of Michigan. Thank you, Sarah Blumberg, Mariana Moreno-Nava, Alina Yan, Samuel Meinel, Yuru Chen and Michael Atie for your hard work and contribution to the projects.

In addition, I would like to thank people who helped me with bioinformatics portion of my thesis projects. Learning a new skill set is never easy, I am so grateful that Bioinformatics is such a welcoming community. Thank you to Dr. Stephen T. Guest for his encouragement and guidance in the PhD/MS Bioinformatics program. I also appreciate the help and guidance provided by Rebecca Tagett from the University of Michigan Bioinformatics Core and Professor Lana Garmire. And thank you to an incredible online community to help and solve problems and share tutorials.

I would like to thank all other past or current members of the Nagrath lab; they are the people who filled this journey with joy, support and late day snacks. To Mina Zeinali, Molly Kozminsky, Ting-Wen Lo, Sarah Owen, Emma Purcell, Kaylee Smith, Brittany Rupp, Harrison Ball, Nna-Emeka Onukwugha, Yolanda Zhang, Scott Smith, Abha Kumari, and Yuru Chen, I am so glad we shared part of this Ph.D. journey together and thank you so much for constantly brightening my days. No matter where in the world we end up, I know all of you will be achieving amazing things. I wish all of you all the best and hope we all can keep in touch.

I would like to thank my friends and family, especially my parents, the Broses family, Dr. Rong Duan for their support and love through the years.

Table of Contents

List of Tables

List of Figures

Abstract

Circulating tumor cells (CTCs) are the seeds of cancer metastasis and can be accessed through a simple blood draw. Recent developments in nanomaterials and microfluidic devices have enabled the invention of highly sensitive microfluidic platforms such as the graphene oxide (GO) chip. Such novel microfluidic devices have drastically advanced the isolation and characterization of CTCs, revealing that these rare cells may reflect disease status in cancer patients. However, further investigations in the context of clinical treatment studies are still needed to fully elucidate the value of CTCs as biomarkers. Additionally, targeting these rare CTCs might be a feasible therapeutic strategy to control cancer metastasis.

In this thesis work, I first optimized the GO chip workflow to isolate CTCs from 16 metastatic bladder cancer patients. Interestingly, I found that patients with CTCs > 3/mL had worse overall survival. Additionally, through amplicon-based targeted sequencing and a novel, customized bioinformatic analysis pipeline to remove variances from contaminating white blood cell (WBC) signals, I found that several tumor-related genes, including KRT5, KRT10, MMP-2, and AKR1C2, were significantly upregulated in patients with metastatic disease.

This similar workflow was then applied to longitudinal studies in stage III non-small-cell lung cancer (NSCLC), in which I developed analytical methods to correlate CTC counts and RNA expressions with clinical outcomes. CTCs were isolated and enumerated from 26 NSCLC patients and 6 time points across chemoradiation and immunotherapy treatment. The PD-L1 expression and RNA profile of these CTCs were characterized using on-chip immunofluorescent staining and microarray, respectively. I found that some CTC metrics, including a larger decrease in CTC

counts after therapy started, and having ≤ 50% PD-L1+ CTCs at single time points, significantly predicted longer, progression-free survival. Compared to pretreatment, significant upregulations of genes related to cancer metastasis, invasion, proliferation, and resistance were found in CTC samples during chemoradiation.

To explore potential therapies against these residual metastatic seeds, I hypothesized the critical role of NK cells in eliminating CTCs based on existing literature and investigated the CTC–NK interaction using novel single-cell resolution characterization methods. Through quantified NK cytotoxicity, 2 in-house CTC lines were both highly sensitive to NK-mediated killing compared to other lung-cancer-cell lines. By calculating an NK and epithelial to mesenchymal transition (EMT) score from bulk and single-cell RNA sequencing of CTC samples, I found a strong correlation between the NK-sensitive phenotype and EMT. In other words, CTCs, especially those with mesenchymal phenotypes, are highly sensitive to NK-mediated killing and have NK-sensitive signatures at the RNA and protein levels.

Lastly, I adapted the GO platform to isolate patient-specific NK cells and generate a novel therapeutic agent, NK-derived exosomes. Compared to NK cells, exosomes can potentially infiltrate biological barriers and are less influenced by the immunosuppressive tumor microenvironment. In a small cohort of NSCLC patients, I isolated NK cells and CTCs and produced NK exosomes through a 12-hour, on-chip incubation. The NK cell and NK exosome concentrations showed correlations with bloodborne CTC numbers. And preliminary results then demonstrated that the NK exosomes harvested from the NK-GO chip had cytotoxic effects on in-house derived CTCs.

The findings in this thesis strongly demonstrate the value of CTCs as biomarkers and therapeutic targets in clinical cancer management. Further, the methods developed in this work

could be further applied to larger studies to advance the clinical utility of CTC-based liquid biopsies.

Chapter 1 Introduction

1.1 Cancer metastasis, liquid biopsy, and circulating tumor cells

1.1.1 Cancer metastasis

Cancer metastasis refers to the spread of cancer (i.e., new tumor formation) to a secondary site in the body. Metastasis is a systemic disease associated with 90% of cancer-related mortalities. The metastatic seeding process starts relatively early, often during tumor formation and sometimes even before the cancer diagnosis[1,2]. Subpopulations of tumor cells that have increased invasiveness and mobility can enter the bloodstream and spread throughout the body[3]. While most of these disseminated tumor cells fail to initiate a secondary tumor, a few succeed with the help of other cell types along the way[4]. The survival of these disseminated tumor cells might be a primary reason for cancer relapse after surgical removal of local tumors. Extensive research is creating new options for monitoring and targeting this multistep metastasis process[5–7].

1.1.2 Liquid biopsy and the promise of personalized medicine

Liquid biopsy is emerging as a popular tool for metastasis research, both biologically and clinically. Liquid biopsy uses various analytical techniques to study biomarkers in bodily fluids, primarily blood. Because these bodily fluid samples can be accessed without surgical procedures and are minimally invasive, studying these biomarkers can potentially enable early tumor detection, personalized medicine, treatment response, and residual disease monitoring. The available biomarkers include circulating tumor DNA (ctDNA), circulating tumor cells (CTCs), extracellular vesicles (EVs), metabolites, and RNA molecules[8]. Among these biomarkers, only

assays using ctDNA and CTCs have been approved by the FDA. This thesis focuses on developing new pipelines for the characterization, analysis, and targeting of CTCs in the context of cancer immunotherapy.

CTCs are rare cells that are shed from solid tumors into the bloodstream. They are metastatic seeds that initiate a secondary tumor. CTC profiling can give comprehensive information on DNA, RNA, and protein levels, providing a direct window into metastasis in action. In addition, CTCs are fully intact live cells, which allows for drug screening through expansion and patient-derived xenograft models. Recent advances in isolation, characterization, and expansion technologies have made it possible to interrogate these CTCs and provide relevant clinical information.

1.2 CTC isolation methods

1.2.1 Overview of CTC isolation principles

CTCs were discovered over 150 years ago by the Australian pathologist Thomas Ashworth in the blood samples of metastatic cancer patients[9]. Isolation and characterization technological developments have helped CTCs become one of the most popular topics in cancer research. CTCs are found in a low concentration and with high background signals in clinical blood samples. There are approximately one to 10 CTCs per mL, with millions of white blood cells (WBCs) and billions of red blood cells (RBCs) in the background. It is worth noting that CTC counts vary based on cancer type, cancer stage, and tumor burden. In late-stage metastatic lung cancer patients, hundreds of CTCs can be found in one mL of patient blood samples[10,11].

The isolation methods can be divided into two main categories, immunoaffinity-based and physical property-based technologies. Immunoaffinity-based technologies take advantage of CTCs' unique cell-surface protein expression and use antibodies against these markers to detect

CTCs from peripheral blood mononuclear cells (PBMCs) or whole blood. CTCs have absent expressions of leukocyte markers and positive expressions of epithelial-cancer-cell markers, including epithelial-cell-adhesion molecule (EpCAM) and cytokeratin (CK) markers. Most physical property-based technologies are size-based, taking advantage of the fact that CTCs are generally larger compared to WBCs[12].

1.2.2 Immunoaffinity-based technologies

The immunoaffinity-based separation concept has long been used in traditional cell sorting, such as magnetic-activated cell sorting (MACS) and fluorescence-activated cell sorting (FACS). The first FDA-approved CTC isolation device, CellSearch™, uses magnetic beads conjugated with antibodies against EpCAM. The device captures CTCs from 7.5mL of patient blood samples; the enriched samples are then fixed and stained with cytokeratin and white-blood-cell markers to further identify the CTCs. Many large-scale clinical studies have used this technology to show the clinical implications of CTCs[13–15]. Although the CellSearch™ system represented a breakthrough in CTC isolation technology, its limitations have been discussed by many researchers[16,17]. The main limitations include the lack of a release mechanism, lack of compatibility for downstream molecular or expansion assays, and sole dependency on EpCAM cell-surface expression. These deficiencies have motivated biologists and engineers to collaborate to develop new CTC isolation methods.

Microfluidic devices are emerging as a popular tool for in vitro diagnostics because of their low cost, small size, low reagent use, and high sensitivity. The CTC-chip, a pioneering invention by Nagrath et al., uses anti-EpCAM-coated microposts under controlled laminar flow conditions to separate viable CTCs from peripheral whole blood samples[18]. CTCs were identified in 115 of 116 (99%) samples from patients with metastatic lung, prostate, pancreatic, breast, and colon

cancer. The herringbone chip, developed 2 years after the CTC chip, provides an enhanced, high-throughput platform for CTC isolation. The herringbone chip contains 8 microchannels with patterned chevrons or herringbones on their upper surfaces. These patterns significantly increase the interactions between target CTCs and the antibody-coated chip surface by introducing micro vortices into the fluid flow and forcing the cells to the antibody-coated surface. CTCs were detected in 14 of 15 (93%) patients with prostate cancer. To capture different subtypes of CTCs, Pecot et al. used antibody cocktails against a variety of cell surface antigens, such as EpCAM, Human Epidermal Growth Factor Receptor (HER2), Mucin 1 (MUC1), Epidermal Growth Factor Receptor (EGFR), c-MET, N-cadherin, and mesenchymal stem cell antigen[19]. Detection of both Cytokeratin $(CK)^+$ and CK^- CTCs was reported in breast, ovarian, and colorectal cancer.

The rapid development of nanomaterials has enhanced the functionality of CTC capture and characterization. The graphene oxide (GO) chip, developed previously within the Nagrath lab, uses angstrom high 2D gold patterns on a silicon substrate to increase capture sensitivity[20]. As shown in Figure 1-1A, GO chip is 24.6 mm × 60mm by size and have over 50,000 gold flowers patterned on top of the silicon wafer. GO, as a nanomaterial with a high surface-area-to-volume ratio, dramatically increases the number of active sites for cell capture. The 1000 Å gold layer provides a rough surface that can influence the device's flow pattern, allowing for better interaction between cells and anti-EpCAM antibodies. Capturing antibodies, such as anti-EpCAM, are then conjugated onto the GO through PEG molecules, crosslinkers, and avidin. On average, the device captured 73% of cancer cells from mock samples, even with only 3 to 5 spiked cancer cells. Follow-up studies showed successful characterization of CTCs from breast[21], prostate[22], and lung cancer patients[23].

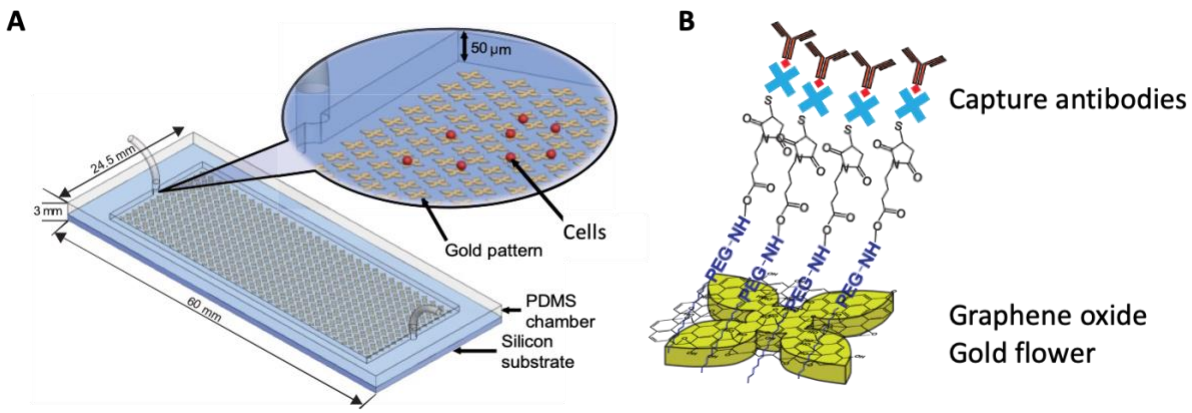

Figure 1-1 GO chip platform, adapted from[20]*. (A) The schematic drawing of a GO chip; (B) Enlarged images of the GO chip chemistry to conjugate antibodies on to GO chips.*

1.2.3 Physical property-based technologies

The use of CTCs' physical characteristics for isolation has gained popularity because of its promising ability to capture the $EpCAM^-$ CTC population. Different techniques, such as filtration, acoustic separation, and inertial focusing, are used in various isolation-method designs. The isolation by size of epithelial tumor cells (ISET) assay is the earliest filtration-based system for CTC isolation from peripheral blood[24]. In this assay, blood samples are diluted 10 times and processed through a membrane with 8 μm cylindrical pores. CTCs were then detected by positive immunostaining of cytokeratin (KL1) and negative immunostaining of CD45 (LCA). The sensitivity tests with cell-line mock samples and liver-cancer-patient samples showed successful isolation of low concentrations of CTCs (0–5/mL). In a follow-up study, CTCs were detected in 23 of 44 liver cancer patients and were associated with shorter survival[25]. Despite the initial success, the first-generation filtration membranes often ran into problems such as pore clogging, high-contaminating WBCs, and compatibility of downstream analyses.

Based on similar principles, microfluidic devices with microgaps and microposts are being developed to enhance isolation performance. One of these microfluidic-based systems, the Parsortix™ system, recently became the second CTC isolation technology to receive clearance

from the FDA[26]. The key isolation device in the Parsortix™ semiautomated system uses a "step" configuration in the channel heights. Smaller cells are forced to pass through, and larger cells are retained in the device[27]. After the isolation step, captured cells can be collected in small volumes for downstream analysis by an opposite change in flow direction. Xu et al. calculated an average of 92% capture efficiency when spiking fluorescently labeled cell-line samples in different concentrations, ranging from 3 to 1,000 cells per mL. Additionally, this system is compatible with various downstream applications, including fluorescence in situ hybridization (FISH)[28], bulk RNA sequencing[29], and single-cell RNA sequencing[30]. Clinical studies in breast[29], lung[31], prostate[32], and ovarian cancer[33] have successfully used the Parsortix™ system to identify and characterize CTCs. Although Parsortix™ has improved antigen-independent cell isolation in many aspects compared to the original ISET filters, it is limited by its low throughput. As stated by Kitz et al., it takes approximately 7 hours for the entire workflow, and the system can only process one sample at a time[34].

Inertial focusing devices are promising alternatives to increasing throughput while maintaining the advantages of a filtration system. CTC-iChip, for example, can process whole blood samples at 8 mL/hour and sort 10^7 cells per second at high efficiency[35]. The integrated system first eliminates smaller particles such as RBCs, platelets, and plasma proteins by hydrodynamic size-based sorting, then it uses inertial focusing to streamline cells, which enables magnetic beads-based cell separation. The downstream applications of the CTC-iChip include using digital droplet PCR to retrieve RNA signatures from hepatocellular carcinoma (HCC)[36]. The Labyrinth device, another approach developed in the Nagrath lab, uses a series of sharp corners to force particles of different sizes to form other streamlines. This device can process samples at 2.5

mL/min, and the recovery rate from spiked cancer cells in PBS and blood was over 90%. CTCs were successfully detected in pancreatic, breast, and lung cancer patients[11].

1.3 CTC detection and characterization methods

1.3.1 Protein and metabolic analysis

Immunostaining is one of the most widely used CTC detection methods. It is used by many isolation technologies, including CellSearch™, CTC-chip, and Parsortix™. CTCs are often identified by the positive stain of CK and the negative stain of WBC marker CD45. Other markers can be used in the identification panel for different cancer types, such as ASGPR and GPC3 in liver cancer and HER2 and EGFR in breast cancer[37]. Beyond CTC detection, multiplex immunostaining panels can be used to profile specific protein expression on identified CTCs. For instance, incorporating epithelial markers (EpCAM, CK, and E-Cadherin) and mesenchymal markers (Vimentin, fibronectin-1, and N-cadherin) can identify different subtypes of CTCs in the EMT spectrum[11,33,38]. PD-L1 is frequently detected in the CTCs isolated from late-stage breast[39] cancer and NSCLC patients[40]. In addition, detecting cancer stem cell markers like CD44 and TWIST1 on CTCs is predictive of a worse prognosis in hormone receptor-negative breast cancer patients[41].

While convenient and compatible with most isolation technologies, immunostaining is often limited by its multiplexing capacity and qualitative nature. This field urgently needs novel, advanced cell proteomic and metabolic methods to aid understanding of the functional signature of single CTCs[42]. Several different approaches have been developed to fill this gap. For example, Sinkala et al. developed a microfluidic single-cell western-blot system, which can conduct 8-plex protein analysis for patient-derived CTCs[43]. This assay was tested on 3 cancer-cell lines and a cohort of 12 breast cancer patients, and it observed the intra- and inter-patient heterogeneity of

CTCs. Another approach based on single-cell mass spectrometry that focuses on CTC metabolic profiling was developed around the same time[44]. In a cohort of advanced gastric and colorectal cancer patients, 119 compounds were identified as upregulated in CTCs compared to lymphocytes, with 75 being glycerophospholipids (GPLs). In addition, unique metabolic profile clustering was found between gastric and colorectal cancers and between CTCs and lymphocytes.

Furthermore, a recent study incorporated surface-enhanced Raman spectroscopy (SERS) to characterize the protein expression of single CTCs in melanoma patients[45]. SERS is a powerful optical tool with narrow emission peaks to allow ultrasensitive biomolecule detection with better multiplexing capacity, an alternative to fluorescent signals. Although that paper only tested 3 expression markers on patient-derived CTCs, a higher power of multiplexing in tissue samples, up to 26 markers, has been revealed using similar technologies[46].

1.3.2 RNA analysis

1.3.2.1 Bulk RNA analysis methods

The profiling of CTCs on the transcript level is technically challenging because they have an inherently low RNA quantity and quality after multiple handlings in the enrichment process. Quantitative, real-time polymerase chain reaction (qRT-PCR) is a molecular biology technique commonly used to amplify and quantify specific cancer-related genes in enriched CTC samples. For example, Strati et al. investigated a panel of breast cancer-related gene transcripts in CTCs isolated with immunomagnetic beads[47], including CK-19, MAGE-A3, HER-2, TWIST1, hTERT α+β+, and mammaglobin. Similar workflows have been successfully conducted in many other studies to investigate the expression of a small set of cancer signatures in CTCs[48–50].

Some studies have exploited microarray or bulk sequencing platforms to incorporate larger sets of genes and conduct clustering and differential expression analysis. Smirnov et al. used

microarray to show the global gene-expression profile of CTCs isolated immunomagnetically[51]. By comparing the CTC-enriched and CTC-depleted samples (WBCs only), that study could identify novel CTC-associated genes, such as AGR2, FABP1, S100A13, S100A14, and S100A16. Another study performed bulk mRNA sequencing on breast cancer CTCs isolated using fluorescence-activated cell sorting (FACS)[52]. Despite a 23.9% dropout rate based on library quality, the authors successfully identified significant genes and pathways in CTCs compared to peripheral blood and primary tumors. In addition, a 75-gene signature that had the highest expression in both CTCs and primary tumors was identified and had prognostic values in the cancer genome atlas (TCGA) datasets.

1.3.2.2 Single-cell analysis methods

Contaminated WBC signals pose a critical challenge to the use of CTC molecular characterization for bulk profiling methods. Because of CTCs' rare frequency in blood, most current CTC enrichment samples struggle to obtain a pure CTC population. One potential solution is to further partition these enriched CTC samples into single cells and profile them individually. Several approaches have been experimented with by multiple groups. For example, Szczerba et al. used a micromanipulator to select CTCs, CTC clusters, and WBCs after Parsortix™-based isolation. The transcriptome profiles of individual CTCs and CTC-neutrophil clusters showed a high proliferative nature of CTC-neutrophil clusters[30].

The Chromium (10X Genomics) single-cell sequencing platform provides another single-cell partitioning approach. Using this platform, D'Avola et al. successfully identified CTCs and performed differential expression analysis by comparing CTCs to other blood cells[53]. The differential gene analysis showed the upregulation of a series of oncogenic driver genes in hepatocellular carcinoma such as IGF2 and other genes related to liver physiology, including

apolipoproteins, coagulation factors, alcohol dehydrogenases, and cytochromes in CTCs. The DEPArray™ system is another single cell partitioning approach that uses dielectrophoresis to exert force on cells and individually move them. So far, the DEPArray system has only been used to analyze CTCs on the DNA level, such as mutations[54] and copy number variations[55].

1.3.2.3 Challenges and approaches in the Bioinformatic analysis of CTCs

The molecular heterogeneity, apoptotic nature, and often-impure samples of CTCs have brought unique challenges to the bioinformatics analysis of CTCs. To my knowledge, there is no current method to deconvolute WBC-contaminated bulk CTC samples. However, deconvolution tools for immune cell populations in tumor microenvironments have been developed. CIBERSORT is a well-known digital algorithm that enumerates and characterizes different cell compositions of complex tissues from bulk expression profile data sets[56]. This tool has not been used in CTC profiling, but it could potentially help procure pure CTC signals.

Different single-cell profiling strategies involving bioinformatically defined CTCs have been developed using the 10X Genomics platform. D'Avola et al. used a loosened filtering strategy to make the consideration of all genes an input, regardless of the percentage of cells expressing them[53]. CTCs were identified as the outliers after principal component analysis (PCA) of the highly variable genes. This method is straightforward but could be conservative, because many CTCs have a high level of heterogeneity. To overcome this, Poonia et al. developed the unCTC R package, which uses a novel method of clustering ("Deep Dictionary Learning") and the K-means clustering cost (DDLK), designed exclusively for the identification and characterization of CTCs[57]. Considering that CTCs are highly heterogeneous and could be hard to identify through an unsupervised clustering method, this method projects the single-cell gene-expression data onto a range of well-understood biological pathways to obtain robust cellular clusters. This tool is a big

step forward in identifying CTCs from sequencing results, and further development of bioinformatics tools specifically for CTCs is urgently needed.

1.4 Current clinical application of CTCs

1.4.1 CTC as a prognostic biomarker

Numerous studies have used CTCs as surrogate biomarkers for many cancer types[58]. In general, the presence of CTCs indicates an invasive and metastatic feature of solid tumors and minimal residual disease. CTC counts are the most common quantifiable metric in these clinical studies and are generally associated with tumor invasiveness and metastatic potential. The value and change in CTC counts could help predict patient outcomes across different cancer stages and monitor the treatment response.

Janni et al. reported a 20.2% CTC detection rate in a meta-analysis of 3,173 non-metastatic breast-cancer patients[59]. Larger tumors, increased lymph node involvement, and a higher histologic tumor grade were found in the CTC-positive patients. Using multivariate Cox regression analysis, CTCs were also shown to be independent prognostic factors for patients' disease-free survival and overall survival. Similar results have been reported in many other studies, showing that CTCs help diagnose and predict recurrence in the early stages of bladder, prostate, lung, and other cancer types[60–64].

Further investigation has led to the discovery of other relevant metrics beyond CTC counts at single time points, such as changes in CTC counts, presence of CTC clusters, and specific invasive CTC phenotypes. For example, Lorente et al. found that a > 30% CTC count that declined between baseline and 4 weeks, 8 weeks, and 12 weeks after treatment was associated with an increased prostate cancer survival rate[65]. In a cohort of 54 metastatic breast cancer patients, elevated counts of CTC clusters and larger CTC cluster sizes were found to correlate with a higher

risk of disease progression and death[66]. In addition, certain CTC phenotypes, such as mesenchymal (represented by the expression of Vimentin and TWIST1) and stemness (represented by the expression of CD24, CD44, and ALDH1), have also been associated with therapy resistance and high relapse rates[67–69].

1.4.2 Screening CTCs for treatment stratification

The Treat CTC trial was the first clinical trial to take advantage of the early prognosis value of CTCs to guide the following adjuvant therapy for HER2 negative breast-cancer patients[70,71]. High-risk patients were defined as having at least one CTC per 7.5 mL. The study screened 1,317 patients and detected positive CTCs in 95. Sixty-three of these high-risk patients were then assigned to observation and were administered 6 cycles of trastuzumab. The study was stopped because the CTC count did not decrease in the treatment arm; nevertheless, it proved the feasibility and clinical potential of CTC-based screening. The study also found that CTC-positive patients were associated with a higher risk of relapse.

Developments in CTC characterization technologies have encouraged the screening of specific molecular subtypes using CTC samples to guide therapeutic decisions. Marchetti et al. reported an 84% (31 of 37 patients) EGFR mutation-detection rate using CTC samples from NSCLC patients, corresponding to the matching tumor tissue[72]. Similar high concordance (85%, 57 of 67 CTC samples; 67%, 8 of 12 patients) in at least one or more somatic mutations and copy number alterations has been reported in metastatic breast cancer[73]. Discordance of expression between CTC and tissue has also been reported, especially for HER2 expression[74–76]. In the tissue of HER2-negative patients, CTCs may acquire a HER2 positive phenotype and exhibit a higher potential for proliferation[77]. Wang et al. observed that patients who had negative HER2 expression in primary tumors but positive expression in CTCs ($\geq$ 2 HER2 + CTCs) and who received anti-

HER2 targeted therapies displayed significantly improved progression-free survival (PFS) compared to those who did not[78]. This difference was not observed in patients with negative HER2 signals in both tissue and CTC samples (< 2 HER2 + CTCs).

Beyond evaluating the expressions of single genes, Kwan et al. developed a 17-gene CTC score to quantify estrogen receptor (ER) signaling during breast cancer treatment, identifying patients who did not respond to endocrine therapy and predicting their early disease progression[79]. Taken together, these findings indicate the unique value of profiling CTCs to guide therapeutic decisions.

1.4.3 CTC expansion and drug testing

In vitro expansion of isolated CTCs aims to take advantage of the proliferative nature of cancer cells and establish patient-derived CTC lines, or mouse models. Current literature on successful cases of CTC expansion and drug testing was summarized nicely by Smit et al.[80] From 2014 to 2020, 358 cases of successful CTC cultures were reported, 42 (12%) of which had established, long-term CTC lines (≥ 6 months). Some of these studies performed drug testing on established CTC lines. Yu et al. comprehensively profiled 6 established, permanent CTC cultures from metastatic, ER-positive breast cancer patients and tested anti-cancer agents against molecular targets and common chemotherapeutics[81]. The authors observed concordance between some of the CTC drug sensitivity results and clinical histories. Similar concordance was also reported in small-cell lung cancer (SCLC)[82]. These findings indicate that CTC-based drug testing models are largely representative of solid tumors' drug sensitivity.

1.4.4 CTC as a biomarker under the context of immunotherapy

1.4.4.1 Cancer immunotherapy

Standard cancer care has been revolutionized by the recent development and clinical use of immunotherapies. Cancer immunotherapies leverage parts of the patients' own immune system to treat diseased tumor cells. Current well-known immunotherapy approaches include immune checkpoint inhibitor (ICI) and adoptive cell-based therapies (e.g., CAR-T therapies). ICI targets the immune checkpoint pathways activated by cancer cells as immune evasion mechanisms. Common immune checkpoint targets include cytotoxic T-lymphocyte antigen-4 (CTLA-4) and programmed death (PD-1). So far, seven ICIs have been approved by the FDA for over 15 cancer types[83]. Adoptive cell therapies, on the other hand, aim to isolate, expand, and engineer immune cell populations in vitro and reintroduce them to patients. CAR-T cell therapy is the only FDA-approved cell-based therapy so far. However, there is a large amount of research continuously being conducted on other cancer immunotherapy approaches.

1.4.4.2 CTC metrics that have predictive value in immunotherapies

Programmed cell death ligand 1 (PD-L1) expression is the best-established predictive biomarker of response to ICI treatment on the PD-1/PD-L1 axis[84,85]. Assessing CTC counts or the PD-L1 expression on CTCs for patients receiving immunotherapies provides a noninvasive approach for treatment monitoring. Many studies have explored such prognostic values of CTCs in the context of cancer immunotherapies.

High PD-L1-positive CTC counts before immunotherapy treatment are associated with a worse survival outcome[40,86–89]. Yue et al. described a correlation between disease outcome and dynamic change in CTC counts or PD-L1-positive/high CTC counts during nivolumab (a PD-1 inhibitor) treatment in a cohort of 35 NSCLC patients[86]. Decreased total CTC or PD-L1 positive/high CTC counts are significantly associated with longer survival. For patients treated

with nivolumab, other studies showed that the presence of CTC or PD-L1-positive CTCs during treatment could potentially indicate a mechanism of therapy escape and are associated with poor PFS[40,86,87]. Possible therapy resistance channels have recently been proposed through the expression of CD47 as an alternative immune-inhibiting signal on CTCs[85,90].

1.5 Targeting CTCs to control metastasis

The isolation and characterization of CTCs have laid the biological foundations for therapeutic targeting of CTCs. Selective targeting of CTCs can serve as an unconventional strategy for controlling cancer metastasis. Compared to other anti-metastasis therapies that inhibit the final steps of the metastatic cascade[6], CTC therapeutics enable potential early intervention and easy access to pharmacological and mechanical targeting interventions[5,91]. Although the CTC therapeutics field is relatively new, several noteworthy discoveries and developments have helped engineer intervention and immunosurveillance of CTCs.

1.5.1 Engineering approaches to selectively eliminate CTCs

Michael R. King et al. developed a series of engineering technologies using the E-selectin (ES) adhesion receptor and tumor necrosis factor-related apoptosis-inducing ligands (TRAIL)[92–95]. The first-generation approach uses a vascular shunt functionalized with ES and TRAIL proteins[92]. The ES protein causes CTCs to adhere and exhibit ES-mediated rolling alongside the shunt, and this rolling process allows for 4 times more efficient exposure to TRAIL molecules, inducing apoptosis in CTCs. The second-generation approach takes advantage of the interaction between CTCs and other blood components, such as leukocytes and platelets, to deliver ES and TRAIL molecules[93–95]. Mitchell et al. developed ES/TRAIL liposomes to functionalize leukocytes in the whole blood[93]. The study showed effective elimination of cancer cells in cell-line spike-in model samples and mouse models, and the functionalization process did not induce significant cell

death in endothelial and leukocyte cells. Moreover, Ortiz-Oetero et al. later tested this therapeutic approach in clinical blood samples from prostate cancer patients in vitro[94]. Significantly fewer CTCs were found in the group with TRAIL therapy compared to the vehicle control.

1.5.2 Leveraging immunotherapies to target CTCs

Efforts have been made to build on current immunotherapy approaches to better target CTC populations. For example, since high CTC counts during PD-1/PD-L1 checkpoint inhibitor treatment indicate an escape mechanism, it has been proposed that these residual CTCs might use CD47 as an alternative immune-suppressing signal. Lian et al. showed that the dual blocking of CD47 and PD-L1 could enhance the inhibition of tumor growth more than CD47 or PD-L1 alone[96]. To enhance the delivery of PD-L1 ICIs, Chen et al. invented a platelet-based anti-PD-L1 drug delivery strategy to target CTCs.

Although the above therapeutic strategies are promising, they fail to leverage one of the crucial players in CTC immune surveillance: natural killer cells. Recent literature has increasingly reviewed the possibilities of targeting CTCs and metastasis using NK-cell based therapies[97–99]. In the following sections I further discuss the biological rationale and advances of NK-cell-based therapies.

1.5.3 NK cell and cancer metastasis

NK cells are an innate part of the immune system. They can identify and kill abnormal cells, including viral infections, cancer cell growth, and tumor spread, without antigen presentation. NK cells are regulated by the balance between a series of activation and inhibition receptors[100–102]. Compared to T cells, this mechanism gives NK cells unique advantages in recognizing stressed cancer cells and eliminating them. For example, one of the escape mechanisms of cancer cells for T-cell-based therapeutics is changing self-expression of the major

histocompatibility complex (MHC) class I molecule. MHC class I molecules should be expressed on all nucleated cells in the human body. They are essential for antigen presentation during T-cell activation and effector T-cell function. Downregulation or loss of MHC class I would impair T-cell-based immunosurveillance but would serve as an activation signal for NK cells[103]. Frequent downregulation of MHC class I expression is found in many solid tumors in cancers such as bladder, breast, lung, and colorectal[104,105] and in disseminated tumor cells in bone marrow[106].

NK cells are also known to play a significant role in controlling cancer metastasis[97,98], supported by an extensive amount of preclinical literature. Higher metastasis burdens were found in NK-cell-depleted mice compared to other immune cell-depleted or immunocompetent control mice[99,107–110]. In the NK-cell-deficient or suppressed mouse models, interventions that boost NK-cell effector functions, such as adoptive transferring of NK cells and IL-15 treatment, have been shown to provide protection against metastasis[111,112].

Because of their exceptional ability to control metastasis in animal models, NK-cell therapies have been carried out in over 600 clinical trials investigating their efficacy against cancer. See ClinicalTrials.gov (search keywords: “natural killer,” “cancer”). One of the popular concepts involves isolating NK cells from peripheral blood samples, expanding and activating them, and infusing them back into patients. Promising clinical response has been shown in KIR-mismatched allogeneic NK-cell-therapy cases in acute myeloid leukemia[113,114]. In metastatic solid tumors, adoptive NK cell therapies have limited tumor infiltration, potentially due to the immune suppressive tumor microenvironment[115]. Other challenges of NK-cell therapies include the loss of cytotoxicity after cryopreservation, inconsistent expansion scale, costly expansion procedures, and unmodified NK cells lacking anti-tumor efficacy[116]. Strategies to improve NK-cell recruitment and infiltration and promote NK-cell activation are active areas of research.

1.5.4 NK cells and CTCs

As a crucial step in the metastatic cascade, CTCs are hypothesized to have unique vulnerability to NK-cell-mediated killing. More and more evidence show the interaction between NK cells and CTCs. An inverse correlation has been found between circulating NK cells and CTCs in breast, lung, colorectal, and liver cancer[85,117–121]. On the one hand, decreased NK cell numbers and cytotoxic activity were found in metastatic cancer patients with high CTC numbers [119–121]. On the other hand, significantly decreased CTC numbers were found after administration of NK cell therapies[117,118].

Efforts have also been made to further explore the biological basis of the CTC–NK interaction. On the molecular level, several studies have discussed the connection between NK activation and epithelial-to-mesenchymal transition, which is often found in CTCs. Using a gene-expression-profile data set during TGF-β-induced EMT, Chockley et al. showed that tumor cells undergoing EMT suggest increased NK susceptibility[122]. Others also had similar findings[123,124]. NK activation signals, such as the downregulation of MHC class I molecules, were observed in CTCs in mouse models and melanoma patients[125,126]. In addition, CTC clusters were found to have increased NK-inhibitory ligands and decreased NK-activating ligands, exhibiting higher resistance to NK-mediated killing compared to single CTCs[124].

1.5.5 Next generation NK based therapy: NK exosomes

1.5.5.1 Exosomes as therapeutics

Cell-based therapies face many challenges regarding tumor infiltration, manufacture, storage, and transportation[127]. For NK-cell-based therapies, infiltration of NK cells into solid tumors is largely influenced by cytokine profiles of tumor microenvironments[128]. Parkhurst et al. observed high levels of circulating NK cells but limited clinical responses in melanoma or renal-

cell carcinoma patients after receiving autologous NK cell therapies[129]. The transferred NK cells in these patients persisted in circulation for weeks to months, and tumor cells could not be lysed in vitro after re-isolation. These limitations have led to the development of cell-free immunotherapy avenues like exosomes.

Exosomes, a type of extracellular vesicles (EVs), are nanoscopic courier vesicles (30–150 nm) secreted by various cells. Exosomes are stable in physiological conditions and have a long circulating half-life in the blood. Their nano-size and abundance are ideal for cancer treatment via effective trafficking to the solid-tumor location and infiltration into the tumor microenvironment[130]. Moreover, exosomes can be modified to increase their delivery capabilities. For example, a polyethylene glycol (PEG) coating can increase circulation time, and functionalizing the PEG coating with anti-EGFR nanobodies can reduce nonspecific interaction with cells[131]. Therefore, exosomes are currently being researched as natural drug carriers or agents for cancer immunotherapy, both of which aim to reduce the spread of cancer throughout the body and inhibit the growth of tumor cells[132,133].

1.5.5.2 NK-cell-derived exosomes

NK-cell-derived exosomes naturally express IFN-γ, FasL, and multiple cytotoxic proteins that can induce apoptosis via multiple killing mechanisms[134,135]. They provide a promising cell-free therapy for cancer treatment. Recent studies have demonstrated the effectiveness of NK-cell-derived exosomes in lysing malignant tumor cells. Boyiadzis et al. isolated, expanded, and activated NK cells from 10 healthy donors[136]. From these expanded NK cells, they collected exosomes from the supernatant and tested the cytotoxicity against K562 and other acute myeloid leukemia cell lines. Zhu et al. also observed a similar cytotoxic effect in NK-cell line-derived exosomes (NK-92MI) against B16F10 (a melanoma cell line) cells[137].

1.5.6 Mission statement and hypothesis

The isolation and characterization of CTCs can provide crucial clinical information in a noninvasive manner. Current widely used technologies are limited by their capture sensitivity and compatibility with newly developed downstream technologies. There is also a critical need to develop bioinformatics methods to deconvolute and analyze CTC expression profiles. Moreover, targeting CTCs could be an effective therapeutic strategy against cancer metastasis. An increasing number of studies are showing promising evidence of the unique immunosurveillance of CTCs by NK cells.

In this thesis, I first optimize and develop protein and RNA co-analysis pipelines for the previously developed graphene oxide-based device (the GO chip). This is demonstrated through a cohort of patients with metastatic muscle-invasive bladder cancer (MIBC) to discover the clinical implication of CTC metrics. Second, I apply modified analytical pipelines to longitudinal studies in non-small-cell lung cancer (NSCLC) patients. Through this, I show that the continuous change of CTCs is a promising biomarker for identifying high-risk patients early in treatment. Next, I investigate the utilization of immunotherapies to eliminate CTCs. In this context, firstly I study the interaction between CTCs and NK cells by visualizing NK-cell-mediated cytotoxicity. I further demonstrated the molecular basis of the vulnerability of patient-derived CTCs in NSCLC. Secondly, I develop an integrated microfluidic system for the biogenesis of NK-cell-derived exosomes and explore the cytotoxic capability of this cell-free immunotherapy against CTCs. Overall, I explore the GO device's ability to characterize CTCs and develop NK-cell-based therapies in clinical studies. The analytical pipelines and characterization methods in this study can be used to further CTC studies in the field. This novel approach to developing NK cell-based therapies provides new directions for cancer treatment development.

Chapter 2 A Molecular Profiling Workflow for CTC Characterization in Patients with Metastatic Bladder Cancer

2.1 Abstract

Assessing the molecular profiles of bladder tumors from patients with advanced disease is crucial for implementing personalized treatment. The current standard of assessing the tumor molecular profile is based on tissue biopsies, which is often limited by their invasive nature. Alternatively, liquid biopsy takes advantage of a non-invasive procedure to access tumor materials, providing potential to monitor tumor molecular profiles longitudinally in a less invasive manner. Circulating tumor cells (CTCs) are one of the key analytes of liquid biopsy. In this study, we developed a protein and mRNA co-analysis workflow for bladder cancer CTCs utilizing the graphene oxide (GO) chip. The GO chip was conjugated with antibodies against both EpCAM and EGFR to isolate CTCs from bladder cancer patients. Following capture, protein and mRNA were analyzed using immunofluorescent staining and ion-torrent-based whole transcriptome sequencing, respectively. This is the first time that the ion-torrent-based whole transcriptome sequencing was used in a downstream application for GO chips. We found that CTC counts per mL were significantly associated with patient disease status at the time of blood draw, and having > 3 CTCs per mL was associated with shorter overall survival. Invasive markers, including EGFR, HER-2, CD31, and ADAM15 were detected in subpopulations of CTCs. Targeted whole transcriptome sequencing showed distinct RNA expression profiles from patients with or without tumor burden at the time of blood draw. In patients with tumor burden, we found significant upregulations of several metastasis-related genes, including KRT5, KRT10, MMP-2, and

AKR1C2, demonstrating the capability of identifying tumor-related RNA signatures from blood using GO chip-based assays.

2.2 Publication information

Zeqi Niu, Molly Kozminsky, Kathleen C. Day, Luke Broses, Sarah Blumberg, Aaron Udager, Phillip L. Palmbos, Mark L. Day, Sunitha Nagrath. "Characterization of Circulating Tumor Cells in Patients with Metastatic Bladder Cancer" (*In preparation*)

2.3 Introduction

Over 81,000 patients will be diagnosed with bladder cancer in the United States in 2022 and about 25% of these patients will have muscle-invasive bladder cancer (MIBC)[138] in which the tumor invades into the muscularis propria which surrounds urothelium. First-line treatment options for these MIBC patients include neoadjuvant chemotherapy and radical cystectomy. Yet, approximately 50% of MIBC patients relapse after radical cystectomy, and most of these relapses are companied with distant metastasis[139]. The five-year survival for metastatic bladder cancer patients is only 6%. Standard of care treatments for these metastatic patients include cisplatin-based systemic chemotherapy and checkpoint inhibitor immunotherapy, however, most develop resistance to therapy and eventually die. Intertumoral molecular heterogeneity drives differential responses and resistance to these therapies, thus contributing to patient mortality[140]. Molecular profiling of MIBC samples has revealed multiple molecular subtypes (i.e. basal, luminal, neuronal), which correlate with patient responses to therapy and overall survival[141]. Therefore, real-time molecular profiling of advanced bladder cancer can enable personalized disease care, and guide novel therapeutic design.

Traditional tissue-based molecular profiling is limited by its invasive nature, resulting in few sample points in time and inability to monitor tumor evolution and response to therapy in real-time. On the contrary, liquid biopsy tests retrieve molecular information about the tumor through non-solid tissues such as blood and urine. The collection procedures are non-invasive and can be repeated throughout the treatment course. Circulating tumor cells (CTCs) are one of the major biomarkers of liquid biopsy tests. As the seeds of metastasis, they offer a unique perspective to understanding the molecular landscape of the metastatic disease and have been proven to be a highly promising prognostic biomarker in different cancer types[23,142,143]. In bladder cancer, detectable CTCs in the early stage, non-muscle invasive bladder cancer (NMIBC) are found to be associated with a significant higher risk for tumor recurrence and progression to muscle-invasive disease[144]. The dynamic changes of CTCs in metastatic patients across baseline and second cycle of chemotherapy are predicative of 3-year progression-free survival (PFS) and overall survival (OS)[145].

Although these findings are highly promising, the profiling of CTCs in bladder cancer has previously been limited by several factors. The majority of CTC studies in bladder cancer utilize the CellSearch™ platform, an FDA-approved CTC isolation approach. This technology uses magnetic beads conjugated to antibodies against EpCAM (epithelial adhesion molecules) for isolation, which are expected to be uniquely expressed on CTCs in the peripheral blood. The advances in microfluidic devices have enabled more pure, sensitive capture of viable CTCs[146,147]. Immunoaffinity-based microfluidic devices use similar principles as the CellSearch technology, but by conjugating antibodies against additional surface proteins, they provide a more versatile capturing capability. We previously developed a graphene oxide nanosheet-based microfluidic device (GO device)[20], successfully isolating CTCs from breast[21], lung[23], and prostate[22] cancer

patients with high purity and sensitivity. The GO device captures CTCs using the near-flat nanostructure patterned on the silicon wafer substrate, making it an ideal platform for downstream immunofluorescence assays and RNA profiling assays.

Immunofluorescent staining of CTC protein expression can be used to infer tumor characteristics. In bladder cancer, high concordance of HER2 status was found between primary tumors, CTCs and lymph node metastasis, suggesting that CTC-based testing could identify candidates for anti-HER2 therapy[148] and high PD-L1 positive CTCs are found to be associated with worse overall survival[149]. Here, we investigated the role of ADAM15, CK7/8, CD21, EGFR and HER2 expression in bladder cancer CTCs to determine whether bladder cancer CTCs expressed these biologically important markers and whether they were associated with clinical outcomes. ADAM15, a type I transmembrane glycoprotein, is known to be involved in cell adhesion and metastasis by modulating tumor-endothelial cell interaction[150,151]. CD31 is an identification marker for endothelial cells. CTCs that are CD31 positive, characterized as circulating tumor-endothelial cells (CTECs), can be generated through cell-fusion or transdifferentiation[152]. These CTECs have hybridized properties of vascularization and motility, and are associated with worse overall survival[153]. In addition, extensive research has shown that the ErbB family of receptor tyrosine kinases, including EGFR, HER2, HER3, and HER4, are also associated with cancer metastasis[22]. We have previously reported that EGFR is a likely driver of prostate cancer bone metastasis. In accordance with this, we also found that EGFR is expressed on prostate cancer CTCs in patients with metastatic disease[154]. In bladder cancer, the overexpression of EGFR and HER2 are positively correlated to the clinical stage, pathologic grade and tumor recurrence[155]. Circulating tumor cell-based EGFR and HER2 profiling assay could be utilized to screen patients for targeted therapies.

Compared with protein immunofluorescent staining, RNA-based assays provide quantitative RNA level expression information. Targeted RT-PCR has been primarily used to evaluate specific gene expression in RNA samples extracted from enriched bladder CTC samples. For example, KRAS, EpCAM, CD133, Survivin, PI3K, VEGF, mTOR and AKT genes were found to have significantly increased expression in CTC-enriched samples[156]. In another study investigating colon and bladder cancer patients, the high expression of EGFR and TNC (tenascin C) from RNAs extracted from blood samples are found to be indicators of worse clinical outcome[157]. However, RT-PCR is often conducted with only limited gene panels, while other technologies, such as microarray and next-generation sequencing may provide a broader picture for the CTC molecular landscape. Osman et al. showed preliminary results from Affymetrix microarray on all nucleated blood cells showed that samples from bladder cancer patients have distinct expression profiles[158]. One of the difficulties for implementing these high-throughput molecular profiling technologies for CTCs is because of their apoptotic nature and low RNA quality and quantity after isolation. In tissue FFPE samples that have similar low RNA quality and quantity, amplicon-based targeted RNA sequencing technology has been used to profile FFPE samples with consistent success[159].

In this study, we used the GO device conjugated with both EpCAM and EGFR to isolate CTCs from metastatic bladder cancer patients. We then established protein and mRNA co-analysis workflow using immunofluorescent staining and amplicon-based whole transcriptome sequencing. Cell line model samples were used to optimize and ensure high capture efficiency and accurate characterization. For patient blood samples, three GO devices were processed in parallel (Figure 2-1). Two of these devices were stained with CTC identification and invasive marker panels, while the other device was used for RNA material extraction. To our knowledge, this is the first time

that amplicon-based whole transcriptome sequencing was used to molecular profile CTCs in bladder cancer. Using this workflow, we showcase the prognostic potential of CTCs in metastatic bladder cancer patients. We aim to advance the biomarker discovery and understanding of cancer metastasis by profiling CTCs at both protein and RNA levels.

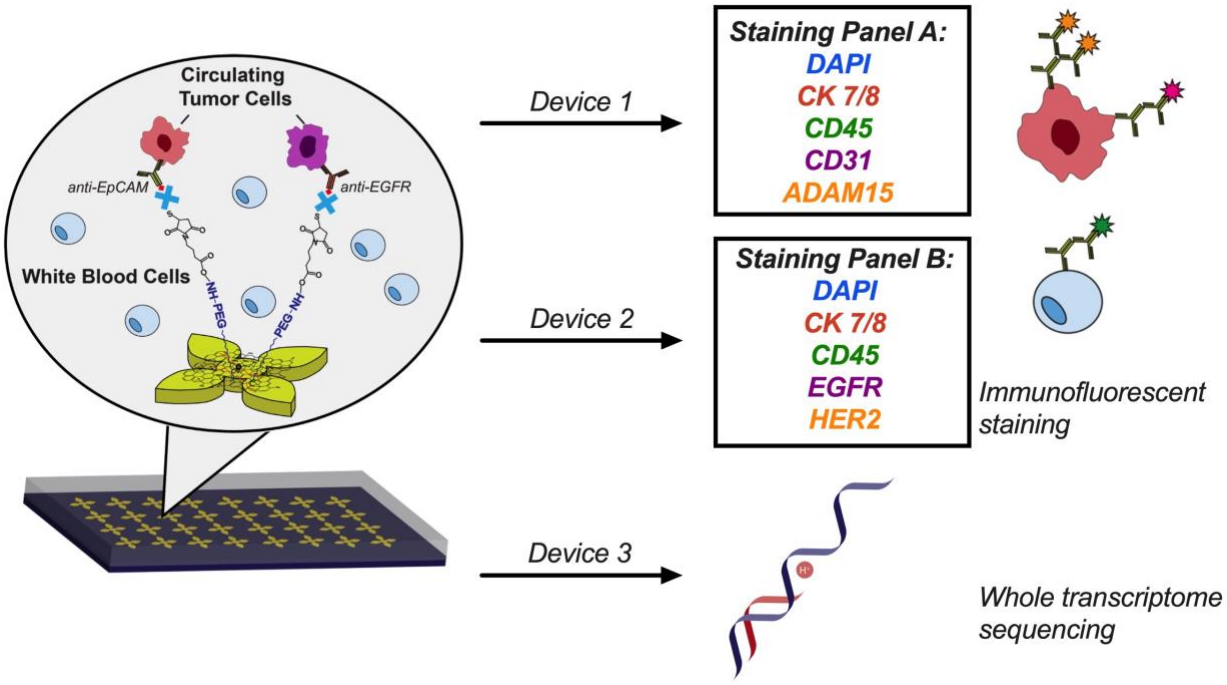

Figure 2-1 Schematic drawing of the GO chip workflow.

2.4 Materials and methods

2.4.1 Cell culture

UC-5, UC-9 and UC-18 cell lines were maintained in DMEM (Gibco) with 10% fetal bovine serum (FBS) (Sigma) and 1% antibiotic-antimycotic (Gibco), at 37°C and 5% CO_2. They were grown to 70 – 80% confluence before subculturing using the TrypLE enzyme (Gibco). Media was replaced every 48 – 72 hours between subculturing. Cell lines were routinely tested and reported negative for mycoplasma contamination (Lonza).

2.4.2 GO chip fabrication and functionalization

The GO chip is fabricated and functionalized, as described previously. Briefly, a chrome layer (100 Å) and gold layer (1000 Å) were first deposited onto the silicon dioxide wafer. A positive photoresist (SPR 220) layer was then coated and exposed to UV light under the mask with designed patterns. The patterns form on the photoresist when immersed in developing reagents and were then etched into the gold and chrome layer. The photoresist was then removed entirely, and the devices were cut into the correct sizes and proceeded to functionalization.

GO suspension was prepared with graphene oxide nanosheets, N, N-dimethylformamide (DMF), Tetrabutylammonium (TBA) hydroxide, and phospholipid-polyethylene–glycol-amine (PL-PEG-NH2). Silicon substrates are immersed in the GO suspension for 10 minutes, followed by the addition of cross-linker compound N-(gamma-maleimidobutyryloxy) succinimide (GMBS) and Neutravidin. The silicon substrate and PDMS were bonded using a corona plasma discharge. Completed GO chips were then stored at 4℃ till sample processing. On the sample processing day, 1mL PBS was first flown through the device at 100 µL/min to wash off the residual Neutravidin. Then, the antibody cocktail containing 20 µg/mL anti-EpCAM, and 20 µg/mL anti-EGFR was processed through a device inlet at 20 µL/min and incubated for 30min, and then through an outlet with the same incubation to ensure even antibody coating. 3% bovine serum albumin (BSA) solution was then processed through the device at 100 µL/min for 1mL, to prevent non-specific binding of WBCs.

2.4.3 Cancer cell isolation from model samples and capture efficiency calculation

Target bladder cell lines were pre-labeled with fluorescent green tracker dye (CellTrackerTM Green CMFDA) and counted before being added to buffer or blood. Cell capture was performed by flowing the model samples through the devices at a flow rate of 1 mL/hr. The cells are then fixed and permeabilized on the chip, followed by staining with DAPI (4', 6-

diamidino-2-phenylindole). The chips are then scanned using an inverted fluorescence microscope and the capture efficiency is calculated using the following equation:

$$\text{capture efficiency (\%)} = \frac{\text{cell number captured on chip}}{\text{total cell number processed}} \times 100\%$$

2.4.4 Patient sample collection and CTC isolation

The experimental protocol was approved by the Ethics (Institutional Review Board) and Scientific Review Committees of the University of Michigan, and all patients gave their informed consent to participate in the study (HUM00041153). For each patient sample, three GO chips were processed in parallel to perform immunofluorescence and RNA extraction within 4 hrs since blood draw. Briefly, 1mL of blood sample was processed through the device at 1 mL/hr, following the capturing antibody incubation and BSA incubation as described above. Then, 6 mL of PBS were processed at 100 μL/min to wash off any unbound, non-specific blood cells. For immunofluorescent staining, the immobilized cells on chip were fixed with 4% paraformaldehyde (PFA).

2.4.5 Immunofluorescent staining and CTC identification

Following 4% PFA fixation and a 1mL PBS wash, the isolated cells were then permeabilized using 0.2% Triton-X100 (Sigma-Aldrich) and incubated for 30min. The devices were then washed with 2mL PBS and blocked with 2% goat serum (ThermoFisher) and 3% BSA to prevent nonspecific staining for 30min. The staining antibodies were then diluted in 1% BSA and flowed through the devices at 50 μL/min and incubated at 4℃ overnight. On the second day, 2mL PBS was flowed through the devices at 100 μL/min to wash off the excess primary antibodies. The secondary antibodies were then prepared, flowed through the devices, and incubated for 1.5 hrs. 2mL of PBS was then again flowed to wash off the excess secondary antibodies. DAPI was

then flowed through the device and incubated for 15min and washed off using 1mL of PBS. Finally, the devices were scanned and analyzed using Nikon Ti2 fluorescent microscope and the Nikon-Elements software. A summary of the antibody products used are shown in Table 1.

Table 1 Summary of antibodies used for the staining panels.

Marker	**Primary antibody**	**Secondary antibody**	**Staining Panels**
CD45	Santa Cruz Sc-70699	Thermofisher A11006	Panel 1 & 2
CK7/8	BD 349205	Thermofisher A21133	Panel 1 & 2
EGFR	Thermofisher 2800005	Thermofisher A21240	Panel 1
HER2	Cell Signaling 2165	Thermofisher SA5-10035	Panel 1
CD31	R&D Systems BBA7	Thermofisher A21240	Panel 2
ADAM15	Novopro 101503	Thermofisher SA5-10035	Panel 2

CTCs were identified as DAPI+/CK7/8+/CD45- based on the staining images. On these identified CTCs, the expressions of the invasive markers were recorded as binary variables for further analysis.

2.4.6 RNA extraction and targeted whole-transcriptome sequencing

RNA extraction was performed on the third parallel device after blood sample processing and PBS washing step. Briefly, 100 µL Arcturus® PicoPure® RNA Extraction buffer (Life Technologies) was flowed through the device at 3mL/hr. The device was then incubated at 42 ℃ for 30 min. Following the incubation, 100 µL ultrapure DEPC water was flowed through the device and the effluent materials were collected. These materials were then purified using Arcturus® PicoPure® RNA Isolation Kit according to the manufacturer's instructions. The resulting 11 µL of purified RNA were stored at -80 ℃ until library preparation.

We performed amplicon-based whole-transcriptome sequencing using the Ion Ampliseq Transcriptome Human Gene Expression Kit (Life Technologies) according to the manufacturer's instructions with approximately 0.3 ng of RNA per sample, allowing for interrogation of ~21,000

RNA transcripts. Library preparation was performed according to the manufacturer's instructions. Technical replicate libraries and templates were independently constructed and sequenced on separate chips. Reads were mapped and quantified using version 5.16.1 of TorrentSuite's (Life Science Technologies) coverageAnalysis plugin with the default parameters.

2.4.7 Bioinformatics analysis and removing white blood cell variance

The read count table were exported into R programming environment for further analysis. We used RUVseq R package[160] to first remove the variance caused by varying WBC signals following the package vignette. Briefly, initial normalization was performed using the upper-quartile method in the EDASeq package[161,162]. To remove WBC related variance, two input parameters are needed including a set of negative control genes and factor number k. For the negative control genes, we first selected a broad range of 1746 leukocyte marker genes from available databases[163,164], and then selected genes that are relevant in our experiments. To do this, we first plotted the average and standard deviation for these 1746 gene expression within the healthy control samples and cell line samples using a density plot format (shown in Figure 2-2). We then set a series of criteria to find the common genes that are highly expressed in processed healthy blood control samples and lowly expressed in cell line control samples in our experiment. The detailed selection criteria are listed in Table 2.

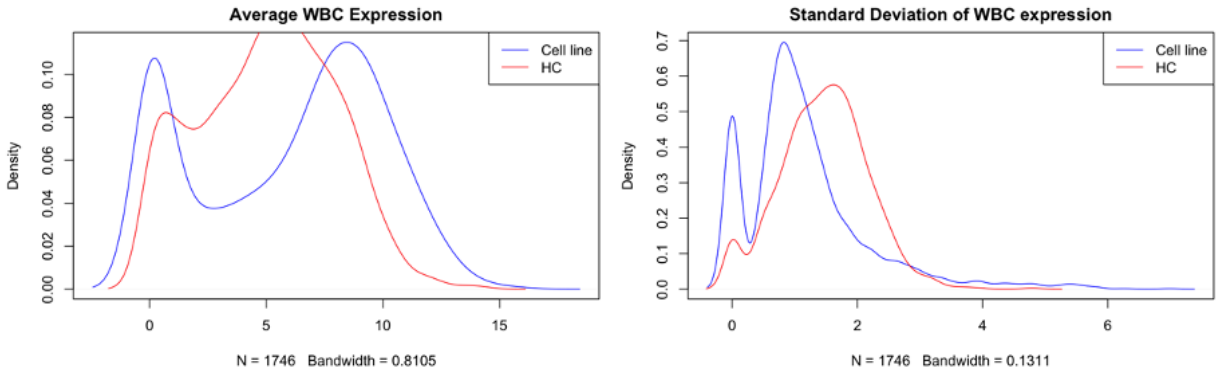

Figure 2-2 Density plots for selected 1746 WBC related genes within cell line samples and healthy control samples.

Table 2 Detailed selection criteria for selecting negative control genes for WBC expression.

Select genes whose average log expression is:	Select genes whose standard deviation is:
$>$ 5 within all healthy control samples	$>$ 1.5 within all healthy control samples
$<$ 4 within all cell line samples	$<$ 0.6 within all healthy control samples

Using this criteria, 84 WBC marker genes were selected as negative control genes. For the factor number k, we experimented with k equals 1 to 5 based on the small patient sample size[160,165]. The resulting differential gene expression did not seem to be affected by the k number. We chose k equals 2 as final output parameter. After performing RUVseq, the design matrix was entered as input with different comparison group into DESeq2 R package. Finally, the adjusted p-val and log fold change results for significantly differentially expressed genes (DEGs, adjusted p-val < 0.05, fold change > 1.5) were exported for interpretation. Disease ontology enrichment analysis[166] were performed on the DEGs through the ClusterProfiler package[167].

2.4.8 Statistical analysis

Comparisons between two groups were performed using unpaired Student's t-tests, two-tailed. Correlation was performed using simple linear regression, and the coefficient of

determination, R^2 was reported. Survival analysis was performed using Kaplan-Meier survival curves using the Log-rank method (Mantel-Cox test). All analysis was conducted in GraphPad Prism V9.

2.5 Results

2.5.1 Isolation of bladder cancer cells and workflow optimization of the GO chip

To test the capture efficiencies of the modified GO chip workflow with anti-EGFR and anti-EpCAM, we spiked human bladder cancer cell lines (UM-UC9, UC5 and UC18) into PBS or healthy control blood. As shown in Figure 2-3A, the capture efficiencies of UC-5 and UC-9 are over 88% regardless of their background solutions. Further, capture required expression of either EGFR or EpCAM with only 12.8% of UC-18 cells (low EGFR, low EpCAM) captured. To further identify the CTCs from non-specifically bound WBCs, immobilized cells were stained with cytokeratin 7/8 (CK7/8, epithelial marker) and CD45 (white blood cell marker). Identified CTCs were then further evaluated for their expression of ADAM15, CD31, EGFR and HER2. Examples of positive control staining images of these markers are shown in Figure 2-3B and Figure 2-3C.

To whether the amplicon-based whole transcriptome sequencing method can accurately represent the RNA expression profile after GO chip isolation, we compared the expression profile from UC-5 and UC-9 captured on chip to previously sequenced UC-5 and UC-9 from cultured conditions. As shown in Figure 2-3D, even with batch effects, expression data from the same cell line still clustered together in the principal component analysis. The expression profiles of cell lines of the same origin between on-chip and cell lines direct from culture are positively correlated (Figure 2-3E, UC-5: $R^2 = 0.6189$; UC-9: $R^2 = 0.7252$). Taken together, these results indicate that the amplicon-based whole transcriptome sequencing is a viable tool to profile samples isolated using the GO chip.

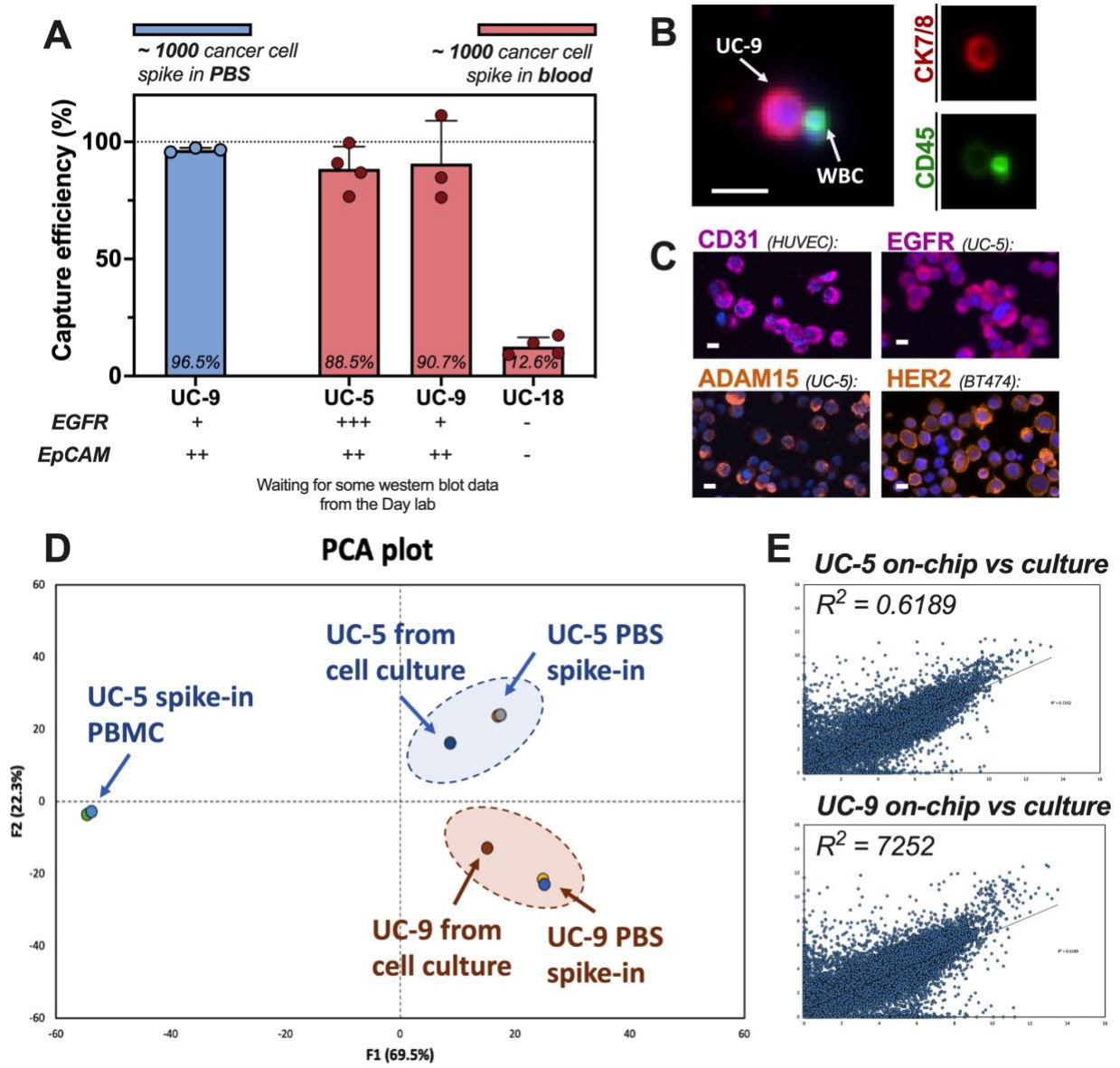

Figure 2-3 Workflow optimization using cell line controls. (A) Capture efficiency of bladder cancer cells spiked into PBS or healthy control blood samples. (B) Staining optimization of Cytokeratin 7/8 (CK 7/8) and CD45 using blood sample spiked with UC-9. (C) Examples of CD31, EGFR, ADAM15 and HER2 staining with corresponding cell lines. (D) Principal component analysis of the RNA expression profile of UC-5 and UC-9 spike-in model samples, as well as expression profile from RNA extracted from culture. (E) Linear correlation of the expression between the UC-5 and UC-9 on-chip samples and the culture samples.

2.5.2 CTC concentrations associate with tumor burden at blood draw and overall survival

Using the optimized workflow, we then analyzed CTC profiles from a pilot cohort of 15 bladder cancer patients, including 14 metastatic patients and 1 non-muscle invasive bladder cancer

(NMIBC) patient. Patient demographic and other clinical information are summarized in Figure 2-4A. In this cohort, 9 patients received pembrolizumab, a PD-1 checkpoint blockade immunotherapy. 14 patients had single time point blood draws, while one patient had blood draws at two sequential time points.

We first sought to compare the CTC per mL between the different blood draw times with respect to their systemic treatments among the metastatic MIBC patients (N = 14). In this cohort, 3 samples were drawn before patient received systemic treatments, while 6 were drawn during the systemic treatment (including 2 samples from one patient drawn at different times during therapy), and 5 after treatment was completed. 1 patient was excluded from this analysis because of loss of follow up. As shown in Figure 2-4B, no significant difference in CTC concentration was found between the different treatment time points, although the before time point had a slightly higher average CTC per mL (9.5 CTCs/mL). We then compared CTCs per mL based on burden of disease at time of blood draw (Figure 2-4C). The disease burden was determined based on radiographic measurements and classified as either, no evidence of disease and metastatic disease (lesions seen on most recent imaging). In addition, 4 control samples from healthy blood were processed using the same protocol to use as a negative control. Significantly higher CTC concentrations were found in patients with metastatic disease (mean 11 CTCs per mL, p-val = 0.0471).

Overall survival from the time of blood draw and CTC measurement was then analyzed to determine the implication of CTC concentration for patient survival. Patients were divided into two groups by their CTC counts being above or below 3 CTC/mL. As shown in Figure 2-4D, patients with >3 CTCs per mL had significantly shorter overall survival time (p-val = 0.0439). The median survival for this higher CTC concentration group is 656.5 days.

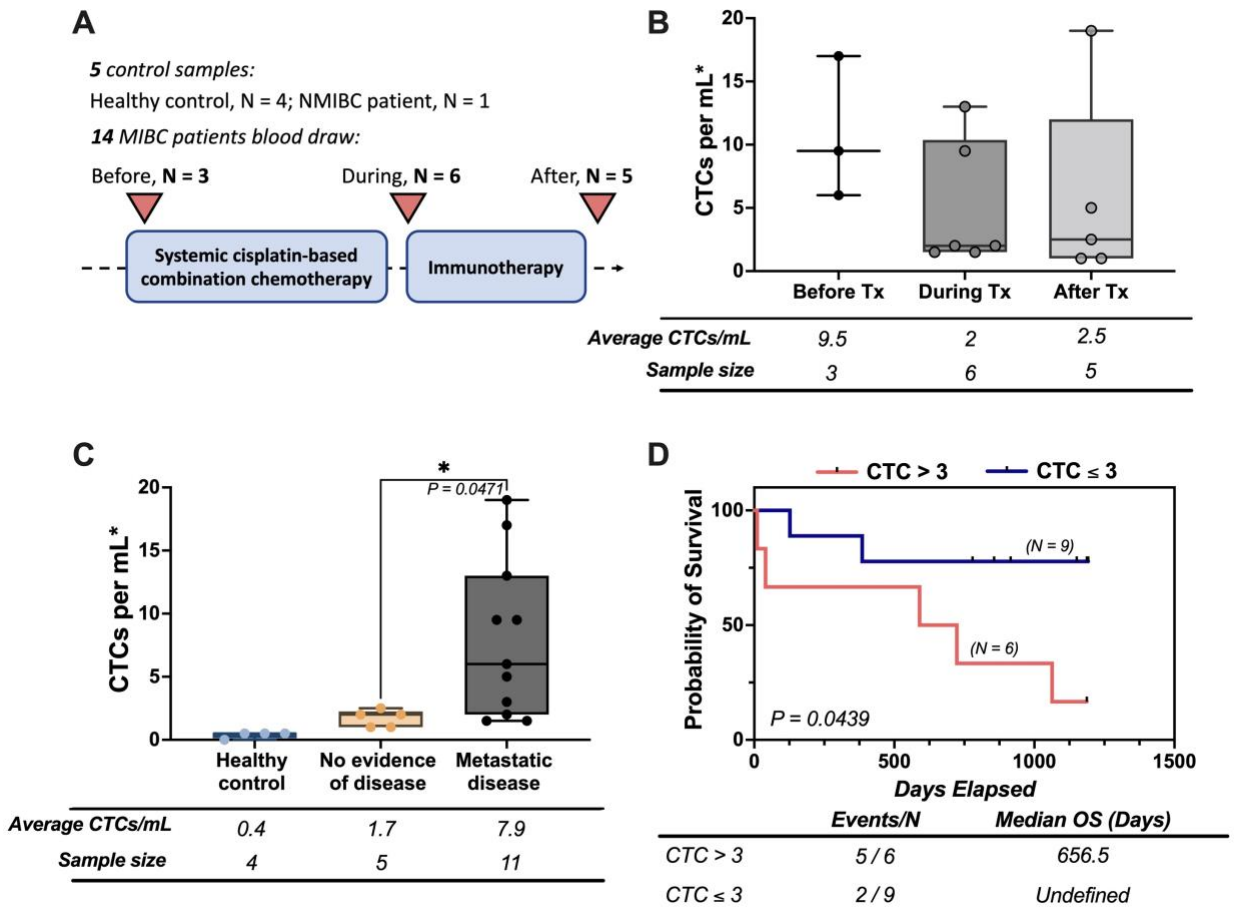

*Figure 2-4 CTC enumeration in a cohort of metastatic muscle-invasive bladder cancer patients. (A) Study overview. (B) CTC per mL from patient blood draws that are before, during and after chemotherapy and immunotherapy. (C) CTC per mL in blood draws from healthy control, patients with no evidence of disease or patients with metastatic disease. (D) Kaplan-Meier curve of CTC per mL greater or less than 3. * CTCs per mL on the y-axis is calculated by averaging the two immunofluorescent staining devices.*

2.5.3 Correlation between the presence of CTCs with invasive marker expression and overall survival

Because ADAM15, CD31, EGFR and HER2 were hypothesized to correlate with increased tumor invasion and metastatic spread, each was evaluated for isolated CTCs from patient samples. Examples of immunofluorescent staining images are shown in Figure 2-5A. 46.7% patients had ADAM15+ CTCs, and for these patients, the median positivity per patient is 33.3%. For CD31, CTCs from 58.3% patients showed positive staining, and in these patients, and median percentage for CD31+ CTCs is 33.3% per mL. Patients who have positive EGFR staining on their CTC

accounts for 66.7% of the pilot cohort, and in these patients, the median positivity per patient is 33.3% per mL. Only 16.7% patients were found to have HER2+ CTCs in our cohort. For each of these patients, 1 CTC per mL was found to have positive HER2 staining. In addition, 58.3% of patients had at least two invasive markers stained positive for their CTCs.

We then correlated these CTC expression profile with overall survival data (Figure 2-5B). Although the comparison did not reach statistical significance because of the limited sample size, patients who had ADAM15+, EGFR+ or HER2+ CTCs tend to have shorter overall survival. These trends were expected based on previous literature stating that these markers are associated with tumor progression. On the contrary, patients who had CD31+ CTC tend to have longer overall survival. This trend was unexpected and could be due to the small sample size in patients without CD31+ CTCs. Overall, the relationship between the invasive marker expression on CTCs need to be verified using a larger cohort, although our preliminary data reveal that expressions of these markers are associated with worse patient survival.

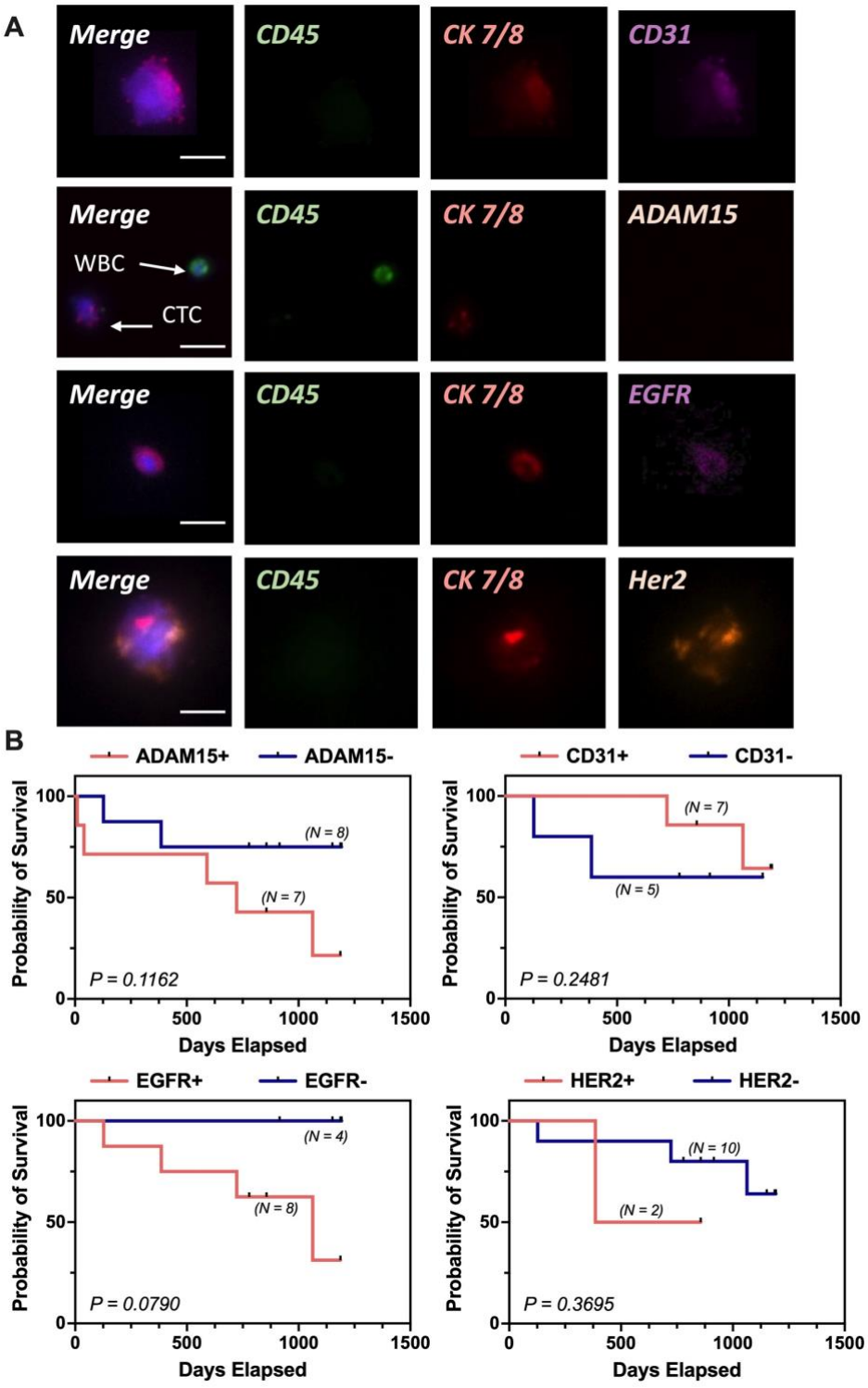

Figure 2-5 Invasive marker expression on bladder cancer patient CTCs. (A) Immunofluorescent images of CTCs with invasive marker expressions. (B) Kaplan-Meier curve of patients with or without single invasive marker presence.

2.5.4 Metastasis related RNA signatures found in patients with metastatic tumor present and high CTC counts

To further investigate CTC expression signatures on the RNA level, amplicon-based targeted RNA sequencing was performed on 13 samples in this cohort, and the results were analyzed using custom pipeline shown in Figure 2-6A. Briefly, the read count table was exported from TorrentSuite software and imported into R programming. We then performed normalization, quality control and unsupervised clustering. As shown in Figure 2-6B, the expression profiles clustered by the sample type suggesting that the RNA signature was being driven by non-tumor RNA. However, when we specifically analyzed the RNA signature of CTC samples, the healthy control samples and patients with no tumor evidence overlapped with each other, whereas those with active tumor clustered separately. We then sought to perform differential gene expression analysis to discover tumor related traits within isolated CTCs. We first used RUVseq R package with a set of selected WBC control genes to remove the variance generated from contaminating WBCs. The differential gene expressions were analyzed between three different groups: 1) healthy controls and patient samples; 2) patients who have active metastatic disease and no tumor evidence; 3) patients who have CTC > 2/mL and $\leq$ 2/mL.

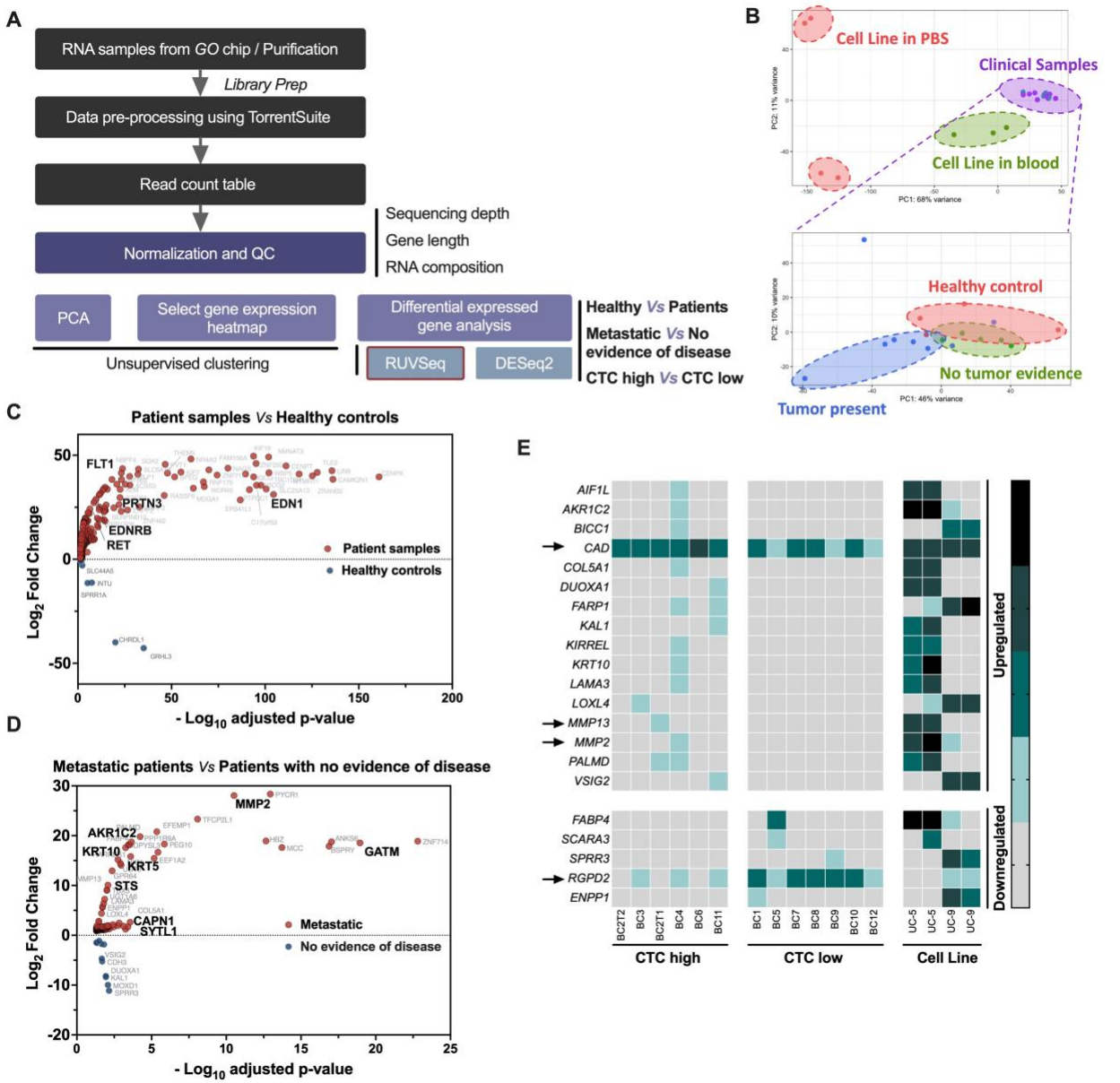

Figure 2-6 RNA expression analysis from CTC samples. (A) RNA analysis workflow overview. (B) Principal component analysis for the RNA expressions. (C)Volcano plot of significantly differentially expressed genes between patient samples (N = 13) and healthy controls (N = 4). (D) Volcano plot of significantly differentially expressed genes between patients with metastatic disease (N = 8) and patients with no evidence of disease at the time of blood draw (N = 5). (E) Normalized expression of DEGs between patients who have CTC > 2 per mL and CTC ≤ 2 per mL.

Between patient samples (N = 13) and healthy controls (N = 4), 216 genes were found to be significantly differentially expressed (adjusted p-val < 0.05, Fold change > 1.5), including 199 upregulated and 17 downregulated genes (Figure 2-6C). Many genes amongst the 199 enriched genes in CTC samples have been shown to be associated with cancer development. Table 3 shows

the enriched disease ontologies from these upregulated genes, with 10 genes being closely associated with urinary system cancer. For example, highly upregulated gene FLT1 (Fms-related tyrosine kinase 1) is the receptor of VEGF (Vascular endothelial growth factor) and is associated with cancer angiogenesis and tumorigenesis. High expression of FLT1 and VEGF have been shown in 40% of urinary bladder cancer patients[168].

Table 3 Top 3 cancer related disease ontologies and their relevant differentially expressed genes between cancer patient and healthy controls.

DISEASE ONTOLOGY	RELEVANT GENES
Urinary System Cancer	FLT1/EDN1/EDNRB/PRTN3/RET/APOE/APOC1/ID1/ALOX5/CDKN1B
Kidney Cancer	FLT1/EDN1/EDNRB/PRTN3/RET/APOE/APOC1/ALOX5/CDKN1B
Prostate Cancer	FLT1/BUB1B/APOE/NR1H3/HSPG2/ID1/CDKN1B

As shown in Figure 2-6D, the comparison between patients with metastatic tumor (N = 8) and patients with no disease evidence (N = 5) resulted 211 differentially expressed genes (adjusted p-val < 0.05, Fold change > 1.5), with 197 of which are upregulated in patients with metastatic tumor present. Interestingly, there were only two common genes (MOXD1 and WDHD1) between this set of DEGs and previous DEGs between patient samples and healthy controls. This might indicate this comparison between different disease status reveal some unique molecular traits that are associated with metastasis. For example, MMP-2 (Matrix Metalloproteinase-2) contributes to almost every key step in the metastatic cascade including EMT, cancer cell survival, proliferation, intravasation and extravasation[169]. Overexpression of AKR1C2 has been shown to aid the development of cisplatin-based chemoresistance and become a high-risk factor in bladder cancer patients[170,171]. STS (Steroid sulfatase) is a steroid sulfate activation enzyme in the androgen signaling pathway that has been known to associate with aggressive tumor characteristics[172]. In

bladder cancer, STS has been shown to promote the invasion capability through the regulation of EMT[173]. Moreover, KRT5 and KRT10 were found to be highly upregulated in the metastatic patient group. These two genes are often found in basal and intermediate subtypes of bladder cancer cells, which are associated with aggressive phenotype as well[174]. Other examples of well-studied metastasis-related markers include GATM[175], SYTL1[176] and CAPN1[177].

We then interrogated the differential expression between patients with high (N = 6) or low (N = 7) CTC concentrations with the cutoff being 2 CTCs/mL. There were 21 differentially expressed genes between these two groups, as shown in Figure 2-6E. Several genes that are related to metastasis including COL5A1, MMP2, MMP13, AKR1C2, KRT10 are detected in some samples in the high CTC group. Although the detections of these genes are sparse among the tested samples, some universally expressed genes such as CAD and RGPD2 showed interesting trends. CAD gene (other name Carbamoyl-Phosphate Synthetase 2, CPS2) showed higher expression in CTC enriched samples, as well as the cell line controls. CAD is involved in the biosynthesis of pyrimidine synthesis and is upregulated in cancer cells[178]. RGPD2, on the other hand, are highly expressed in several CTC low samples, but not in CTC high or cell line controls. This gene is not well studied but shown enriched expression in regulatory T cells. Overall, these results give confidence in our CTC profiling platform to find metastasis related traits.

2.6 Discussion

Molecular profiling of cancer cells is especially crucial for bladder cancer management because of its intertumoral heterogeneity. As part of liquid biopsy, CTCs hold the promise of the dynamic monitoring of cancer and personalized treatments. The detection of CTCs in bladder cancer often struggles with low detection rate and limited molecular profiling analysis. We present a protein and RNA co-analysis workflow using highly sensitive GO device and bioinformatics

pipeline to remove variance from contaminating WBCs. Our pilot study tested this workflow on a small cohort of 16 bladder cancer patients and 5 healthy control samples, and successfully detected CTCs from all 16 samples from cancer patients. The CTC concentrations in patients with metastatic disease are significantly higher than those in healthy controls and patients with no disease evidence at the time of blood draw. We also show that patients with high CTC concentration (> 3 CTCs/mL) potentially have shorter overall survival time. This result is consistent with other studies in the literature using other technologies[179].

We used multiplex immunofluorescent staining to investigate the expression of EGFR, HER-2, CD31 and ADAM15 on isolated CTCs. We hypothesis that the expressions of these markers represent the aggressive CTC subtype that are responsible for vascular invasion and contribute to the survival of CTCs and worse disease outcome. Comparing the survival data for patients with or without invasive marker positive CTCs, patients who had ADAM15+, EGFR+, and HER-2+ CTCs presented shorter overall survival trends. Patients who had CD31+ CTCs had longer overall survival results. We think this might be because of the small sample size of CD31- patients.

For the RNA analysis, we developed a workflow that amplicon-based targeted transcriptome sequencing and bioinformatics methods to profile the DEGs from bulk RNA material in the isolated CTCs. We used a set of 84 WBC marker genes to remove the variance caused by contaminating WBCs in these bulk samples and discovered the DEGs between samples from cancer patients and healthy control, metastatic patients and patients with no disease evidence, and patients with high CTC counts and low CTC counts. Many metastasis-related gene signatures that are well studied in the literature, such as KRT5, KRT10, MMP-2, MMP-13, AKR1C2, GATM, SYTL1 and CAPN1 were found with upregulated expression in metastatic patient

samples. Future studies should investigate correlating expression on CTCs using single cell-based profiling approach to confirm our findings.

It is worth noting that our study has a couple of limitations. Firstly, the sample size for comparison is small due to sample collection difficulties. Larger cohorts in the future with multiple collection time points is needed to further validate our results. Secondly, the removing WBC variance method hypothesizes that the negative control genes are not related to the comparison factor. This means our results are based on the hypothesis that the 84 WBC markers are biologically not related to patient disease status and patient CTC number.

Our results show proof of concept that the GO chip-based workflow can be used to profile CTCs from bladder cancer patients on protein and RNA level. This workflow could be potentially used for larger clinical studies to further explore CTCs prognostic values.

Chapter 3 Analytical Workflow for CTC Characterization in Longitudinal or Multisite Clinical Studies

3.1 Abstract

Although many studies have shown the initial prognostic value of the CTCs, efforts for profiling and analyzing CTC in longitudinal clinical studies are still needed. The profiling of CTCs on the RNA level is especially challenging because of the inherent low RNA quantity and quality after multiple handling in the enrichment process. Microarray transcriptome profiling can be a promising approach for CTC analysis because of its compatibility with low-quality and quantity RNA materials. Here, I developed an analytical workflow after profiling CTCs using the GO chip and microarray in a cohort with locally advanced (stage III) NSCLC patients treated with chemoradiation and immunotherapy. CTC-related metrics were characterized on multiple fronts, such as CTC counts per mL, the change of CTC counts over time, protein expressions, and RNA expressions, and their correlations with patient outcomes were explored. We found that CTC decreases in counts per mL after the start of chemoradiation therapy and having $\leq$ 50% PD-L1+ CTCs significantly predicts longer progression-free survival. From paired differential gene expression analysis of RNA profiles, we found significant upregulations of genes that related to cancer metastasis, invasion, proliferation, and resistance in CTC samples during chemoradiation treatment. I then applied this workflow to other clinical studies and developed a bioinformatic workflow to remove the variance from contaminating WBCs in the CTC samples. Overall, the workflow developed in this chapter could be further applied to other clinical studies to elucidate the value of CTCs as biomarker further.

3.2 Manuscript information

Emma Purcell, **Zeqi Niu**, Sarah Owen, Madeline Grzesik, Abbie Radomski, Anna Kaehr, Heather Fairbairn, Shruti Jolly, and Sunitha Nagrath. "Circulating Tumor Cells Isolated from Stage III NSCLC Patients Using Microfluidic Graphene Oxide (GO) Chip Predicts Progression Free Survival."*(In submission)*

Kaylee Smith, Jess Jana, **Zeqi Niu**, Zach Gdowski, Scott Smith, Emma Purcell, Ted Lawrence, Kyle Cuneo, and Sunitha Nagrath. "Circulating tumor cells as a biomarker to predict patient outcomes in hepatocellular carcinoma." *(In preparation)*

Shirish M. Gadgeel, Karen Dziubek, Misako Nagasaka, Thomas Braun, Khaled Hassan, Haiying Cheng, Antoinette Wozniak, Balazs Halmos, James Stevenson, Pradnya Patil, Nathan Pennell, Mary Jo Fidler, Philip Bonomi, Angel Qin, **Zeqi Niu**, Sunitha Nagrath, Gregory P. Kalemkerian. "Pembrolizumab in combination with platinum-based chemotherapy in recurrent EGFR/ALK+ Non-Small Cell Lung Cancer (NSCLC)." *(In preparation)*

3.3 Introduction

CTC-based liquid biopsy provides new hope in implementing personalized treatment plans. In non-small cell lung cancer (NSCLC), previous CTC studies are mostly performed using the CellSearch platform, and have correlated CTC counts to timepoints during treatment[40,87,180,181]. We previously demonstrated the utility of the GO chip workflow in a cohort of stage I-III NSCLC patients, finding increasing PD-L1+ CTCs after chemoradiation treatment[23]. Additionally, we used RT-qPCR to further profile the isolated CTCs and found that PD-L1 and LGALS3BP were significantly upregulated in the CTCs of patients with earlier progression of their cancer. However, a more comprehensive analytical pipeline is needed to correlate CTC counts over time and patient survival, as well as profile CTCs on the RNA level.

The profiling of CTCs on the RNA level is technically challenging because of the inherent low RNA quantity and quality after multiple handling in the enrichment process. The current widely used technology, RT-qPCR, can amplify and quantify specific cancer-related genes in the enriched CTC samples, yet this assay is limited to only a small number of pre-selected gene sets. Alternatively, the microarray transcriptome profiling technologies are compatible with low-quality RNA materials (such as FFPE tissue samples) and low RNA input (minimum 0.01ng for the Clariom S PICO assay).

To further expand the clinical value of CTCs, we use the GO chip and microarray technologies to profile CTCs from locally advanced (stage III) NSCLC patients treated with chemoradiation and immunotherapy. The cohort for this study all received combination chemotherapy and radiation for six weeks, with the majority of patients receiving subsequent maintenance durvalumab for 1 year following their chemoradiation. We collected blood samples with six timepoints for each patient across the treatment course, making this the first study that monitored patients for their CTC profiles across both chemoradiation and durvalumab therapy. Moreover, an analytical workflow was developed to correlate the CTC counts and RNA information to patient survival outcomes. I then applied this workflow to other similar clinical studies in NSCLC and hepatocellular carcinoma (HCC). The methods developed in this chapter could be further streamlined and applied to future CTC studies.

3.4 Materials and methods

3.4.1 CTC profiling workflow

CTCs were isolated from whole blood using GO[20,23] chips similar as described above. The device is functionalized to tether the following capture antibodies on the surface for CTC isolation: anti-EpCAM, anti-EGFR, and anti-CD133. EpCAM and EGFR are expected to be highly

expressed in lung cancer CTCs[19], and CD133 is a stem-cell-like marker linked to tumorigenic phenotypes in lung cancer[182]. As shown in Figure 3-1, two GO chips were run in parallel for each patient blood sample, one for CTC enumeration and one for RNA extraction of captured CTCs. For the CTC enumeration chip, CTCs were identified and counted DAPI+/CK+/CD45- cells using immunofluorescent staining. Identified CTCs were then evaluated for their staining of PD-L1 (Biolegend, NC0043617). CTC count and PD-L1 data were then compared to clinical metrics to generate CTC profiles that were assessed for their ability to predict patient outcomes. For the RNA chip, the extracted and purified RNA materials were sent to Fisher scientific for Clariom™ S PICO human microarray assay. The read count data were then returned to our lab for further bioinformatic analysis.

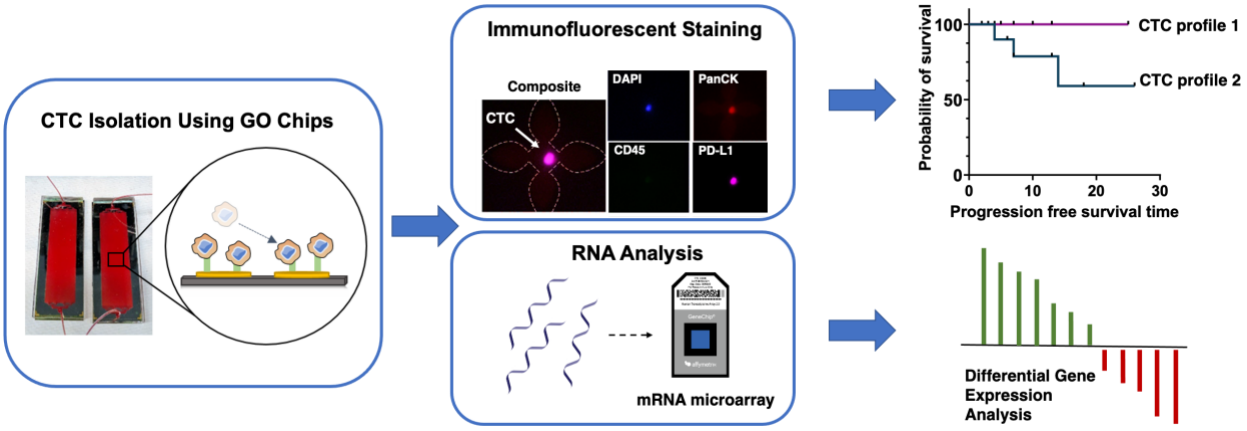

Figure 3-1 The schematic of CTC isolation and analysis using GO platform.

3.4.2 Patient cohort overview

Patients were profiled through both combined chemotherapy and radiation therapy (chemoradiation, chemo-RT) and immunotherapy for a total of six timepoints. These time points include pre-treatment (pre-TX), during chemoradiation treatment (Week 1 and Week 4), one month after chemoradiation (Week10), and during immunotherapy (Week 18 and Week 30). Patients underwent an adaptive radiation plan for a total of six weeks, that is, for the first four

weeks, patients received the same radiation dose, however, the dose for the final two weeks was determined based on the patient's FDG-PET scan at week 4 of chemoradiation. Following radiation, most patients (16/26) had a 1-month treatment break before starting anti-PD-L1 immunotherapy, durvalumab. Some patients, however, were enrolled before durvalumab became the standard of care. Of these, 2 patients received a different immunotherapy, 8 patients received no immunotherapy, and 1 died during radiation.

A

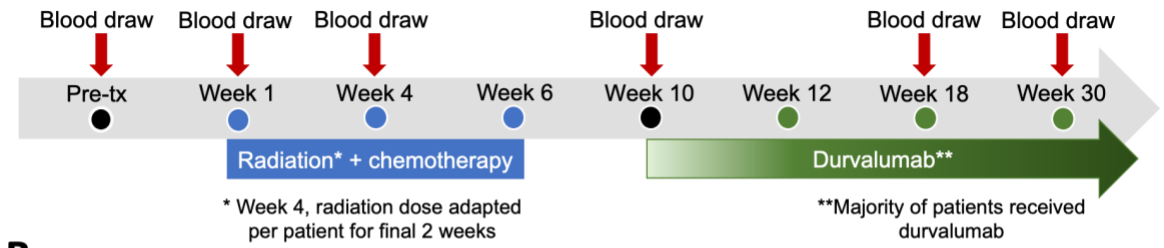

B

Clinical Characteristic		n (%)
Total Patients	26	—
Age	mean = 67	range = 50-83
Sex	F	7 (27%)
	M	19 (73%)
Stage	IIIA	11 (42%)
	IIIB	15 (58%)
Histology	Adenocarcinmoa	12 (46%)
	Squamous cell	12 (46%)
	Poorly differenciated NSCLC	2 (8%)
Immunotherapy following chemoradiation	None	8 (30%)
	Durvalumab	16 (62%)
	Pembrolizumab	1 (4%)
	Atezolizumab	1 (4%)

Figure 3-2 Patient treatment timeline and demographic overview. (A) The timeline of patient sample draws corresponding to treatments. The black timepoints indicate no treatment, the blue time points are during

radiation therapy, and the green time points are during durvalumab for most patients. (B) Patient clinical information summary.

3.4.3 Survival analysis

Progression-free survival (PFS) time was calculated between the radiation treatment start date and the date of progression or last contact. To test the association between CTC metrics and PFS, patients are divided to two comparison groups using the factor of interest (Table 4). The cutoff is selected to ensure either group can have comparable number of samples. To represent CTC changes between two time points, we calculated %CTC change using the following formula:

$$\%\ change = \frac{(CTCs\ at\ time\ 1 - CTCs\ at\ time\ 2)}{CTCs\ at\ time\ 1} \times\ 100\%$$

Table 4 Comparison groups for PFS survival analysis

Factor of interest	**Group 1**	**Group 2**
CTC count at single time point (CTC counts / mL)	CTC Pre-TX > 10	CTC Pre-TX ≤ 10
	CTC Week1 > 10	CTC Week1 ≤ 10
	CTC Week4 > 10	CTC Week4 ≤ 10
	CTC Week10 > 10	CTC Week10 ≤ 10
	CTC Week18 > 5	CTC Week18 ≤ 5
	CTC Week30 > 5	CTC Week30 ≤ 5
%CTC change between two time points	Pre-TX → Week 1 > 0	Pre-TX → Week 1 ≤ 0
	Pre-TX → Week 4 > 0	Pre-TX → Week 4 ≤ 0
	Pre-TX → Week 4 > -75%	Pre-TX → Week 4 ≤ -75%
%PD-L1+ CTC at single time point	%PD-L1 Pre-TX > 50%	%PD-L1 Pre-TX ≤ 50%
	%PD-L1 Week1 > 50%	%PD-L1 Week1 ≤ 50%
	%PD-L1 Week4 > 50%	%PD-L1 Week4 ≤ 50%
	%PD-L1 Week10 > 50%	%PD-L1 Week10 ≤ 50%
	%PD-L1 Week18 > 50%	%PD-L1 Week18 ≤ 50%
	%PD-L1 Week30 > 50%	%PD-L1 Week30 ≤ 50%

3.4.4 Expression microarray analysis

3.4.4.1 Normalization, quality control and filtering step

Microarray data processing procedures were followed in R programming environment (4.0.2). Briefly, raw intensities were imported as CEL files using the oligo package[183]. The intensities were then normalized and summarized into expression values probe-level using a robust multichip average (RMA) method[184]. The probesets were then annotated with gene names using clariomshumanhttranscriptcluster.db package. Duplicate mappings were removed by selecting the probesets with highest average expression across all samples. Quality control plots, including normalized unscaled standard error (NUSE), relative log expression (RLE) as well as principal component analysis (PCA) were generated to identify and remove potential outliers in the dataset. Before proceeding to differential gene expression analysis, we applied a filtering step to remove the low expressing genes. Median expressions of every gene across all the samples were calculated, and genes that have lower median expressions (< half of all expression medians) were removed. After this filtering, 9256 total genes were left and analyzed for differential gene expression.

3.4.4.2 Design formula for identifying differentially expressed genes

Differentially expressed genes were then calculated using different design formulas using the limma package[185], shown in Table 5. These comparison groups were set up to decipher the RNA profile in CTCs across chemo-radiation and between progressing and stable patients. A paired-sample design was used for the comparisons between different time points (indicated by *). For comparisons based on CTC counts, the CTC high group was defined by CTC per mL > 50 and the CTC low group was defined by CTC per mL < 20.

*Table 5 Comparison group summary for differential gene expression analysis. * indicate paired analysis was performed.*

Comparison range	Group 1	Group 2
All samples	Healthy control	Cancer patients
	PD-L1 high	PD-L1 low

Cancer patients	Pre-TX*	Week4*
	Pre-TX*	Week10*
	Progressing	Stable
	CTC high	CTC low
Progressing patients	Pre-TX	Week4
	Pre-TX	Week10
Stable patients	Pre-TX	Week4
	Pre-TX	Week10
Pre-TX samples	Progressing	Stable
Week4 samples	Progressing	Stable
Week10 samples	Progressing	Stable

3.4.4.3 Correlation between gene expression and survival

To assess how gene expressions are correlated with PFS time, we used the survival and RegParallel package to perform univariant cox regression survival analysis with gene expression. We identified genes from single time point RNA profiles that significantly stratify patients with future progressions. To showcase the stratification of patients, we then performed principal component analysis based on the significant genes.

3.4.5 Application of analysis pipeline to other clinical studies

3.4.5.1 General analysis workflow

We generalized the analysis workflow for similar clinical studies as shown in Figure 3-3. Close coordination is needed for this pipeline between the technology labs and clinical labs. Briefly, after blood samples were collected from the hospital, they are usually transported to different location for sample processing on the microfluidic devices. Protein characterizations and RNA extractions were then performed on the enriched samples. Through the protein characterizations, CTCs are usually detected and quantified by the positive staining of cancer specific markers, and negative staining of WBC markers. For RNA samples, targeted approaches such as amplicon-based targeted sequencing or microarray could be feasible as they were designed

to handle low quality samples. The CTC counts and filtered RNA data are then tested as biomarkers for patient clinical outcome information.

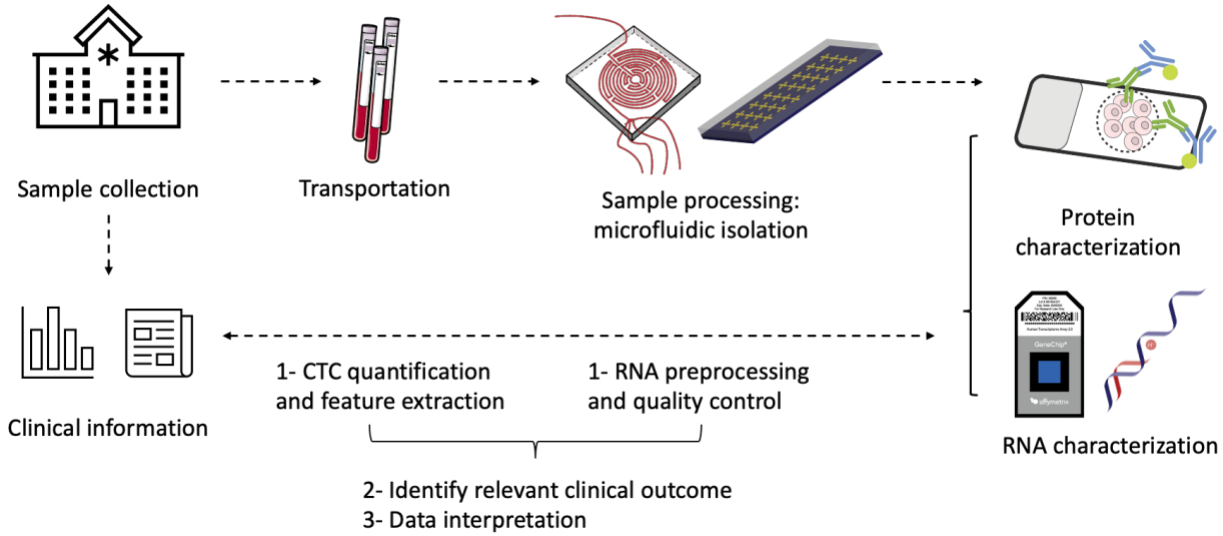

Figure 3-3 General CTC analysis workflow using microfluidic devices.

3.4.5.2 Other study cohorts overview

We applied this workflow to two other clinical studies as shown in Figure 3-4. For study I, we collected blood samples from a cohort of 29 patients with hepatocellular carcinoma (HCC). These patients are enrolled in a pilot study for individualized adaptive radiation therapies, where the treatment dose was adjusted based on patients' liver function. The majority of patients had three blood draws across the treatment course: before the start of radiation, post round 1 radiation treatment, and post the completion of radiation treatment. These blood samples were processed through the labyrinth device developed by our group[186] and analyzed for CTCs using a similar protocol as previous study[187]. RNA was extracted and purified from the enriched CTC samples and sent to Fisher scientific for Clariom^{TM} S PICO human microarray assay. The read count data was then returned to our lab for further bioinformatic analysis.

For study II, blood samples were collected from a multicenter phase II study in NSCLC. Patients with EGFR mutation and ALK positive were enrolled to receive pembrolizumab in

combination with platinum-based doublet chemotherapy. Blood samples were collected from 23 patients and processed 24hrs after blood draw to ensure enough time of transportation. During transportation, the blood samples were kept in K2EDTA tubes and at 4℃. For 11 out of the 23 patients, we were able to collect two blood draws: before treatment start and before cycle 3 of the treatment. We analyzed CTCs using similar GO chip protocols for lung cancer[23], where anti-EpCAM, EGFR and CD133 are used as capturing antibodies and anti-pan-CK, CD45 and PD-L1 as detecting antibodies. The RNA materials were extracted and purified, then sent to perform amplicon-based targeted sequencing. The read count data were then returned to our lab for further bioinformatic analysis.

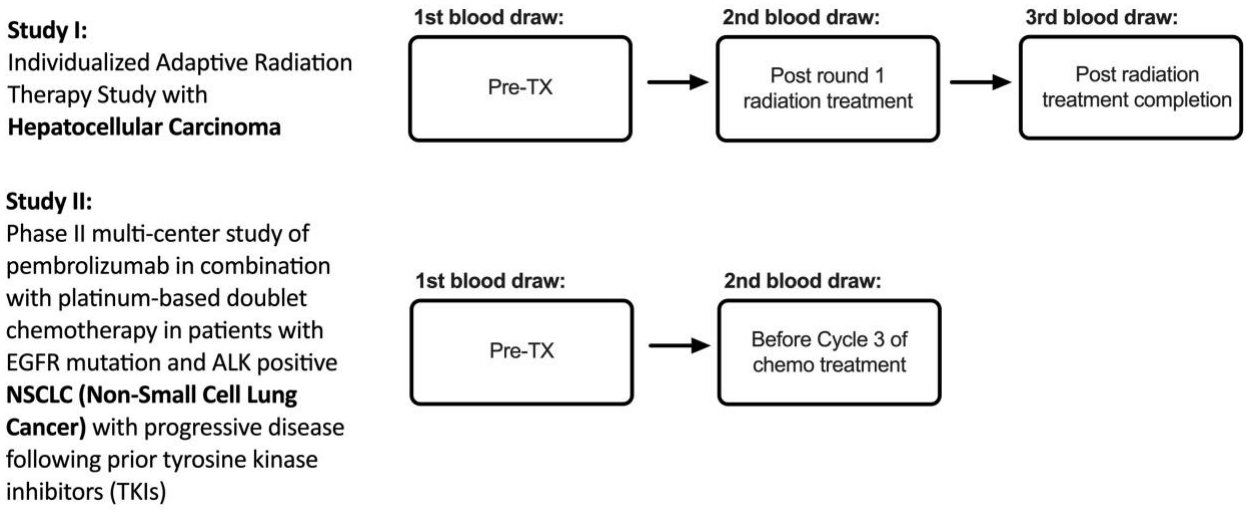

Figure 3-4 Schematic overview of other study cohorts.

3.4.5.3 Remove WBC contaminations using RUV package

One of the challenges in implementing this workflow in these studies were the lack of statistical significance when comparing RNA profiles between different groups. While the sample sizes were small in these two cohorts, we also hypothesized that this problem could be caused by the high WBC contamination in microfluidic technologies. As shown in Figure 3-5, for GO chips,

the final product include 56 – 5000 WBCs and 0 – 500 CTCs[22]. For the labyrinth device, it is estimated that the final product includes 10,000 – 20,000 WBCs and around 100 CTCs.

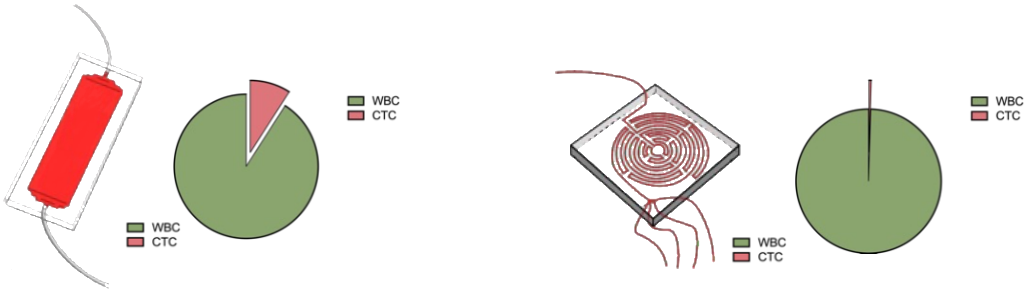

Final product of the **GO chip**:
WBC: 56 - 5,000; **CTC**: 0 - 500

Final product of the **Labyrinth**:
WBC: 10,000 – 20,000; **CTC**: ~100

Figure 3-5 Final enriched product components of the microfluidic devices.

To tackle this problem and increase the statistical significance, we used *remove unwanted variable* method to regress out the variations between WBCs. We used RUV R package for microarray data and RUVseq package for targeted sequencing data. Two input parameters are needed including a set of negative control genes and factor number k. The negative control genes were selected similar as described in the previous chapter. Using these negative control genes, we tested different k selections by plotting the canonical correlations between negative controls or full gene sets and the factors of interest. An example is shown in Figure 3-6 from the HCC cohort. K factor is selected by choosing the smallest k to ensure low correlation between negative controls and the factor of interest, and high correlation between full gene sets and the factor of interest. In the case for the HCC cohort, k = 10 was chosen for further analysis.

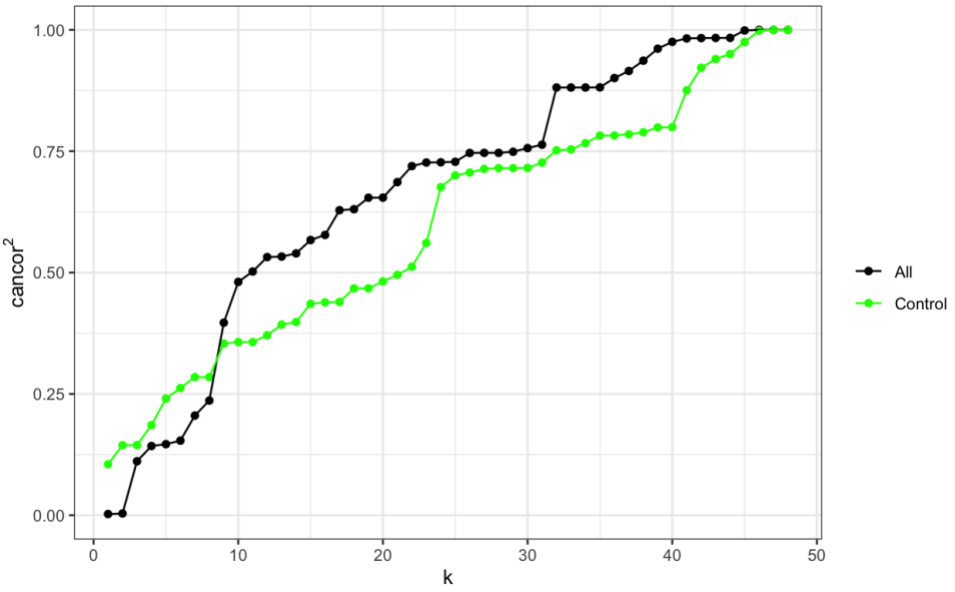

Figure 3-6 Canonical correlation graph to choose the k factor in RUV analysis.

3.5 Results

In this section, the majority of results are demonstrated using the RDART dataset in stage III NSCLC. Results of interests in the other two studies were briefly discussed in 3.5.5 section.

3.5.1 Total CTC counts and PD-L1+ percentage as predictive biomarkers for PFS

We first tested the CTC total counts and PD-L1+ percentage at single time points as predictive biomarkers for patient outcomes. The disease status was assessed by two radiation oncologists using the RECIST criteria. The average follow-up time was 12.4 ± 8.5 months (range = 0-31.3 months), where 0 months follow-up indicated patients were deceased within 1 month of chemoradiation. For total CTC counts, no significant PFS time difference was found between the high and low CTC count groups. At Pre-TX, Week 18, and Week 30 time points, patients with higher total CTCs per mL showed a longer PFS time trend; however, at Week 1, Week 4, and Week 10 time points, higher total CTC per mL tend to have shorter PFS time. For PD-L1+ CTC percentage, higher PD-L1% are associated with shorter PFS time in all time points. Only Week 1

reached statistical significance (p-val = 0.040), while Pre-TX and Week 18 were close to statistical significance (Pre-TX p-val = 0.059, Week 18 p-val = 0.053). This finding is consistent with recent reports indicating that higher PD-L1 on CTCs is correlated with shorter survival, with several studies specifically investigating patients receiving either anti-PD-1 or anti-PD-L1 immunotherapies[23,87,188].

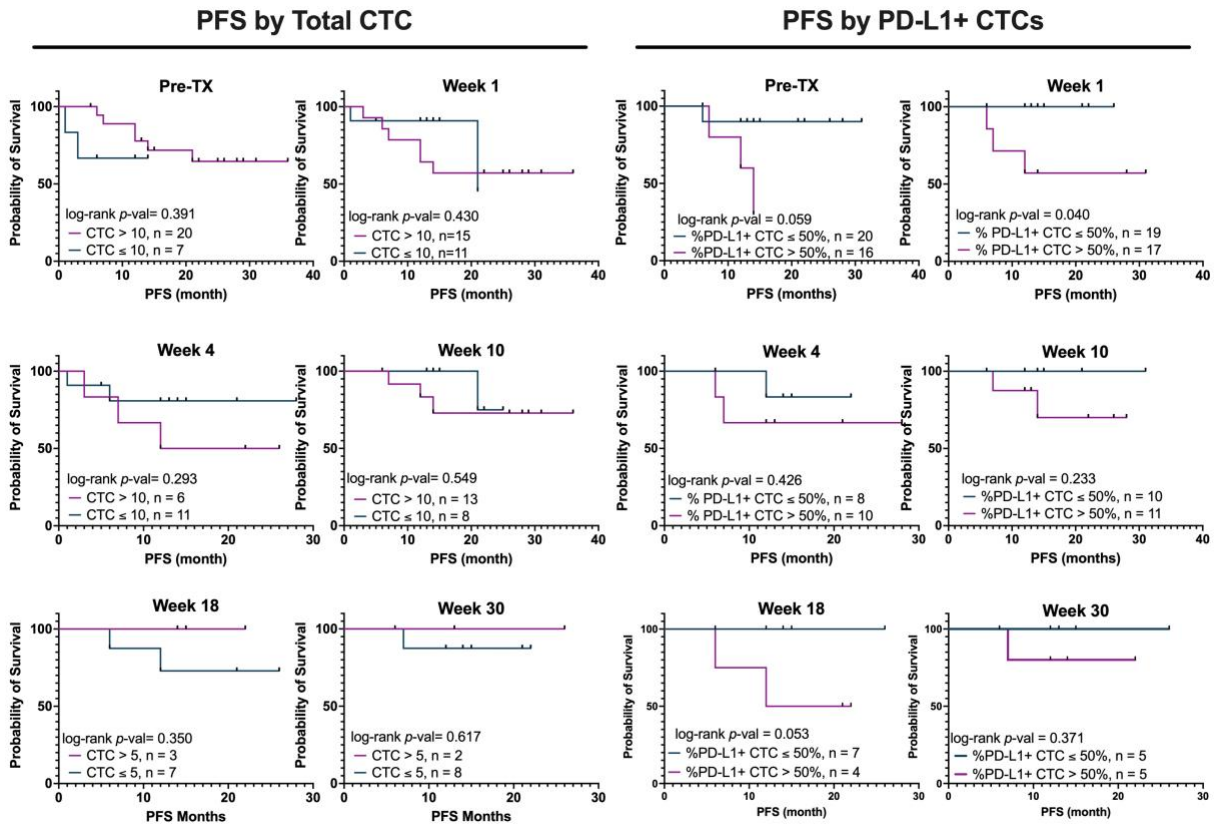

Figure 3-7 PFS by total CTC counts or percentage PD-L1+ at single time points.

3.5.2 Decrease in CTCs during radiation predicts longer PFS

We observed a significant decrease in CTC counts from pre-TX to Week 1, Week 10 and Week 30. As shown in Figure 3-8A, average CTC counts per mL decrease as patients going through both chemoradiation and immunotherapy. For patients who received durvalumab immunotherapy, a significant decrease in PD-L1+ CTC counts was observed between baseline and Week 18 (the first time point during durvalumab, Figure 3-8B).

To investigate how these CTC changes are related to patient outcome, we calculated the percentage CTC change for each patient as described in the method section. We divided the patients into two groups: percent CTC change greater or less than 75%. As shown in Figure 3-8C, a significant difference (p-val = 0.0076) can be observed between the two groups. Among the patients who had a greater than 75% decrease in CTC counts between baseline and Week4 were all stable. These patients had an average monitoring time of 21 months. This data strongly indicates that lack of CTC decrease is an early indicator of future progression.

We then wanted to investigate how does the CTC change prediction compare to the prediction by gross tumor volume (GTV). We plotted receiver operator characteristic curves (ROC) for the two metrics percent change in GTV and CTCs between pre-TX and W4. ROC analysis assesses the accuracy with which a new patient added to the cohort would be correctly predicted to be stable or progressing. Using percent change in GTV to predict future progression led to a low area under the curve (AUC) of only 0.56, while, using percent change in CTCs led to an AUC of 0.88 (p=0.02), Figure 3-8D.

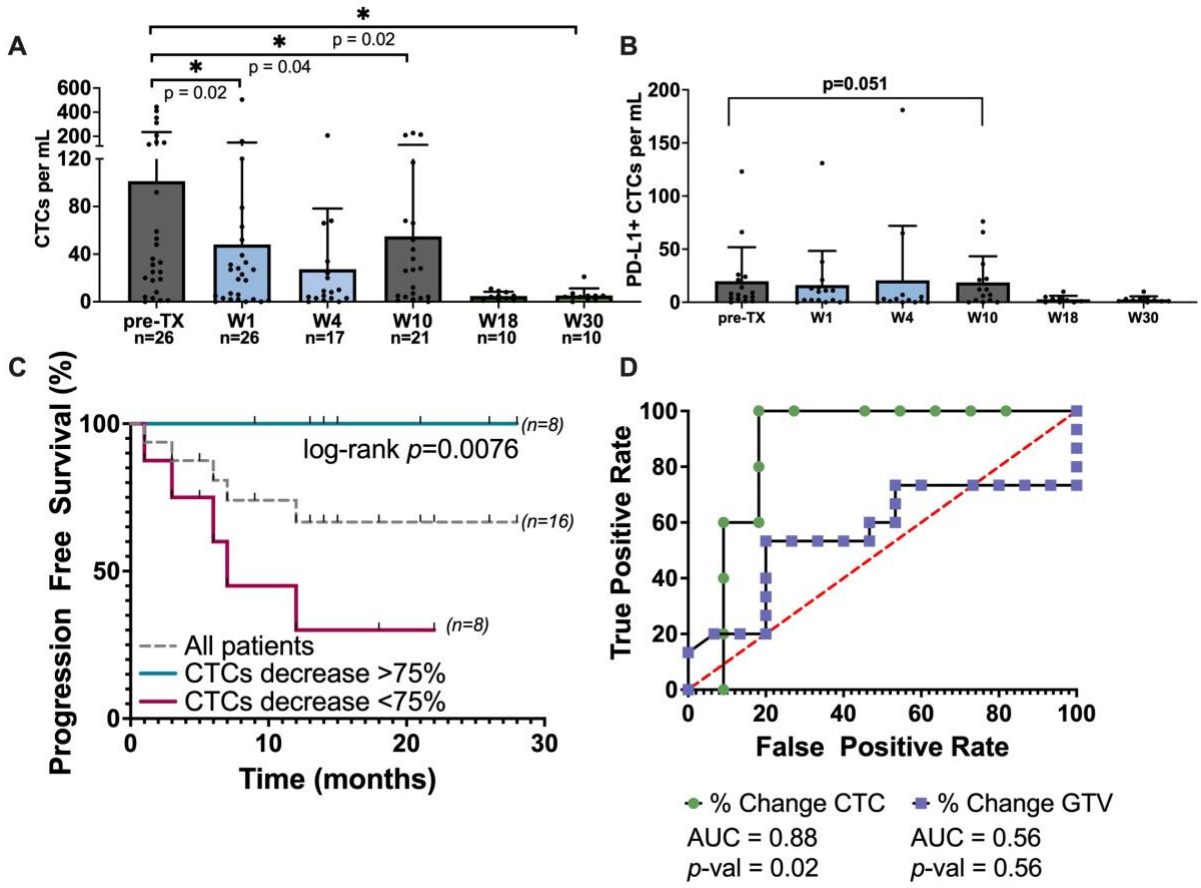

Figure 3-8 The change in CTC counts and its prognostic value. (A) Bar plot of CTCs per mL at each time point for all patients. (B) Bar plot of PD-L1+ CTCs per mL at each time points for patients received durvalumab. (C) Kaplan Meier curves demonstrating the difference in PFS between patient groups determined by the percent change in CTCs between pre-TX and Week 4 for CTCs decreasing by more or less than 75%. (D) Receiver operator characteristic (ROC) curve of change in CTCs and change in GTV between Pre-TX and Week 4 timepoints.

3.5.3 CTCs acquire proliferative and invasive phenotype during chemo-radiation treatment

Three time points from the RNA samples: Pre-TX, Week 4 (during treatment), and Week 10 (after treatment) were selected to perform microarray expression profiling. We first aimed to identify cancer specific signatures by comparing the samples from cancer patients and healthy controls. Reassuringly, we found PTPRCAP gene significantly highly expressed in healthy controls, and S100A2 gene significantly highly expressed in cancer patients (Figure 3-9A). The protein version of PTPRCAP, CD45, is commonly used as a WBC marker in immunofluorescent assays. S100A2 is commonly upregulated in tumor and play a crucial role in metastasis[189].

Next, we categorized the samples by their CTC counts into three groups (high, >50 CTCs, medium, 20-50 CTCs, low, <20 CTCs) and performed DEG analysis between the high and low groups of samples to further analyze signatures associated with CTCs. Interestingly, G3BP1 was found significantly differentially expressed (adjusted *p*-val = 0.04, Figure 3-9B). In several studies, G3BP1 was shown to promote tumor growth and metastasis[190], indicating that patients with higher CTCs could have a higher risk for metastasis or that G3BP1 is related to the release of CTCs from a tumor.

We then performed differential gene expression analysis between pre-TX, W4, and W10 timepoints to identify the transcriptomic changes during chemoradiation. All p-values are reported as false discovery rate (FDR) adjusted p-values, $p < 0.05$ were considered significant. Excitingly, there were 97 DEGs between pre-TX and W4 (during chemoradiation). We plotted the top 50 DEGs based on log-fold change were displayed in a heatmap, Figure 3-9D where samples are largely sorted by timepoint (n=23/28 samples), pre-TX vs W4, using unbiased clustering. Each gene in the top 50 genes was investigated manually to identify relevant literature related to cellular proliferation, invasion, drug resistance, metastasis, prognosis, and cancer-related genes, as displayed in the annotation in Figure 3-9D**.** CTCs isolated during chemoradiation (W4) showed greater expression of genes related to aggressive and proliferative phenotypes.

Lastly, patients were classified as either having sustained clinical stability or progression at a future date. While no genes were identified to be differentially expressed between the stable and progressing groups, 7 genes were upregulated between pre-TX and Week 4 within the stable patients. Of these genes, 3 were also upregulated in a comparison of all patients between the two timepoints (MMP9, MCEMP1, S100A9). The remaining 4 genes were unique to only patients with sustained stability (HK3, TSPO, SHKBP1, RGL4), Figure 3-9E. HK3 expression has been shown

to correlate to improved immune cell infiltration and predicts immunotherapy response[191]. Similarly, preliminary results indicate that SHKBP1 was associated with epithelial to mesenchymal transition and lymph node metastasis.[192] Taken together, these indicate that stable patients have CTCs with less metastatic gene expression profiles during radiation compared to patients who will have progression.

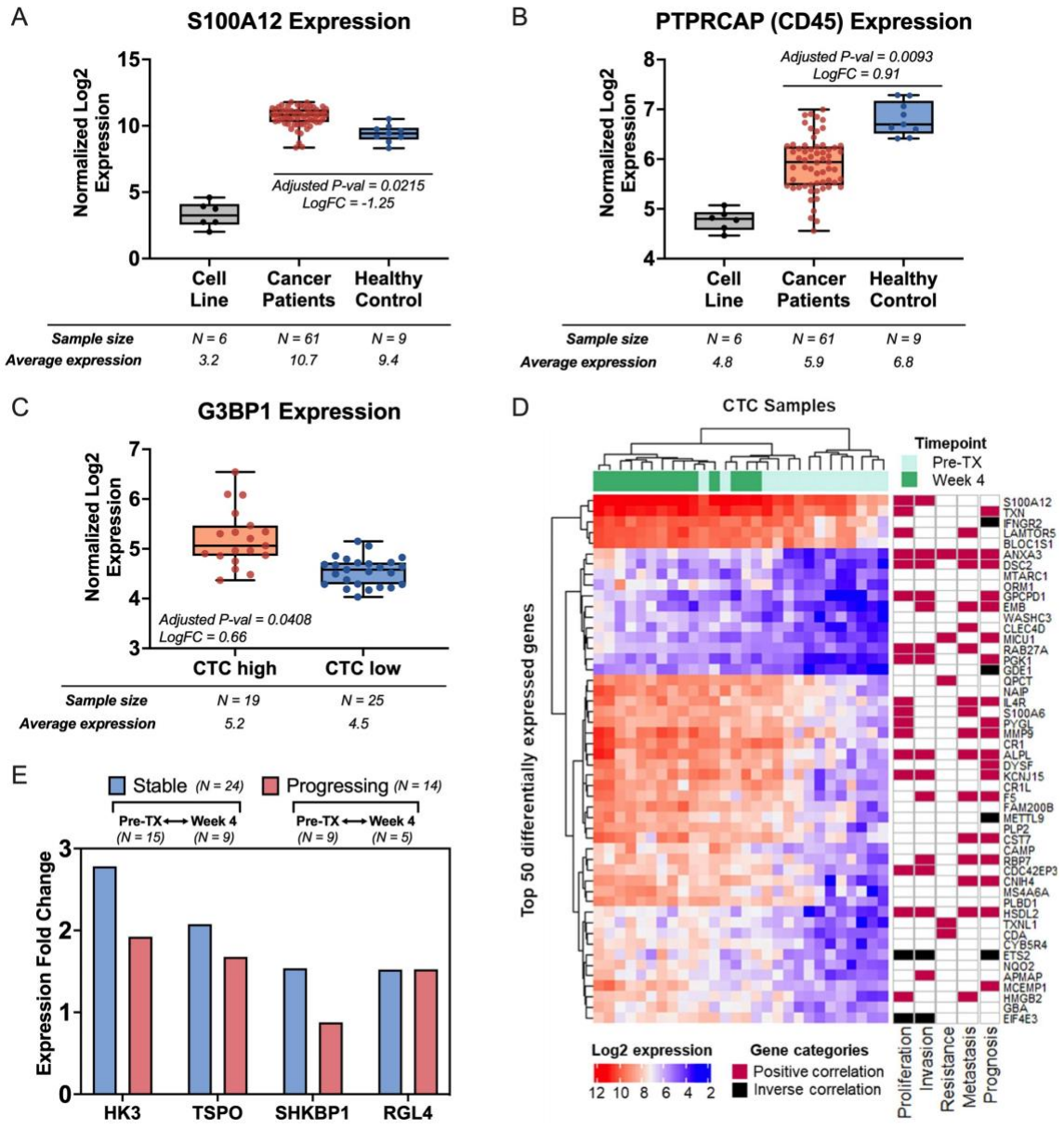

Figure 3-9 Differential expression analysis for microarray RNA samples. (A) Normalized Log_2 Expression of S100A2 gene between cell line, cancer patients and healthy controls. (B) Normalized Log_2 Expression of

PTPRCAP gene between cell line, cancer patients and healthy controls. (C) Normalized Log_2 Expression of G3BP1 gene between cell line, cancer patients and healthy controls. (D) Top 50 differentially expressed genes between pre-TX and Week 4. (E) Fold change for four differential expressed genes between pre-TX and Week4 timepoints that had different trends in stable or progressing patients.

3.5.4 Identifying genes that predict patient PFS

After identifying gene expression changes between timepoints, we then aimed to determine an RNA signature that was predictive of PFS. Univariant Cox regression survival analysis was performed to identify predictive genes against PFS at each of the three time points (pre-TX, W4, and W10). With a p-value cutoff of 0.01, we identified 146 genes at pre-TX, 145 genes at W4, and 72 genes at W10 that were associated with PFS. The full list of these genes is summarized in Appendix A. To reduce the dimensions of the predictive metrics and show the combined prognostic value of the gene set, we calculated a principal component analysis (PCA) score based on the selected predictor genes for patients at each time point. The analysis pipeline schematic is shown in Figure 3-10A, and prediction results from each time point is shown in Figure 3-10B-D. Each of the three timepoints had obvious and significant differences in PFS based on principle component 1 (PC1), $p<0.0001$. These results demonstrate the highly predictive nature of this multi-gene analysis.

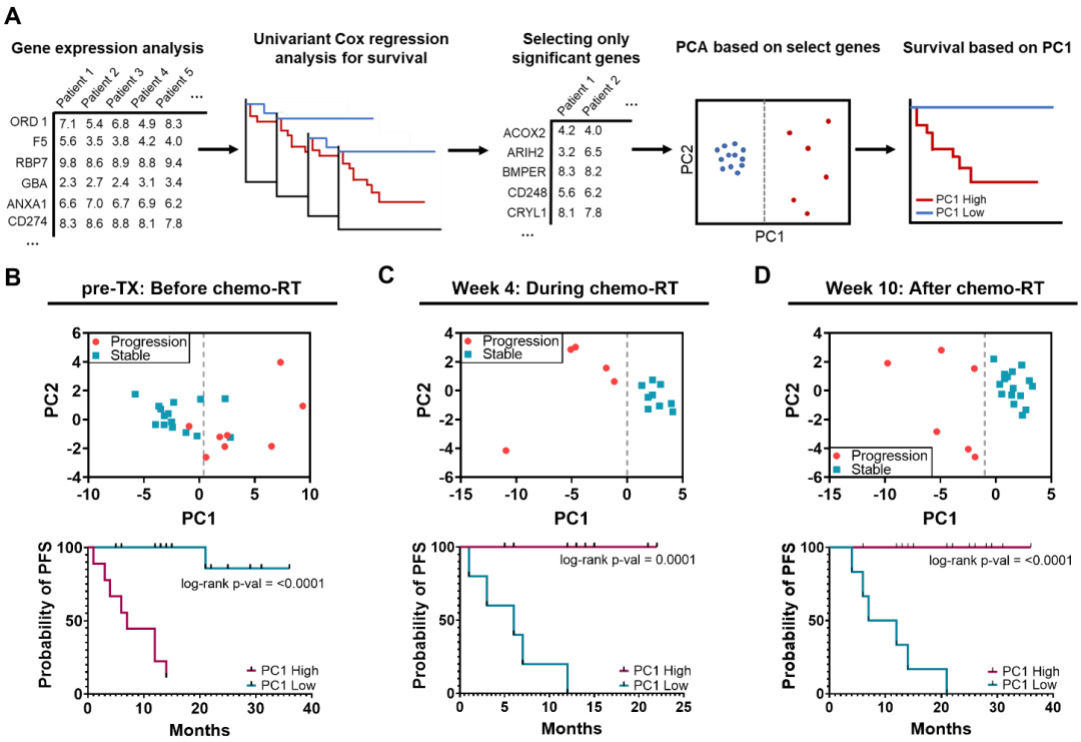

Figure 3-10 Identifying genes that can predict PFS. (A) Schematic in generating principal component based predictive metrics for survival. (B) Principal components from identified gene sets that predicts PFS.

3.5.5 Using RUV method for RNA analysis in other clinical studies

We then applied these RNA analysis methods to other clinical studies. In doing this, we faced the challenge of no significant difference were found between the different comparison groups. We hypothesized that this was because of the various WBC contamination in the enriched bulk CTC samples, so we developed methods to use RUV R package to remove the variances that were caused by contaminating WBCs. The RUV package takes pre-defined WBC marker genes and calculate a modified design formula for the differential gene comparison. As shown in Figure 3-11A, after WBC adjustment in the HCC study, we found 85 downregulated genes between pre-TX and post round 1 chemotherapy. Interestingly, 21 of these downregulated genes are related to liver function (Figure 3-11B), indicating potential decreased liver function during chemoradiation treatment.

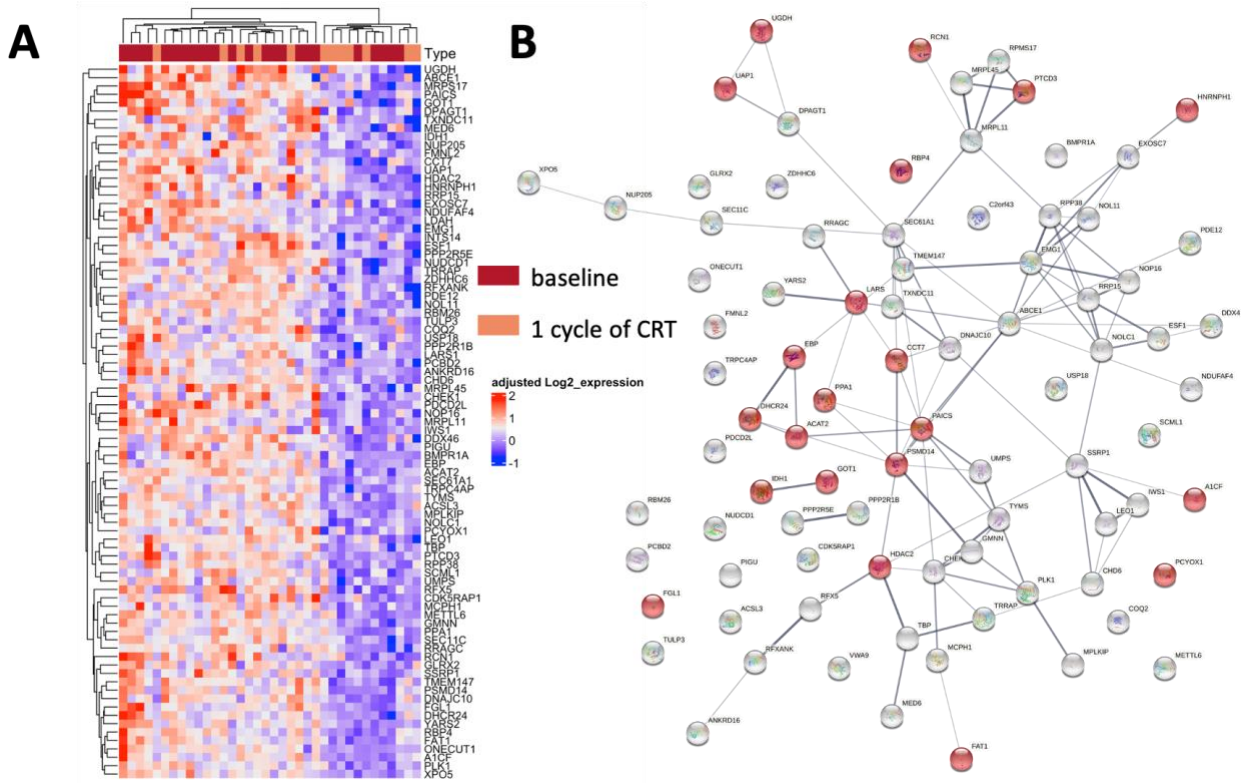

Figure 3-11 Differentially expressed genes in enriched CTC samples between baseline and post cycle 1 of chemoradiation treatment. (A) Heatmap of 85 significantly down regulated genes after chemoradiation treatment. (B) The gene network analyzed using the STRING tool. Highlighted genes are highly expressed in liver tissue.

3.6 Discussion

In this chapter, I developed analysis workflows for the profiling of CTCs using microfluidic devices and microarray to elucidate their role as biomarkers to predict patient PFS. The workflow development was performed in a cohort of locally advanced (stage III) NSCLC patients treated with chemoradiation and immunotherapy.

CTCs were enumerated at six timepoints across radiation therapy and immunotherapy. We found that absolute number of CTCs at single time points did not correlate with progression-free survival time. For patients who went on to receive durvalumab immunotherapy, high PD-L1+ CTC subpopulation percentage at single time points may be associated with shorter PFS. This finding is consistent with recent reports indicating that higher PD-L1 on CTCs is correlated with shorter

survival, with several studies specifically investigating patients receiving either anti-PD-1 or anti-PD-L1 immunotherapies[23,87,188]. One of the explanation for this could be that only blocking PD-L1 is insufficient to halt the immune evasion mechanism on CTCs, blocking other signaling pathways, such as CD47 might be necessary for increasing the immunotherapy efficacy[96]. Additionally, when looking at the dynamic change of CTC counts between time points, we found that having a larger percent decrease in CTCs between pre-TX and Week4 of chemoradiation was significantly associated with longer PFS.

We then performed differential gene expression analysis using Affymetrix Clariom S PICO microarrays. There were significantly upregulated genes between pre-TX and W4 that corresponded to a CTC phenotype that was invasive, proliferative, and potentially immune evasive. These CTCs may represent the cells that are escaping chemotherapy or radiative cell death, and hence have increased proliferative or aggressive phenotypes, however future studies would be needed to fully elucidate the effects of these transcriptomic changes on phenotypic changes. We also correlated the gene expression at single time points with PFS to identify the predictive gene sets. Principle components were calculated from genes that were significantly associated ($p\text{-val} < 0.01$) to PFS to showcase the highly predictive power of these genes. This method effectively captured the highly significant transcriptomic difference between the CTCs of progressing and stable patients ($p\text{-val} = <0.0001$).

When applying this analysis workflow to other clinical studies, we faced the challenge of the lack of statistical significance between the different comparison groups. To solve this problem, we developed RUV package-based workflow to remove the variance generated from contaminating WBCs. We found 85 significantly downregulated genes in the HCC study, comparing CTC samples from post cycle 1 of chemoradiation and pre-treatment. 21 of these

downregulated genes are found related to liver function, which could indicate the decrease of CTCs and liver function during treatment.

In summary, the clinical and RNA analysis workflow developed in this chapter could be widely applied to future CTC clinical studies.

Chapter 4 Single-cell Characterization of Circulating Tumor Cells in Non-Small Cell Lung Cancer on Their NK Sensitivity

4.1 Abstract

Natural killer (NK) cell-based therapies are being actively explored as an option for increasing the efficacy of current immunotherapies for non-small cell lung cancer (NSCLC). As part of the innate immune system, NK cells have been proven to be crucial in limiting distant metastasis in pre-clinical models. Tumor cells in circulation (circulating tumor cells, CTCs) serve as the seeds of distant metastasis, especially those that exhibit a transition to mesenchymal phenotypes. Few studies have investigated these CTCs as targets of the NK cells in the circulation.

In this work, we systematically assessed the capabilities of NK cell-mediated CTC recognition and cytotoxicity using various quantitative methods. Using in-house established patient-derived CTC lines, we visualized NK-mediated cytotoxicity using live cell imaging and quantitative fluorescent image-based dose-response modeling. Then, we evaluated NK ligand expressions at the single-cell level of these established CTC lines and fresh CTCs isolated from NSCLC patients. We identified that CTCs, especially those with mesenchymal phenotypes, are highly sensitive to NK-mediated killing and have NK-sensitive signatures at the RNA and protein levels. In addition, we found a strong correlation between NK and EMT scores based on relevant marker expressions in lung cancer cell lines including CTC lines. Lastly, we developed a single-cell RNA sequencing workflow for fresh isolated CTCs, and found CTCs unbiasedly cluster with platelets, although exhibiting higher rates of ribosomal genes. This study aims to showcase NK-

related biomarkers and novel characterization assays for CTCs and help guide NK-based CTC therapies with the ultimate goal of reducing distant metastasis.

4.2 Publication information

Zeqi Niu¶, Sarah Owen¶, Yuru Chen, Nina Perry, Alina Yan, Zach Gdowski, Mina Zeinali, Lana Garmire, Venkat Keshimouni, Nithya Ramnath, and Sunitha Nagrath. "Single-cell characterization of natural killer cell sensitivity of circulating tumor cells in non-small cell lung cancer" *(In submission)*

4.3 Introduction

Immunotherapies have changed the treatment paradigm for NSCLC across all stages. In earlier stages, FDA has approved immune checkpoint inhibitors (ICIs) as maintenance therapies to reduce the risk of distant metastasis and improve disease-free survival[193,194] and following chemo-radiation treatment for stage III NSCLC[195,196]. The use of ICI in this setting has led to an over 15% improvement in progression-free survival (48-month PFS 35.3% for the treatment group versus 19.5% for placebo)[195]. However, the majority of patients still recur. For example, in unresectable stage III NSCLC, the use of maintenance durvalumab still leaves 64.7% who recur and progress. Several mechanisms of therapy resistance have been proposed[197]. One of the rate-limiting steps for ICI efficacy is the necessity for the HLA class I presentation on the tumor cells for recognition by activated T cells following ICI therapy. It is well known that NSCLCs lose MHC class I proteins with advancing stages[104,198]. The loss of HLA molecules is associated with reduced tumor-infiltrating T-lymphocytes[198], leading to primary or acquired ICI resistance. Alternative approaches that are agnostic of HLA class I proteins include NK cell-based approaches, either by themselves or in combination with ICI as maintenance therapies.

As part of the innate immune system, NK cells do not rely on antigen presentation for activation. Their function is regulated by a complex balance of activating and inhibiting ligands on the surface of malignant cells. For instance, MHC class I molecules serve as an inhibitory ligand for killer cell immunoglobulin-like receptors (KIRs) on NK cells. The absence of MHC class I triggers the activation of NK-mediated cytolytic activity, making them a promising cancer therapeutic candidate[199]. Several studies have shown that NK cells are crucial players in cancer immune surveillance, particularly in controlling cancer metastasis[200]. In immune-deficient mice with T cell, NKT cell, or NK cell depletion, there is a significantly higher incidence of metastasis in NK cell-depleted mice[122,201–203]. Additionally, hyperactivation or adoptive transfer of NK cells resulted in superior metastatic control[201]. Therefore, NK-based therapies are being proposed to target metastasis resulting from circulating tumor cells (CTCs)[97].

CTCs, considered the seeds of metastasis, are shed from solid tumors into the bloodstream and travel to a distant organ to form new tumors. CTCs can be isolated through serial blood draws throughout the disease or treatment course and serve as prognostic biomarkers across solid organ cancers[146,204]. They are known to go through epithelial to mesenchymal transition (EMT), which equips the cells with enhanced competence to survive in the bloodstream[205]. Studies have demonstrated worse disease outcomes with increasing CTC numbers during treatment[206], the presence of CTC clusters[207,208], and specific mesenchymal and stemness phenotype markers[67,68]. Interestingly, CTC numbers are inversely correlated with circulating NK cell numbers and activity in different types of cancer[121,209,210].

Although the role of NK cells in limiting the growth of distant metastasis has been extensively studied using transgenic mouse models[122,200–203], the interplay between CTCs and NK cells has been further explored only recently. For example, Brodbeck et al. first used computer

modeling in perforin-deficient mouse models to investigate quantitative cytotoxicity between NK cells and CTCs[211]. Based on the mathematical model, roughly 80% of CTCs were killed through the perforin-dependent killing of NK cells. Moreover, EMT phenotypes, which are frequently found in CTCs, are found to be associated with NK-sensitive phenotypes in pre-clinical experiments[122–124]. For example, E-cadherin downregulates during the EMT process[212], and serves as an NK cell inhibitor through bindings with the KLRG1 receptor. MHC class I downregulation, one of the most studied NK activation mechanisms, is found in disseminated tumor cells (DTCs) in bone marrow[213], CTCs in animal models[125], as well as CTCs from melanoma patients[214]. These findings indirectly suggest that CTCs may be inherently susceptible to NK cell-mediated cell death. *However, to our best knowledge, there is no study that has investigated NK susceptibility and NK-related marker expressions directly in CTCs isolated from cancer patients.*

Advances in microfluidic technologies during the last decade have enabled the consistent isolation and characterization of CTCs from cancer patients[215]. CTCs are usually identified by positive immunofluorescent staining of epithelial marker (e.g., Cytokeratin) and negative staining of white blood cell (WBC) marker (e.g., CD45). Although this widely used method is sufficient in quantifying CTCs, developments of CTC characterization more extensively and drug testing assays are urgently needed. These methodology developments are often hampered by the limited CTC numbers. One solution is to increase the CTC number by in vitro expansion to perform drug testing and bulk sequencing assays. Although with low success rates, several studies[216–218], including our lab, have developed stable CTC lines. Another solution is to use technologies with lower detection limits. Several recent studies have performed CTC single cell RNA-seq via several different approaches, including Chromium (10X Genomics)[53], Smart-Seq assay[214], or individual micromanipulation[219].

Our lab previously developed a high-throughput label-free microfluidic device, the labyrinth device, to enrich CTCs for potential single-cell analysis[186]. This work aims to decipher the NK cell sensitivity of NSCLC patient-derived CTCs via various single-cell resolution assays. We visualized the CTC killing process through live imaging, and quantitatively tested the NK sensitivity of in-house derived CTC lines. To investigate the NK-CTC interaction on the molecular level, we evaluated the protein and RNA expression of NK-related ligands and their correlation with EMT signatures. For the first time, we established a workflow of single-cell RNA sequencing and analysis for both epithelial and mesenchymal CTCs using Labyrinth and Chromium (10X Genomics). The single-cell sequencing results showed detection rates of ribosomal proteins in CTCs and no clear association between the EMT status and HLA class I expressions. Overall, the results of this study showcase the NK sensitivity and NK-related biomarkers on CTCs and help guide NK-based CTC therapies with the ultimate goal of reducing distant metastasis.

4.4 Materials and methods

4.4.1 Cell culture

Cells were maintained at 37°C and 5% CO_2. Cells were grown to 70 - 80% confluence before subculturing using 0.05% Trypsin-EDTA (Gibco). H1975, H1650, H3255, H441, A549, CTC-Lu1, and CTC-Lu2 cells were maintained in RPMI-1640 (Gibco) supplemented with 10% fetal bovine serum (FBS) (Sigma) and 1% Antibiotic-antimycotic (Gibco). NK-92®MI cells were maintained in suspension culture in Minimum Essential Medium $-\alpha$ (MEM-α) supplemented with 10% FBS (Sigma), 12.5% horse serum and 1% Antibiotic-antimycotic (Gibco). Media was exchanged every 48-72 hours between subculturing. Cell lines were routinely tested and reported negative for mycoplasma contamination (Lonza).

4.4.2 NK cell cytotoxicity live imaging

CTC-Lu2 cells were seeded at 2×10^3 cells per well in an 18-well μ-Slide (ibidi) and incubated at 37 ℃, 5% CO_2 overnight to adhere. The culture media was replaced with MEM-α containing 1×10^4 NK-92®MI cells before the start of the experiment. The slide was then live imaged under Nanolive 3D Explorer with 30s intervals for 1 hr sessions. The images and videos were then processed through the Nanolive software Steve. The screenshot images were focus stacked together to be able to visualize both NK cells and cancer cells.

4.4.3 Quantitative NK cytotoxicity assays and data analysis

Cancer cells were passaged using 0.05% Trypsin-EDTA and incubated with cell tracker red CMTPX (Invitrogen) for 45 min in serum free media, and washed with phosphate buffered saline (PBS) three times. The cells were then counted using a hemocytometer and diluted to a concentration of 50,000 cells/mL. 5,000 cells (100 μL of the cell solution) were seeded into each well of a 96-well plate (Corning) and adhered to the plate overnight. The next morning NK-92®MI cells were collected and resuspended in 1:1 mix of RPMI-1640 and MEM-α. Cells were then counted by hemocytometer and diluted to the appropriate concentration to seed 100 μL of NK cell suspension to each well, containing the indicated effector (NK cell) to target (cancer) (E:T) ratios. After preparing the NK cell dilutions, media was gently removed from each well in 96-well plate and replaced with NK cell suspension. The co-culture was incubated for four hours.

At the end of the four-hour co-culture incubation period, each well was washed with 200 μL PBS, then stained with a cocktail containing Calcein-AM (BD bioscience) for live cell staining and Hoechst (Invitrogen, final concentration 10 μg/mL) for nuclei staining. After incubating in dark at 37°C for 20min, the staining reagents were gently removed from each well and replaced

with PBS. The plate was then scanned with three channels (DAPI, FITC, Cy3) using a Nikon Ti2 inverted fluorescent microscope at 10X magnification.

The images are then batch analyzed using the "General Analysis" module using the NIS-elements software. Specifically, "Remove Average Background" function was first applied to preprocess the images. For Calcein-AM and cell tracker detection, appropriate intensity and size thresholding was then set based on each cell line image to ensure optimal cell counts. "Bright spot detection" function was used for cell nuclei detection. Post processing functions such as "Morpho Separate Objects", "Fill Holes", "Smooth" were used accordingly based on the cell morphology. An intersection function was then set to select cell tracker dye, Calcein-AM and cell nuclei positive cells and generate a combined binary layer. From this layer, total object number, which correspond to live cancer cell number in each well, was recorded to form a count table. Percent cytotoxicity was then calculated using the following equation:

$$\%\ Cytotoxicity = \left(1 - \frac{Live\ cancer\ cell\ count_{at\ certain\ E:T\ ratio}}{Total\ live\ cancer\ cell\ count_{in\ ctrl\ wells}}\right) \times 100\%$$

Percent cytotoxicity and E:T ratio was fitted to a built-in nonlinear three-parameter dose response curve in GraphPad Prism 8.4.0. Area under the curves (AUCs) were calculated using Prism built-in AUC function with Y=0 as baseline.

4.4.4 Sample collection and labyrinth processing

The experimental protocol was approved by the Ethics (Institutional Review Board) and Scientific Review Committees of the University of Michigan, and all patients gave their informed consent to participate in the study (HUM00119934). All patients had a diagnosis of metastatic EGFR mutant or ALK mutant lung adenocarcinoma. Specifically, two patients carried mutations in Anaplastic lymphoma kinase (ALK) and six carried mutations in epidermal growth factor

receptor (EGFR) based on screening of the primary tumor. Most patients were receiving kinase inhibitor treatments; however, one patient (patient 2) was originally receiving chemotherapy until next generation sequencing results were available and identified an EGFR mutation, at which point the patient began kinase inhibitor therapy.

Blood samples were collected in EDTA tubes and processed through the Labyrinth within 2 hours of collection. Red blood cells (RBCs) were removed with Ficoll-Paque™ PLUS Media (GE Healthcare) based on density separation principles, following the manufacturer's protocol prior to processing in the Labyrinth. After RBC depletion, the plasma and blood mononuclear cells (PBMCs) fractions were collected and diluted 1:5 with phosphate buffered saline (PBS) based on the original blood volume. The subsequent diluted sample was processed through the Labyrinth at a flow rate of 2500 μL/min. The resultant from outlet 2 was collected. The CTC-enriched sample was used for immunofluorescent staining.

4.4.5 Immunofluorescence and fluorescent microscopy

To perform immunofluorescent staining, cells either from culture or from the Labyrinth outlet 2 product were processed using Cytospin Cytocentrifuge (ThermoFisher Scientific). A poly-lysine coated slide was placed into the cytospin funnel (ThermoFisher Scientific), cell suspension was added to each cytospin funnel and cytocentrifuged at 800 revolutions/min (RPM) for 10 min. Samples were then fixed using 4% paraformaldehyde (PFA) and cytocentrifuged at 800 RPM for an additional 10 min. The cells on the glass slides were covered with PBS and stored at 4°C until used for immunofluorescence. Two slides were prepared from each patient sample or cell line, for the following staining of panel 1 and panel 2 respectively (Table 6).

Table 6 Immunofluorescence staining conditions of the two designed panels

Staining Panel	**Channel**	**Primary Antibody**	**Catalog number**	**Host (Isotype)**	**Staining cocktail dilution**	**Catalog number** (All purchased through Thermofisher)	**Staining cocktail dilution**
Panel 1 & 2	Cy3	Pan Cytokeratin (panCK)	BioRad MCA1907T	Mouse (IgG1)	1:100	A21123	1:100
Panel 1 & 2	FITC	CD45	enQuire 5788-MSM9	Mouse (IgG2b)	1:100	A21141	1:100
Panel 1	Cy5	HLA-A/B/C	Thermo/eBioscience 14-9983-82	Mouse (IgG2a)	1:50	A21241	1:100
Panel 1	Cy7	E-Cadherin	Cell signaling 31955	Rabbit (IgG)	1:50	SA5-10035	1:100
Panel 2	Cy5	MICA/B	Abclonal A12622/A9802	Rabbit (IgG)	1:50	A21245	1:100
Panel 2	Cy7	CADM1	MBL International CM004-3	Chicken (IgY)	1:50	SA5-10075	1:100

Cells or samples on slides were permeabilized with 0.2% Triton X-100 solution for 3 min. Slides were then washed 3 times with PBS, followed by blocking using 10% goat serum for 30 min at room temperature. Primary antibody cocktails with following concentrations (table) for each marker were prepared in blocking reagent (10% goat serum) and applied to cover the whole slide sample surface. Slides with primary antibodies are then incubated at 4°C overnight. On the following day, slides were washed with PBS for 3 times, with 5 min incubation each time. Secondary antibody cocktails with concentrations shown below were prepared in blocking reagent and applied to cover the sample area for 1.5 hrs. This was followed by three 5 min PBS washes. The coverslips were then mounted onto the sample areas with Gold prolong antifade mountant reagent with DAPI (ThermoFisher Scientific). The entire sample area of the stained slides was scanned using a Nikon Ti2 inverted fluorescent microscope at 20X magnification.

4.4.6 CTC analysis and enumeration

The images from the scanned patient sample slides were manually analyzed using the NIS-Elements software (Nikon). CTCs were defined as DAPI+/panCK+/CD45-, while WBCs were defined as DAPI+/panCK-/CD45+. CTCs were further characterized by their expression of NK inhibitors (Panel 1) or NK activators (Panel 2) using the following method.

4.4.7 Quantitative fluorescent intensity data export

For patient sample slides, because MHC class I expressions in platelets are generating background noises, a background subtraction step was done on panel 1 (MHC class I, E-cadherin) using the subtract background function in ImageJ. The rolling ball radius for the algorithm was set to the pixel number of the largest cell of interest on each image. The processed images were exported as TIFF images and imported to NIS-Elements (Nikon) for further analysis. For cell line samples, this step was skipped.

The Regions of Interest (ROIs) were defined for each selected cell (cell line, CTC, or WBC) manually based on panCK (or CD45 for WBC) and DAPI staining using the ROI autodetection or drawing tool. Raw intensity values for each channel were exported using the ROI statistics module. Normalized intensity z-score for a single marker (inhibitor or activator) was calculated using the following formula:

$$Intensity\ z-score = \frac{x-\mu}{\sigma}$$

For each cancer cell line, x is the intensity of a cell that were chosen randomly across the slide. μ and σ is the mean and standard deviation, respectively, of intensities for each marker across the different cell lines. Over 300 cells per cell line were selected for the data export to generate Figure 4-2D.

For CTC isolated from cancer patients, x is the raw intensity of defined ROI around identified CTCs. μ and σ are the mean and standard deviation, respectively, of the intensities of all CTCs found between different patients that were stained with the same marker. NK sensitivity score for each cell line was calculated using $(\sum Intensity\ z-score\ of\ NK\ activators - \sum Intensity\ z-score\ of\ NK\ inhibitors)$ and normalized to 0 to 100 scale using linear transformation.

4.4.8 Bulk RNA sequencing

Cells were seeded with 1.5×10^5 cells per well in 12-well plates. After 72 hrs, the cells were lysed using 700 µL TRIzol™ Reagent (Life Technologies) and incubated for 5 min at room temperature on a plate rocker. RNA was then isolated and purified using the Total RNA Purification kit (Norgen) under the manufacturer's instructions. The purified RNA samples were then submitted to the Advanced Genomics Core at the University of Michigan for library prep and next-generation sequencing. Input RNA is normalized to 200ng per sample. The RNA library was prepared with Poly(A) mRNA Magnetic Isolation Module (New England BioLabs), NEBNext Ultra II Directional RNA Library Prep Kit for Illumina (New England BioLabs), and NEBNext Multiplex Oligos for Illumina Unique dual (New England BioLabs). The libraries were pooled and sequenced on 2.5% of the Illumina NovaSeq S4 Paired-end 150bp, according to manufacturer's recommended protocols. Bcl2fastq2 Conversion Software (Illumina) is used to generate de-multiplexed FastQ files.

4.4.9 RNA sequencing analysis

Raw data processing was also performed at the Advanced Genomics Core of the University of Michigan. Briefly, snakemake[220] was used to manage the bioinformatics workflow in a reproducible manner. The reads were trimmed using Cutadapt[221] and were evaluated with FastQC[222] to determine quality of the data. Reads were mapped to the reference genome GRCh38 (ENSEMBL) using STAR[223], and assigned count estimates to genes with RSEM v1.3.3[224]. Alignment options followed ENCODE standards for RNA-seq. QC metrics from several different steps in the pipeline were aggregated by multiQC v1.7[225]. The RSEM were then accessed in R programming environment. To increase data power, we incorporated RNA-seq data from cancer cell line enclopedia (CCLE)[112] for commercial cell lines using ComBat-seq[226]. Normalization and

differential gene expression analysis were then performed between NK sensitive cell lines and NK resistant cell lines using DESeq2[227].

4.4.10 Calculation of NK and EMT scores from bulk RNA-seq and CCLE

Transcripts per million (TPM) results were used for the score calculation. Only lung adenocarcinoma cell lines were selected (by searching pattern: "lung" in primary_disease column and "adeno" in Subtype column) from the CCLE dataset. 80 cell lines were selected through the subsetting. NK and EMT scores were calculated using NK (Table 7) and EMT[228] related genes from the literature. For each sample, the calculation formulas are following:

$$NK\ raw\ score = (\sum TPM\ of\ NK\ activators - \sum TPM\ of\ NK\ inhibitors)$$

$$EMT\ raw\ score = (\sum TPM\ of\ mesenchymal\ genes - \sum TPM\ of\ epithelial\ genes)$$

These raw scores were then normalized to 0 to 100 scale through a linear transformation:

$$NK\ \ score = \frac{NK\ raw\ score - NK_{min}}{NK_{max} - NK_{min}} \times 100$$

$$EMT\ \ score = \frac{EMT\ raw\ score - E_{min}}{E_{max} - E_{min}} \times 100$$

Simple linear regression was then performed between the EMT and NK scores in GraphPad V9.4.0.

Table 7 NK-related markers selected from literature[100,229].

Activators			**Inhibitors**	
Ligand	Ligand alias	NK receptor	Ligand	NK receptor
PVR	CD155, NECL5	DNAM1, TIGIT	HLA-A	KIR
NECTIN1	CD111	CD96	HLA-B	KIR
NECTIN2	CD112	DNAM1, TIGIT	HLA-E	CD94
NECTIN3	CD113	TIGIT	HLA-C	KIR
MICA		NKG2D	CDH1[230]	KLRG1
MICB		NKG2D	CDH2	KLRG1

ULBP1		NKG2D	CDH4	KLRG1
ULBP2		NKG2D	CEACAM5	CEACAM1
ULBP3		NKG2D	CEACAM1[231]	NKG2D
RAET1E	ULBP4	NKG2D	CLEC2D	CD161
RAET1G	ULBP5	NKG2D	PCNA	NKp44
RAET1L	ULBP6	NKG2D		
CD48		2B4		
VIM[232]		NKp46		
HLA-G[233]		KIR2DL4, CD94		
BAG6		NKp30		
NCR3LG1	B7-H6	NKp30		
CADM1[122]		CRTAM		
CD70		CD27		

4.4.11 Single-cell RNA sequencing

Single-cell RNA sequencing was performed using 10X Genomics and Illumina sequencing platform according to manufacturer's recommended protocols. Briefly, nanoliter-scale Gel Beads-in-emulsion (GEMs) are generated by combining barcoded Single Cell 3′ v3 Gel Beads, a Master Mix containing CTC samples, and Partitioning Oil onto Chromium Chip B. Then the Gel Beads are dissolved, primers are released, and any co-partitioned cells are lysed. The cell lysate, primers and Master Mix containing reverse transcription (RT) reagents are incubated to produce barcoded, full-length cDNA from poly-adenylated mRNA. After incubation, GEMs are broken, and pooled fractions are recovered. Silane magnetic beads are used to purify the first strand cDNAs from the post GEM-RT reaction mixture, which includes leftover biochemical reagents and primers. Barcoded, full-length cDNA is amplified via PCR to generate sufficient mass for library construction and sequencing. A Chromium Single Cell 3’ Gene Expression library comprises standard Illumina paired-end constructs that begin and end with P5 and P7. The 16 bp 10x Barcode and 12 bp UMI are encoded in Read 1, while Read 2 is used to sequence the cDNA fragments. Sample index sequences are incorporated as the i7 index read. TruSeq Read 1 and Read 2 are standard Illumina sequencing primer sites used in paired-end sequencing.

4.4.12 Single cell RNA sequencing data analysis

Single cell analysis tool package Seurat[234] was used following the result expression matrix from CellRanger. Cells with over 20% mitochondrial contamination were excluded from the analysis to exclude dying and low-quality cells. The dataset was normalized and scaled following the Seurat package vignettes. We then performed Principal Component Analysis (PCA) and non-linear UMAP dimensional reduction to visualize the dataset in two-dimensional space. Blood cells were identified based on a list of canonical blood cell markers, including platelets (PPBP, PF4), NK cell (NKG7, GNLY), T cell (CD3D, CD3G, TRBC2, TRAC). To select CTCs, we first selected potential cancer cells by the negative expression of all above immune cell markers (NKG7, GNLY, CD3D, CD3G, TRBC2, and TRAC) plus CD45(PTPRC). We then calculated the EMT score using the method described above and selected the cells that have the top 10% and bottom 10% EMT score. In other words, we identified CTCs by the most epithelial (low EMT score) and most mesenchymal (high EMT score) profiles among the non-leukocyte population. This strategy diagram is shown in Figure 4-5A. Differential expression gene features are tested using statistical framework MAST. All analysis were performed in R programming environment.

4.4.13 Statistical analysis

Statistical analysis was performed using GraphPad Prism 9.4.0. Significance and p-values between samples were determined using a two-sided unpaired t-tests assuming a Gaussian distribution, with a 95% confidence level. Plotted error bars represent standard deviation. In simple linear regression, R^2 represent goodness of fit.

4.5 Results

4.5.1 Study overview and rationale

The research questions of this study can be divided into two parts; 1) Is there direct evidence of NK sensitivity on CTCs? 2) What molecular traits are related to this sensitivity? To first test the hypothesis of CTC being highly sensitive to NK-mediated killing, we first visualized NK-mediated cytotoxicity against CTC lines using 3D live cell imaging. We then developed an image-based cytotoxicity assay to evaluate the NK-mediated cytotoxicity quantitatively. This assay was tested using lung cancer cell lines, including CTC-derived cell lines (Figure 4-1A).

To gain more insights into the molecular mechanisms of CTC-NK interaction, we performed a series of quantitative assays for RNA and protein expression on fresh CTCs and CTC lines (Figure 4-1B). For protein expressions, we designed two multi-color immunofluorescence (IF) staining panels and evaluated the quantitative intensity data for well-known NK cell inhibitors and NK cell activators. Due to the channel limitation of IF assays, we only included two NK inhibitors: MHC class I molecules (Gene name: HLA-A/B/C) and E-cadherin[230] (Gene name: CDH1), as well as two NK activators: MHC class I chain-related proteins A and B (MICA/B)[235] and cell adhesion molecule 1 (CADM1)[236]. The working mechanisms of E-cadherin and MHC class I molecules have been described above. MICA/B expressions are often induced by various stress or DNA damage responses and can activate NK cells by binding to NKG2D receptors. CADM1 is a cell adhesion molecule that has recently been found to activate NK cells through the binding with class I-restricted T cell-associated molecule (CRTAM) receptor. There is little work done on evaluating the expressions for MICA/B and CADM1 on CTCs isolated from patients.

Although these markers predict NK sensitivity to some degree, the complexity of NK regulation can hardly be explained by only four characteristics. We then performed RNA profiling assays, which provide expression snapshots for more NK ligands. Bulk-sequencing was performed

for CTC lines, and single-cell sequencing through Chromium (10X Genomics) was performed for fresh isolated CTCs.

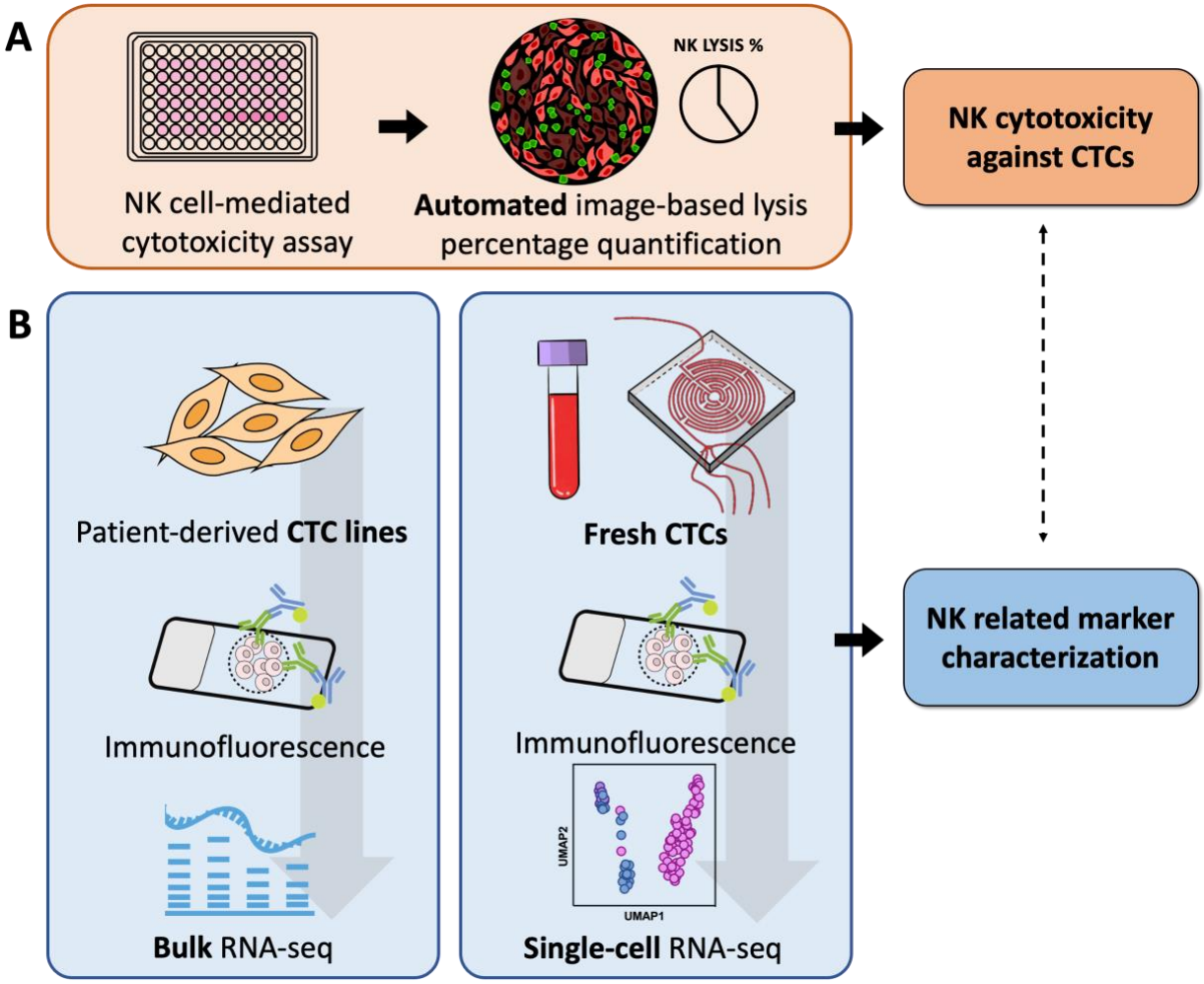

Figure 4-1 Schematic diagram of characterizing NK sensitivity in patient-derived CTCs. (A) NK cytotoxicity assays using an image-based workflow. (B) Protein and RNA level characterization for NK-related ligands in fresh isolated and patient-derived CTC lines.

4.5.2 Patient-derived NSCLC CTC lines are sensitive to NK-mediated cytotoxicity

We first observed NK cell-mediated killing with in-house derived CTC lines using 3D live cell imaging. An example of three NK-92®MI cells (smaller in cell size, indicated by blue arrows and texts) killing one CTC-Lu2 cell is shown in Figure 4-2A. Within 26min, the CTC-Lu2 cell went through apoptosis.

To further assess the NK sensitivity of the CTC lines quantitatively, we developed a novel semi-automatic imaging-based co-culture cytotoxicity assay. Seven cancer cell lines, including two CTC lines (CTC-Lu1 and CTC-Lu2), were fluorescently labeled (Cy3) and incubated for four hours with NK-92®MI under ten different effectors to target (E:T) ratios. After the incubation, cells were stained with Calcein-AM and Hoechst, followed by imaging under a fluorescent microscope. Calcein-AM staining (FITC) helps identify the living cells after the incubation, while Hoechst (DAPI) identifies the nuclei. An automatic counting algorithm was defined in the NIS-Elements imaging software to batch process the images and count the live cancer cells (Cy3, FITC, and DAPI positive). The percent cytotoxicity was calculated using live cancer cell counts and fit to a three-parameter dose-response curve. Figure 4-2B shows the fitted cytotoxicity percentage hyperbolic curve with the 95% confidence interval. CTC-Lu1 and CTC-Lu2 had the highest cytotoxicity percentages at all E:T ratios. At E:T ratio 20, over 90% of the CTC-Lu1 and CTC-Lu2 were killed after four hours of incubation. These results indicate that the two in-house derived CTC lines are susceptible to NK cell killing. To compare the rankings of NK sensitivity in all cell lines, the area under the curves (AUCs) were calculated using the fitted hyperbolic curves. The orders of established lung cell lines are consistent with cytotoxicity results reported by another study[123] (Figure S1). For the following characterization, we categorized CTC-Lu2, CTC-Lu1, and H441 cell lines as NK sensitive, and H1975, H3255, H1650, and A549 as NK resistant.

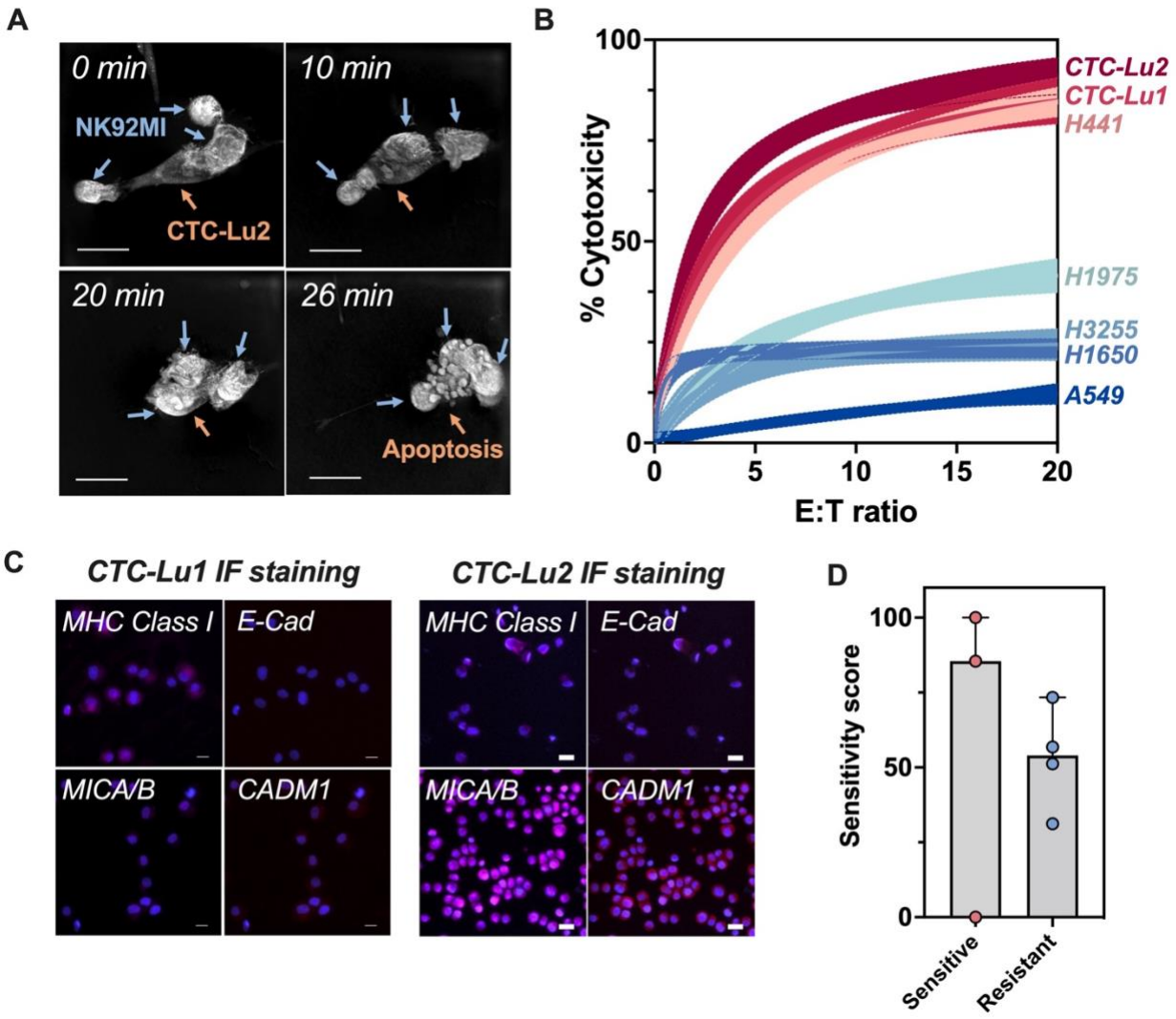

Figure 4-2 NK-mediated cytotoxicity and key NK-related protein expression in expanded CTC and other lung cancer cell lines. (A) 3D live cell imaging of several NK cells killing a CTC-Lu2 cell. (B) Percent cytotoxicity across ten different effectors to target (E:T) cell ratios fitted to a three-parameter dose-response curve. (C) Immunofluorescent staining of CTC-Lu2 lines with NK-related markers. (D) Overall NK sensitivity score of the lung cell lines tested by sensitivity phenotype.

To investigate the contributing molecular mechanism for this CTC-NK sensitivity, we developed a quantitative immunofluorescence assay to evaluate protein expression with single-cell resolution. Briefly, two parallel staining panels were designed to distinguish CTCs from WBCs and evaluate expressions of four NK-related markers. CTCs are defined by the positive stain of cancer cell marker pan-cytokeratin (panCK) and the negative stain of WBC marker CD45. The NK-related markers include two inhibitory ligands, MHC class I molecules and E-cadherin,

and two activating ligands, MICA/B and CADM1. Examples of fluorescent staining of our in-house CTC lines are shown in Figure 4-2C.

Raw fluorescent intensities of each marker were then exported per cell and normalized using z-score normalization across all the cell line samples. To assess overall NK sensitivity, we calculated a prediction score by assigning equal weights to each marker (Figure 4-2D). Briefly, for each cell line, raw sensitivity values were calculated using (∑NK activator z-scores - ∑NK inhibitor z-scores). The raw sensitivity values were then ranked between the seven cell lines and normalized to a scale of 0 to 100 by a linear transformation. These normalized values represent the NK sensitivity score. Since the downregulation of NK inhibiting markers and upregulation of NK activating markers correlates to sensitive NK phenotype, a higher sensitivity score is expected for NK sensitive phenotype. The results show that the sensitive cell lines (CTC-Lu1, CTC-Lu2, H441) have a higher median sensitivity score than the other cell lines based on these four markers.

4.5.3 Predicted NK sensitivity from NK ligands' RNA expressions correlates with EMT signatures in lung cancer cell lines

The number of markers that can be evaluated simultaneously for immunofluorescence assays is often limited. NK cell regulation involves multiple pathways, and NK activation could result from a combination of more than four ligands[100]. To evaluate a more comprehensive collection of NK-related markers at the RNA level, we performed bulk RNA sequencing on the set of seven lung cancer cell lines, including the two CTC lines. We first selected a panel of NK-related ligands from the literature (Table 7), including 19 activating and 11 inhibiting ligands. As shown in Figure 4-3A, NK-sensitive cell lines (red) show higher expression than NK-resistant cell lines (blue) in NK activator ligands such as MICB and NECTIN3. For NK inhibitor ligands such as CDH1 and CEACAM1, NK-sensitive cell lines show lower expression than NK-resistant cell

lines. However, this trend is not consistent among all the NK activators and inhibitors. To assess overall sensitivity, we calculated the NK score based on these 30 markers and showed that the sensitive cell lines (CTC-Lu1, CTC-Lu2, H441) had a higher median sensitivity score value (Figure 4-3B). Compared with the score based on immunofluorescence staining, a larger difference in sensitivity score was observed between the sensitive and resistant groups (mean difference = 36.5, compared with mean difference = 8.7 based on immunofluorescence staining).

We then performed an exploratory differential analysis between the NK-sensitive and NK-resistant cell lines. To increase the power, we integrated the expression data for non-CTC lines from the Cancer Cell Line Encyclopedia (CCLE)[112] as duplicates in addition to the in-house bulk sequencing data. We discovered 1304 genes that were significantly differentially expressed between sensitive and resistant cell lines (cutoff of adjusted p-val < 0.05, fold change > 1.5), including 372 significantly upregulated genes and 932 significantly downregulated genes (Figure 4-3C). Among these, we highlighted the genes that are known to associate with EMT[228] or NK function (Table 7). Specifically, genes that were previously found[228] upregulated during EMT (red), such as VIM, DDR2, CDH11, and DCN, were upregulated in the NK-sensitive cell group. Conversely, genes that are downregulated during EMT[228] (blue), FGFR2, KLK5, IGFBP2, COL17A1, CA2, ABCA12, S100A8, KLK7, ARTN, and PTPN3 were downregulated in the NK-sensitive group. From these results, we suspect that NK sensitivity may correlate with EMT.

Additionally, NK-related ligands show interesting differential expressions. MICB, an NK activator, was significantly highly upregulated in NK sensitive group. Other NK activators, BAG6, NECTIN2, NECTIN3, VIM, and CADM1, were upregulated but did not reach statistical significance. NK inhibitors, including SERPINB4, were downregulated but did not reach statistical significance. HLA-G, which serves as an NK inhibitor and NK activator depending on whether

surface or soluble form, is highly upregulated in the NK-sensitive cell lines[233,237]. The most differentially expressed genes (Log_2 fold change > 2) were then analyzed for gene ontology overrepresentations. Genes related to blood circulation, cell adhesion, icosanoid metabolic process, and humoral immune response were highly enriched (Figure 4-3D). The process of EMT and natural killer cells mediated cytotoxicity were also found to be overrepresented although not reaching statistical significance.

To further explore the correlation between NK ligands and EMT signatures, we calculated EMT scores (see methods) for the seven lung cell lines, with higher EMT scores indicating more mesenchymal phenotypes. Interestingly, the NK sensitivity scores and EMT scores had a high positive correlation (Figure 4-3E, yellow, $R^2 = 0.7694$, p-val = 0.0095). It is also worth noting that the two CTC lines both had high NK sensitivity and EMT scores, indicating their NK sensitive and mesenchymal phenotype. Moreover, we analyzed a set of 80 lung adenocarcinoma (LUAD) cell lines from CCLE using similar methods. Excitingly, the NK sensitivity scores for these cell lines also highly correlate with EMT scores (Figure 4-3E, gray, $R^2 = 0.5202$, p-val < 0.0001).

In summary, the bulk RNA-seq results show a close correlation between predicted NK sensitivity calculated from NK ligands and EMT status in lung cancer cell lines. Especially, in-house derived CTC lines were predicted NK sensitive and mesenchymal based on ligand expressions.

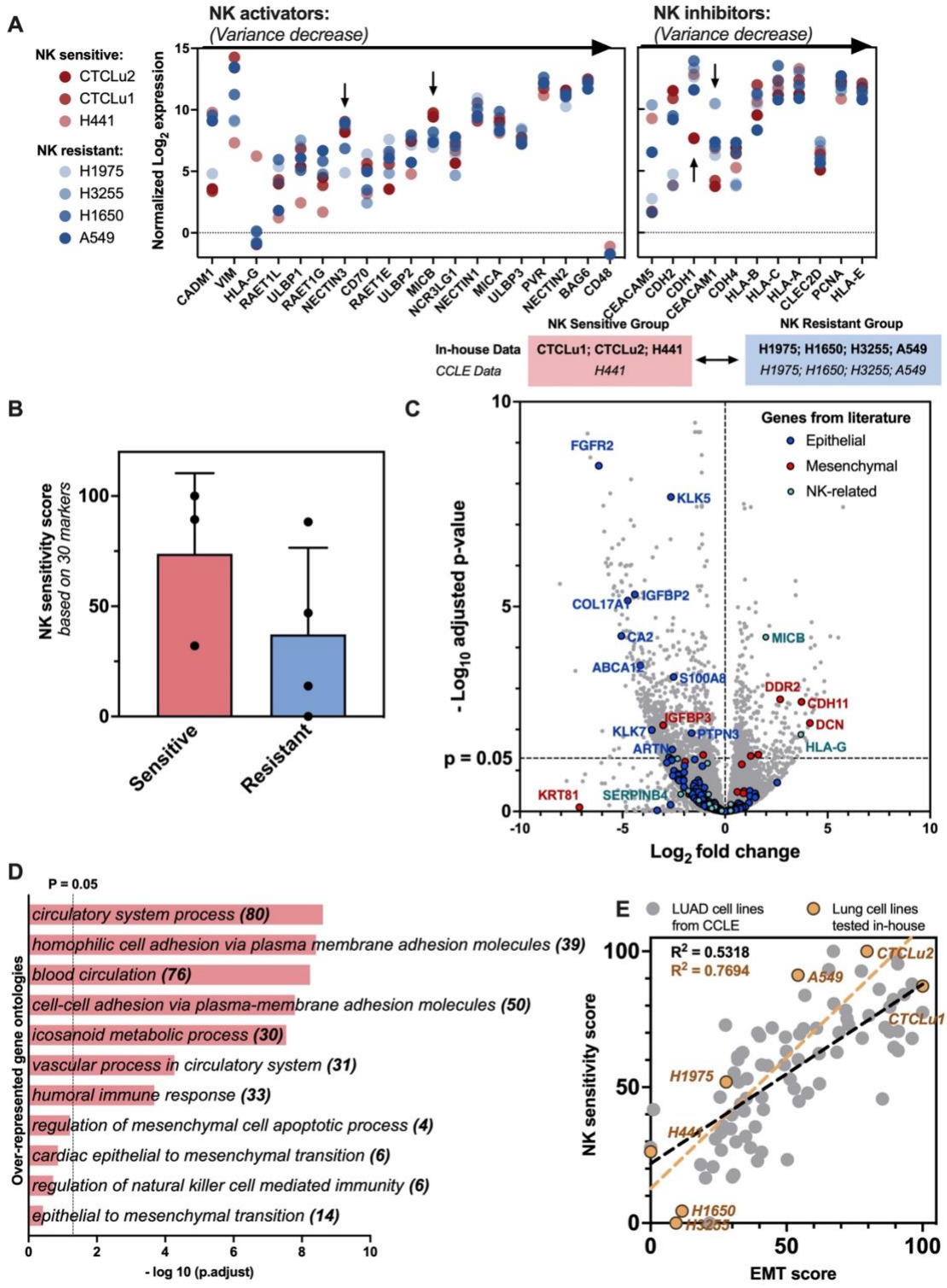

Figure 4-3 Bulk RNA-sequencing of lung cancer cell lines. (A) Normalized Log_2 expression of 30 NK-related ligands, including 19 activating and 11 inhibiting ligands. Ligands were arranged in the graph by the variance between the seven cell lines (descending from left to right). (B) NK sensitivity score calculated based on the 30 NK ligands. (C) Differentially expressed genes between NK sensitive phenotype and NK resistant phenotype. EMT-related and NK-related genes were labeled in colors. (D) Over-represented gene

ontologies. The relevant gene count for each ontology is indicated in the parenthesis. (E) Correlation between NK sensitivity score and EMT score. Lung cell lines from the in-house bulk sequencing dataset are labeled in yellow, and lung adenocarcinoma (LUAD) cell lines from CCLE are marked in gray.

4.5.4 NK ligand expressions on Day-0 patient CTCs predict NK-sensitive phenotypes

We were then interested to see if these NK-sensitive signatures could be found in freshly isolated CTCs from patients. A similar quantitative immunofluorescence assay was performed to evaluate NK-related marker expression from eight late-stage metastatic NSCLC patients. The average patient age was 62 years old and was well distributed between males and females. Four patients had two or more time points collected, while the remaining four only had a single time point. CTCs were isolated from blood samples using the labyrinth workflow[186]. The high-throughput label-free device allows the isolation of heterogeneous CTC subpopulations, independent of surface protein expression. After isolation, immunofluorescent staining was performed using the two staining panels described above, shown in Figure 4-4A. We then exported the intensity values from individual CTCs and surrounding WBCs as internal controls. Z-score normalization was performed for all exported cells within each marker, adjusting for the background variations.

We found that CTCs have interesting protein expression profiles compared to the control WBCs (Figure 4-4B). For NK inhibitors: MHC class I and E-cadherin, the median expression level in CTCs is lower than in WBCs. Conversely, NK activators: MICA/B and CADM1 showed slightly higher median expression in CTCs than WBCs.

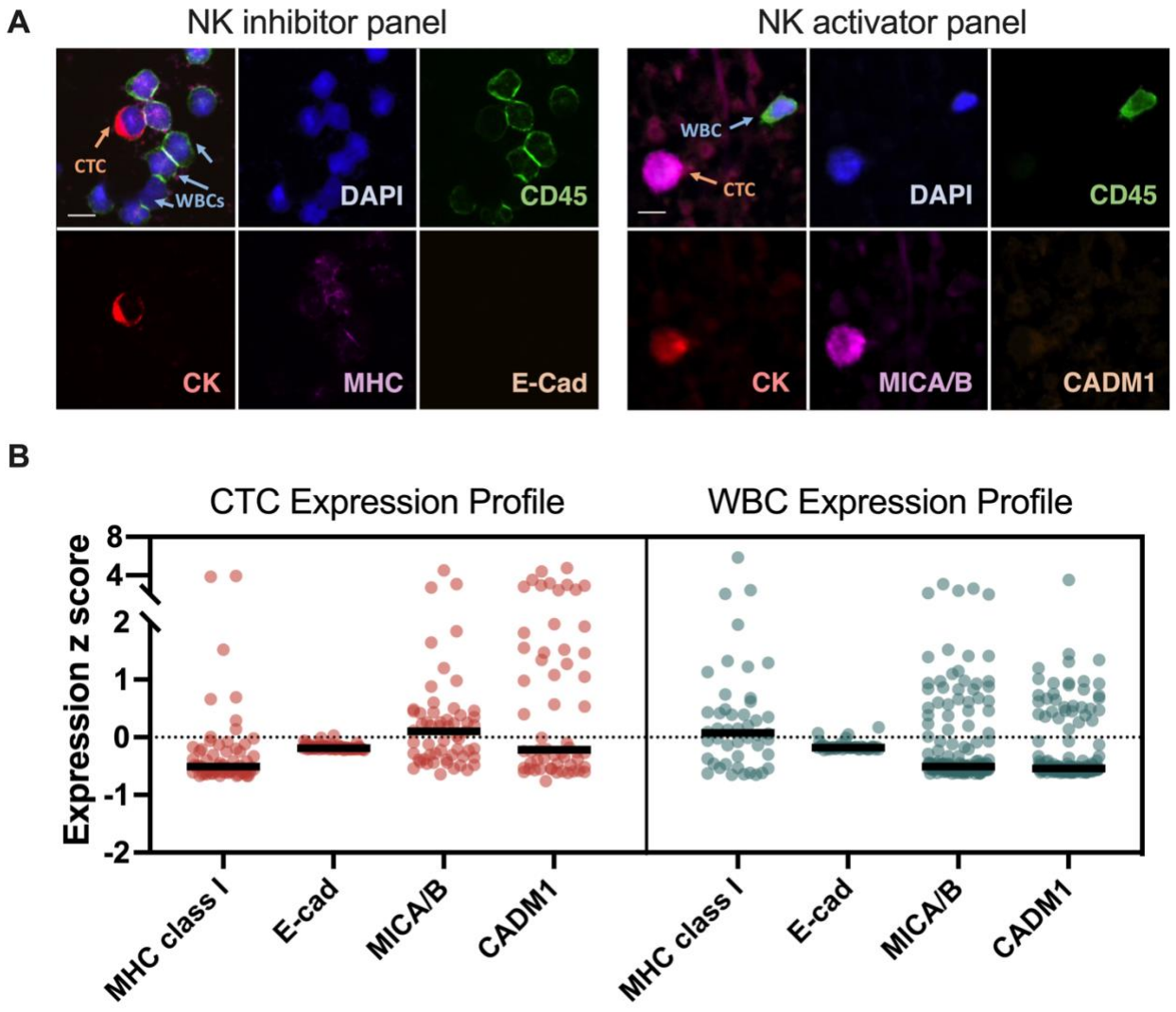

Figure 4-4 Key NK regulator protein expression in freshly isolated CTCs. (A) Examples of immunofluorescent staining from the two panels. CTCs were identified as DAPI+/panCK+/CD45-. (B) Z-score normalized fluorescent intensities of identified CTC and WBC populations.

4.5.5 Heterogenous EMT profiles observed but not correlated with HLA loss from single-cell RNA sequencing on patient CTCs

To explore the correlation between EMT and NK-related signatures at the RNA level in freshly isolated CTCs, we performed single-cell sequencing on enriched CTC samples from three patients in the cohort. Patient blood samples were first enriched through previously described Labyrinth[186]. We then selected CTCs by the negative expression of immune cell markers and the top 10% epithelial or mesenchymal cells based on the calculated EMT score. This CTC selection

strategy is described in Figure 4-5A and the methods. We first performed the uniform manifold approximation and projection (UMAP) dimension reduction analysis to reveal the major cell types of these enriched samples (Figure 4-5B). Platelets, neutrophils, NK, and T cells were identified using canonical markers, along with the CTCs.

Interestingly, these CTCs clustered with platelets in the UMAP analysis. We were not surprised by this result because frequent platelet coating of CTCs has been shown in other studies[238]. To differentiate between these two groups, we analyzed the differential gene expressions. A representative volcano plot of the differential expressed genes in Pt-2 is shown in Figure 6B. Known cancer-related genes such as MALAT1, EEF1A1, S100A10, VIM, S100A6, COL1A1, and COL3A1 were highly expressed in CTCs. Platelet marker genes, such as PF4 and PPBP, were highly expressed in platelets. These expression profiles increased our confidence in this CTC identification strategy. The complete list of significant DEGs and their detection percentage in the two groups are shown in Figure 6C. Interestingly, many genes in the ribosomal protein group, such as RPL18A, RPL32, RPL13, and RPL19 upregulated in CTCs.

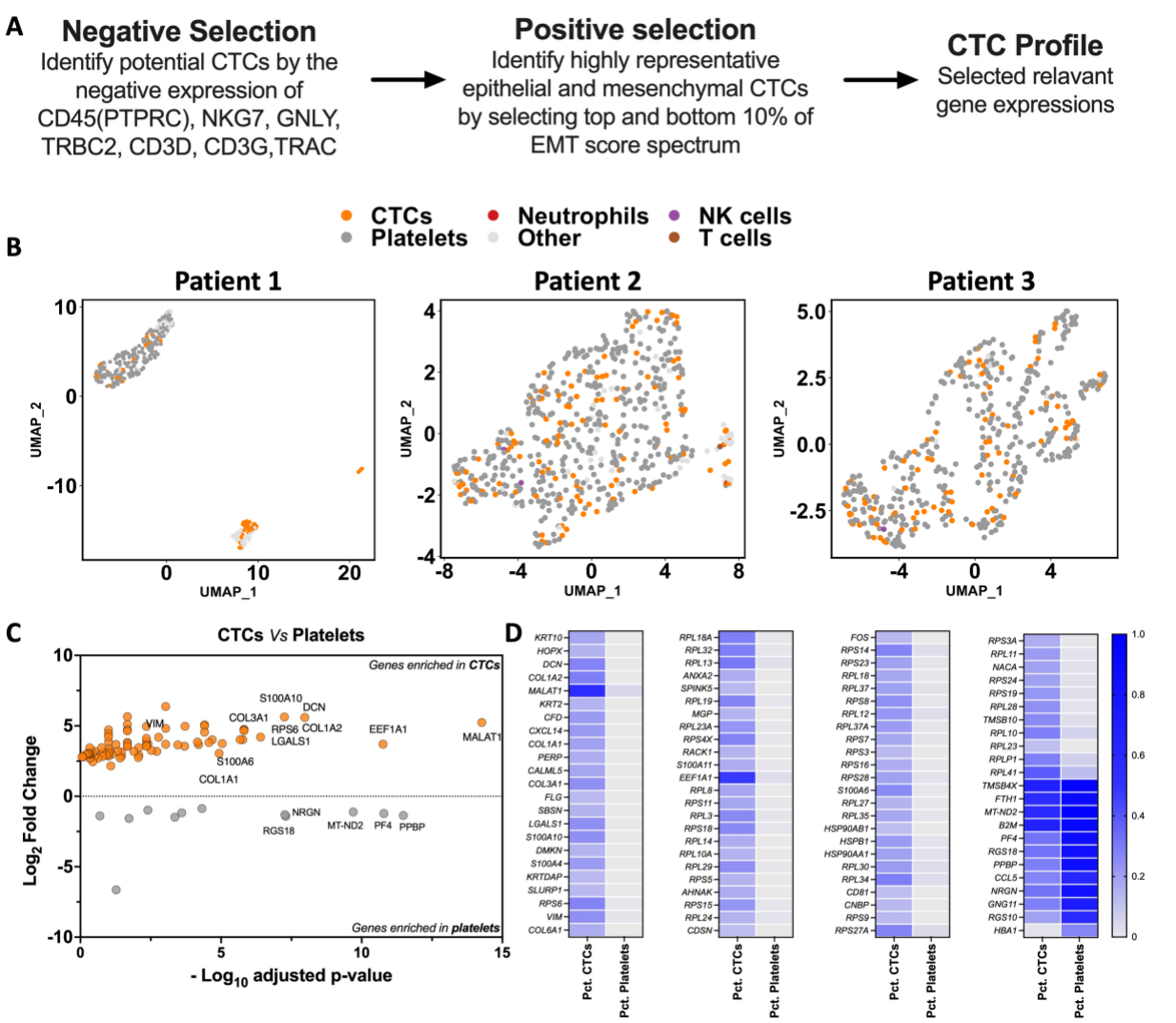

Figure 4-5 Single-cell RNA profiling of freshly isolated CTCs. (A) Schematic of CTC selecting strategy. (B) 2-D UMAP dimension reduction analysis showing clusters of CTCs and platelets. (C) Volcano plot of differential expressed genes between CTCs and platelets. (D) List of differentially expressed genes and the detection rate within the CTC and platelet groups.

We then interrogated the expression of NK, EMT, and other lung cancer-related genes in these identified CTCs. We plotted the genes with consistent non-zero expressions (expressed by at least two cells) in heatmaps (Figure 4-6A). We arranged these CTCs based on their EMT score from high (mesenchymal) to low (Epithelial). As expected, common mesenchymal markers, such as VIM, COL3A1, and COL3A2, were highly expressed in the mesenchymal CTCs of Pt2. Conversely, epithelial markers, such as TACSTD2[239], were highly expressed in the epithelial CTCs. Because of the low coverage of the sequencing experiment, only four HLA class I alleles

(HLA-A, HLA-B, HLA-C, and HLA-E) among the NK ligands had consistent non-zero expressions. We did not see a clear difference in HLA class I expression between epithelial and mesenchymal cells. We then quantified the frequency of zero expressions for the four HLA class I alleles for mesenchymal or epithelial cells and observed similar indifference between the two groups (Figure 4-6B).

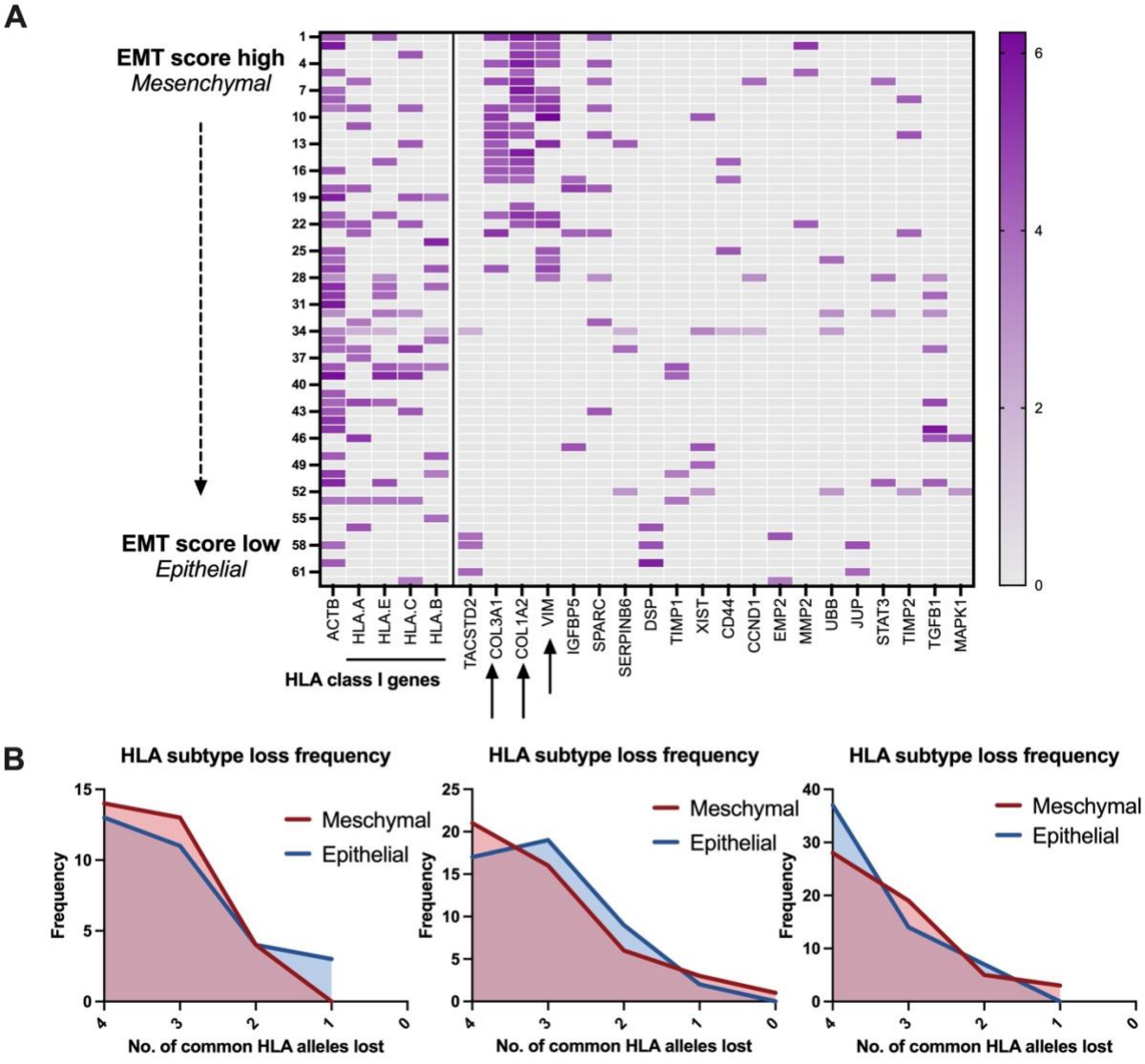

Figure 4-6 Clustering and further analysis of the single-cell datasets. (A) Heatmap of the NK and cancer-related RNA expressions in selected CTCs in Pt-2. CTCs are arranged based on EMT scores from high to low. (B) Frequency density plot of zero expressions of the four common HLA alleles: HLA-A, HLA-B, HLA-C, and HLA-E.

4.6 Discussion

Despite rising evidence supporting NK cells' role in halting distant metastasis, little work has been done to characterize the NK sensitivity on patient-derived CTCs. The rarity of CTCs in the blood limits their compatibility with traditional cytotoxicity assays, which require large starting cell numbers. Several studies, including our group, have developed techniques to expand CTCs to larger numbers[216–218,240,241]. Two NSCLC patient-derived CTC lines were successfully established by our group[241]. Using these established CTC lines, we were able to capture NK-CTC cytotoxicity in real-time and quantify this sensitivity with a set of lung cancer cell lines. Excitingly, we found that the CTC lines were both highly sensitive to NK-mediated killing compared to other cell lines. To our knowledge, this is the first time that NK sensitivity of patient-derived CTC lines has been shown.

Although CTC expansion offers ex vivo drug testing possibilities, its application for personalized medicine is limited mainly because of the inconsistent success rates and long culture times[240,242]. To explore CTC biomarkers for NK-based therapies and investigate the molecular mechanism of this sensitivity, we selected four key NK regulators, including MHC class I, E-Cadherin, MICA/B, and CADM1, to evaluate their expressions on the protein level. We calculated an overall sensitivity score by assigning equal weights with opposite signs to the inhibiting (-1) and activating markers (+1). Higher scores are anticipated to have a higher sensitivity to NK-mediated killing. We observed a slightly higher median NK score based on four markers in the NK-sensitive lung cancer cell lines. We used a similar method to calculate the NK score for freshly isolated day-0 CTCs and hypothesized a correlation with patient disease status. However, we did not observe any difference in the NK scores by patient disease status. This could be due to the limited numbers of patient samples or the limited four markers in the calculation.

To overcome this, we performed bulk and single-cell sequencing on CTC lines and freshly isolated CTCs, respectively. We first performed differential gene expression analysis using the bulk sequencing data on the lung cancer cell lines. NK-sensitive cell lines have upregulated mesenchymal genes, including DDR2, CDH11, and downregulated epithelial genes such as FGFR2 and KLK5. These mesenchymal-like expression profiles validate our unique patient-derived CTC line model. Based on this trend, we calculated NK and EMT scores calculated based on known markers from the bulk sequencing results. The two in-house derived CTC lines showed high NK and EMT scores, reflecting their mesenchymal and NK-sensitive phenotype. We also found a strong correlation between EMT signatures and NK ligands in both our dataset and lung cell lines from the CCLE database. Our finding using CTC lines is consistent with previous findings in preclinical[122] and colon cancer cell line model[236].

We then established an integrated single-cell RNA analysis workflow using the label-free labyrinth device and Chromium (10X Genomics). CTCs were defined by cells with no immune cell marker expressions and were highly epithelial or mesenchymal based on the EMT score. These CTCs were found to cluster with platelets in the UMAP analyses. We suspect this could be because of the platelet coating of some of these CTCs, which has been shown in other studies. Differentially expressed genes were then identified between CTCs and platelets, showing cancer or platelet markers in either of the groups. Interestingly, we found high detection rates of ribosomal genes, such as RPL35 and RPL13, in the CTC population. These ribosomal genes have also been shown to be upregulated in other studies using in vivo CRISPR screenings in CTCs[243]. There have been increasing discussions about the crucial role of ribosome biogenesis downstream of EMT and in multiple steps of metastasis[244,245]. Additionally, we found no clear associations between EMT

signatures and HLA allele expressions. This was also consistent with previous findings by Chockley et al. in the expression of MHC class I in response to TGF-β-induced EMT[122].

The limitations of this study include 1) Sample size. Cytotoxicity and bulk RNA-seq were only performed with two patient-derived CTC lines. In contrast, fresh CTC immunofluorescence and single-cell RNA-seq were tested in eight and three patients, respectively. 2) Low coverage in the single-cell sequencing experiment. 3) Lack of NK receptor profiling. Future NK sensitivity metrics could include co-profiling patient isolated NK cells and patient-derived CTCs to investigate NK-based immune surveillance against CTCs further and design personalized NK-based therapies.

Despite these limitations, our study presents a comprehensive workflow for assessing the NK sensitivity of CTCs on a single-cell level. Using this workflow, we identified that CTCs, especially those with mesenchymal phenotypes, are highly sensitive to NK-mediated killing and have NK-sensitive signatures on both protein and RNA levels. We believe our work serves as a proof-of-concept study that provides the initial foundation for NK-based therapy design to target CTCs and metastasis and could be built upon in future studies with larger cohorts and includes patient-derived NK cells.

Chapter 5 Development of a Streamlined Microfluidic Workflow to Harvest Cytotoxic NK-Cell Derived Exosomes

5.1 Abstract

Since the recognition between Natural Killer (NK) cells and cancer cells does not require antigen presentation, NK cells are being actively studied for use in adoptive cell therapies in the rapidly evolving armamentarium of cancer immunotherapy. In addition to utilizing NK cells, recent studies have shown that exosomes derived from NK cells also exhibit anti-tumor properties Furthermore, these NK cell-derived exosomes exhibit higher stability, greater modification potential, and less immunogenicity compared to NK cells. Therefore, technologies that allow highly sensitive and specific isolation of NK cells and NK cell-derived exosomes can enable personalized NK mediated cancer therapeutics in the future. Here, we propose a novel microfluidic system to collect patient-specific NK cells and on-chip biogenesis of NK-exosomes. In a small cohort of non-small cell lung cancer (NSCLC) patients, we isolated both NK cells and circulating tumor cells (CTCs), and we found NSCLC patients have high numbers of NK and NK-exosomes compared with healthy donors, and these concentrations show a trend of negative and positive correlations with bloodborne CTC numbers, respectively. We further demonstrated the NK-exosomes harvested from NK-GO chip had cytotoxic effect on CTCs. We expect this versatile system can be used for patient-specific NK-based immunotherapies along with CTCs for potential prognostic/diagnostic applications.

5.2 Publication information

Materials in this chapter adapted from: Yoon-Tae Kang*, **Zeqi Niu***, Thomas Hadlock, Emma Purcell, Ting-Wen Lo, Mina Zeinali, Sarah Owen et al. "On-chip biogenesis of circulating NK cell-derived exosomes in non-small cell lung cancer exhibits antitumoral activity." *Advanced Science* 8, no. 6 (2021): 2003747.

*These authors contributed equally.

5.3 Introduction

Cancer immunotherapy has emerged as a promising strategy to treat cancers, most notably by engaging the adaptive immune system (e.g. immune checkpoint inhibitors) or through cell-based approaches (e.g. Adoptive T cell therapies, NK cell therapies) involving the innate immune system[246–248]. The US Federal Drug Administration (FDA) has approved several of these therapies, such as pembrolizumab and ipilimumab (immune checkpoint inhibitors), for both solid organ as well as hematological malignancies in the past decade, revolutionizing treatments of many cancer that were considered incurable in the past[249]. Despite these successes, T cell-based therapies are handicapped by factors including an expensive, time consuming process of engineering and expanding T cells, as well as efficacy limitations arising from low major histocompatibility complex (MHC) expression on tumor cells[250]. To circumvent these issues, other approaches have been proposed, which involve the study of other members of the innate immune system, such as the Natural Killer (NK) cells.

NK cells are lymphocytes that can be cytotoxic against a wide range of cells, having the ability to destroy infectious as well as transformed cells without antigen presentation[251,252]. The high cytotoxicity of NK cells against circulating tumor cells, which are considered as the seed of metastasis, was previously reported[253]. Because of the broad cytotoxicity and rapid reaction,

adoptive NK cell therapy aimed at increasing NK cell numbers may be a promising immunotherapeutic approach. Compared with T cell-based therapies, NK cell therapies are independent of antigen presentation and can be better controlled to reduce the risk of cytokine storms[254]. However, NK cell-based therapies still struggle to overcome some of the innate limitations of cell-based therapies, such as a lack of ability to deliver adequate numbers of NK cells to tumors due to limited targeting capabilities. For example, NK cell therapy for brain cancer is challenging, given the difficulty in crossing the blood brain barrier (BBB) and the blood-tumor barrier (BTB)[255,256]. To overcome these limitations while simultaneously utilizing NK cell's benefits, several newer approaches, such as utilizing NK cell derived-exosomes or microvesicles, have recently been studied by a few groups[137,257] in order to improve NK cell based immunotherapy approaches.

Exosomes are a type of extracellular vesicle (EV) secreted by various cells. They are nanoscopic courier vesicles (30 - 150 nm) carrying lipids, nucleic acids, metabolites and proteins, hence playing a central role in intercellular communication and macromolecule transmission. They also enable transport of proteins that convey genetic information between cells. Almost all membranous cells within the human body secrete exosomes[258], and these exosomes can mimic many of the salient features of their mother cells while also displaying their own distinguishing features. These innate unique protein compositions of exosomes allow for specific cellular uptake and target-homing capabilities, which is differentiated from standard nanoparticle-based drug carriers[133,259]. Exosomes are also characterized as biocompatible and stable in physiological conditions with a long circulating half-life in blood[260]. Therefore, exosomes are currently being considered for use as natural drug carriers or agents for cancer immunotherapy, both of which aim to curtail the spread of cancer throughout the body and retard the growth of tumor cells[261]. In order

to utilize innate merits of exosomes, exosomes have been hybridized with conventional nanoparticles to be used as a drug carrier for cancer chemotherapy[262].

The unique characteristics of exosomes derived from certain immune cells such as NK cells may offer solutions to many of the challenges arising from complications of the tumor microenvironment. Their nano-size and abundance are ideal for cancer treatment via effective trafficking to the solid tumor location and infiltration into the tumor micro-environment[130]. Exosomes derived from NK cells can penetrate several typically problematic barriers including the blood brain barrier and the blood tumor barrier, which has been relatively impenetrable to NK cells. As such, NK cell immunotherapies for cancers such as glioblastoma have been restricted in their efficacy due to reliance on small tumor-induced BBB disruptions for immune cell uptake[263]. Also, infiltration of NK cells into tumors, such as lung cancer, is largely influenced by cytokine profiles of tumor microenvironment, which sometimes impairs NK cell's activities[134].

NK cell-derived exosomes provide an efficient alternative for treatment of certain cancers. They naturally express IFN-γ, FasL and multiple cytotoxic proteins that can induce apoptosis via multiple killing mechanism[134,135]. Exosome's innate cell-cell transfer ability can stimulate further tumor microenvironmental activity or communicate with surrounding cells, activating their cytotoxic effects.

Recent studies have demonstrated the effectiveness of NK cell-derived exosomes in lysing malignant tumor cells, including mediating a significant anti-tumor response against acute myeloid leukemia and melanoma[136,137]. While NK cells have shown promising results despite limited tumor access, exosomes present an option for unhindered tumor access by particles with NK cell properties and associated benefits including stability, consistency, and modification potential[260].

Therefore, selective isolation of NK cells and the subsequent harvesting of exosomes is a promising approach for NK therapies in the future. However, due to the technical challenges of isolating highly pure, live populations of NK cells and the subsequent collection of exosomes derived from these cells, this approach has not been successfully implemented[257]. There have been several separate attempts to optimize specific cell isolation or cell-derived exosome collection, however, to date, there are no streamlined platforms to isolate specific subtypes of cells and to harvest specific exosomes from a heterogeneous sample.

Microfluidics and micro-devices have been utilized for decades for the isolation of cells and vesicles from a complex specimen with higher efficiency and sensitivity than conventional bulky equipment-based isolation. Microfluidic technologies for liquid biopsies have rapidly evolved and have shown success in capturing rare cells, including circulating tumor cells[18,264,265], stem cells [266,267], and extracellular vesicles[267–269], etc. Microfluidic devices functionalized with antibodies to capture specific cell populations are a powerful tool to achieve a high purity isolation with minimal resources and limited quantity of clinical samples[270]. In addition, recent advances of antibody conjugation chemistry offer an advantage to selectively release isolated targets for further downstream analysis and functional studies. Several release strategies have been studied utilizing surface antibody conjugates, including cleavable cross-linkers[271,272], dissociable thermal sensitive polymer substrates[273], and methods that take advantage of competing binding affinities between biotinylated antibodies and biotin derivatives[274–278]. Use of cleavable cross-linkers or dissociable substrates requires special chemicals or condition changes which may be crucial to the final products or might alter the contents of the released targets. Chemical release strategies utilizing competing binding affinities such as the use of biotin to displace antibodies conjugated with biotin analogs with lower streptavidin bond preference have demonstrated notable success in complete

target cleavage under mild conditions[274–278]. However, incorporation of this chemistry into microsystems has rarely been studied.

Given the combined merits of microfluidic devices and chemical release strategies, we propose a streamlined microfluidic platform to harvest NK exosomes (NK-Exos) from viable NK cells isolated on chip, as shown in Figure 5-1. By using a graphene oxide microfluidic chip functionalized with antibodies against natural killer cells (NK-GO chip), we isolate NK cells on chip with high purity and viability. The deposition of two-dimensional GO sheet has a large surface area and provides more binding sites to isolate targets compared to the identical sized device without GO deposition. Thanks to the biocompatibility of GO, the captured and viable NK cells undergo short-term incubation for NK-Exo secretion and the recovery of the NK-Exos is accomplished using anti-CD63 conjugated magnetic beads (ExoBeads). For the functional study of NK-Exos, here, instead of using irreversible binding of biotin to avidin, we used desthiobiotinylated anti-CD63 and avidin-conjugated beads[277]. Therefore, we were able to easily strip the isolated exosomes from the beads using biotin solutions due to competing reactions between biotin and desthiobiotin against avidin[278]. This mild and biocompatible release process enables further nanoparticle tracking analysis and functional studies of NK-Exos. Using clinical blood samples from patients with non-small cell lung cancer (NSCLC) and healthy donors, we compared total NK cell number and NK exosomes in terms of concentration and size, along with their correlation with circulating tumor cell (CTC) number in blood. The isolated and released exosomes were further characterized using in-house CTC-derived cell line cytotoxicity assay to evaluate preliminary therapeutic potential. We believe our novel and versatile platform can set the stage for future work relating to NK exosome-based cancer immunotherapy.

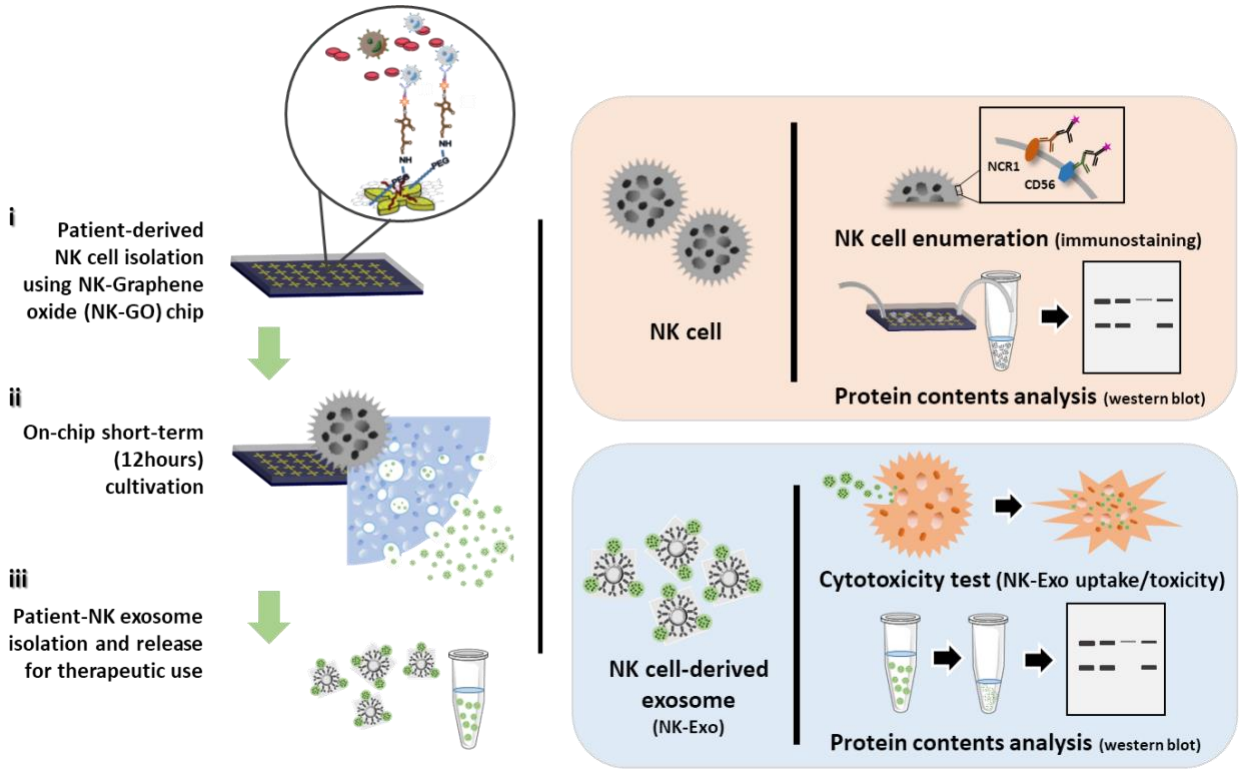

Figure 5-1 Schematic diagram of the microfluidic technology approach for on-chip natural killer (NK) cell isolation, in situ NK cell-derived exosome biogenesis, and recovery for potential therapeutic use of NK exosomes.

5.4 Materials and methods

5.4.1 Cell culture and model sample preparation

NK-92®MI cells were cultured in MEM-alpha (Gibco, USA) containing 20% fetal bovine serum and 1% penicillin-streptomycin solution. In order to prepare model samples for NK cells, NK-92®MI cells were pre-labeled with a CellTracker dye with green (ThermoFisher, USA) and approximately 10^3 to 10^5 NK cells were spiked into 1mL of PBS buffer or whole blood. For NK exosome secretion experiments in well plates, 3 million NK cells were seeded into each 10mm suspension cell culture dish (Corning, USA) with media containing exosome-depleted serum (Gibco, USA). After 48h of cell seeding, supernatant from 8-10 cell culture dishes was collected and centrifuged at 500g for 5 minutes before the supernatant is again centrifuged at 12,000g for 20 minutes. Model samples for NK cell-derived exosomes were prepared by ultra-centrifuging NK

cell culture supernatant. After ultracentrifugation, we measured the exosome concentration using NanoSight (Malvern, UK), and a known concentration of exosomes was spiked for model sample preparation.

5.4.2 Human blood sample preparation

The blood sample collection and experiments were approved by ethics committee (Institutional Review Board and Scientific Review Committee) of the University of Michigan. Informed consent was obtained from all participants of this clinical study and the blood samples of cancer patients were obtained after approval of the institutional review board at the University of Michigan (HUM00119934). All experiments were performed in accordance with the approved guidelines and regulations by the ethics committee at the University of Michigan. The blood samples were used within 2 hours of extraction and each whole blood sample was directly processed by NK-GO chip and Labyrinth for NK cell isolation and CTC isolation, respectively.

5.4.3 NK-GO chip fabrication and surface modification

Graphene oxide microfluidic devices have been used for the high-purity isolation of rare cells[20]. We improved and optimized this device for NK cell applications. Briefly, gold patterned silicon wafers were soaked in graphene oxide (GO) solution for 10 minutes then bonded to a PDMS chamber using a corona discharge. NK-GO chips were injected with GMBS cross-linker in ethanol and incubated for 30 minutes. The device was then washed with PBS and 500 μl of 10% NeutrAvidin in PBS was injected through the device. The prepared GO chips were conjugated with NK cell antibodies using avidin-biotin affinity-based immobilization. Biotinylated antibodies against CD56 were flowed through the device for NK cell capture.

5.4.4 NK cell isolation and on-chip NK cell exosome harvesting

Before processing each sample containing NK cells, we blocked the device with a 3% bovine serum albumin (BSA) solution in PBS to minimize non-specific binding. Cell capture was performed by flowing the sample containing NK cells through the devices using a syringe pump at a flow rate of 1 mL/hr. PBS buffer was then applied to wash away non-bonded cells. After cell isolation and washing, the cells are fixed with 4% PFA solution and permeabilized on the chip, followed by staining with 4', 6-diamidino-2-phenylindole (DAPI) fluorescent dye for staining cell nuclei. The chips are then scanned under fluorescent microscope (Ti2, Nikon, Japan). After scanning, 300µl of MEM-alpha serum free media was then pumped into the device with low flow rate (1mL/hr). 12 hours incubation with the whole device is then performed in 37℃, 5% CO_2 incubator Galaxy 14S (Brunswick, USA).

5.4.5 On-chip NK-92®MI cell enumeration for model sample experiments

The number of cells captured on the chip is obtained by counting CellTracker Dyed/DAPI+ cells on fluorescent images of the device, and the total cell number processed was obtained using different methods depending on background solutions. For the cells spiked in buffer, total cell number can be obtained by counting the cell number in the solution which flowed out of the chips. Under the principle of mass balance, total cell number is simply the sum of cells on chip and cells collected in the waste. When the cells are spiked in healthy blood, the total cell number is obtained by spiking same amount of cell solution into well plates to be counted.

5.4.6 Immunofluorescence staining of cells

In order to verify NK cells in clinical samples, we optimized and set our NK cell staining panel. For staining optimization, NK-92®MI and Jurkat cell slides are using 10 minutes, 800 g spin cycle on a Cytospin 4 (ThermoFisher Scientific, USA), followed by a 10 min 4%

paraformaldehyde (PFA) fixation. Cells are then permeabilized using 0.2% Triton X-100 (Sigma-Aldrich, USA) for 3 minutes, followed by three 5 min washes using phosphate buffer saline (Gibco, USA). The slides are then blocked with 10% goat serum (Invitrogen, USA) for 30 minutes. Following that, the primary antibodies were applied for 1 hr at room temperature. After washing off the primary antibody using another three 5 min PBS washes, secondary antibodies were applied and incubated for 30 minutes. Coverslips were then applied with ProLong Gold antifade reagent with DAPI (Molecular Probes, USA). Primary antibodies against CD56 (A7913, Abclonal, USA) and NCR1 (A14499, Abclonal, USA) and secondary antibody against rabbit IgG (A21245, ThermoFisher, USA) were included in the NK cell staining panel.

5.4.7 NK cell-derived exosomes isolation/release using magnetic beads

For the isolation and release of the captured exosomes, desthiobiotinylated anti-CD63 (Life Technologies Corporation, USA) was used. Biotinylated anti-CD63 was affixed to streptavidin conjugated magnetic beads, DynaBeads T1 (Invitrogen, Norway), as follows. First, 20 to 40µl of 10mg/mL streptavidin conjugated magnetic beads in solution were deposited into a small vial and washed with 0.2 µm filtered PBS multiple times. After that, three different dilution ratios of desthiobiotinylated anti-CD63 (1:5, 1:10, and 1:20) solution in 1% BSA was applied to the magnetic beads. The beads with antibodies underwent a one-hour incubation period. After this incubation, the beads were washed three times with filtered PBS. In each case, a magnet was applied to the side of the vial to secure the beads while the solution was extracted. For the control beads, instead of antibody solution, we used only a 1% BSA solution without antibody reagent and followed the remaining steps the same.

For NK exosomes isolation and release, 200 µl of supernatant from the device was directly applied to the prepared magnetic beads (ExoBead). This mixture was incubated on a rotator for an

hour and magnetic beads were separated using a magnet, followed by PBS washing three times. The beads right after this step underwent SEM or western blot analysis. For the release of the captured exosomes on the beads, 1 mL of 0.5 mM biotin solutions was added to the separated beads, consisting of 1mL of filtered water and 10µl of biotin solution and incubated for 0.5 to 2 hours. The biotin solution was placed in a new tube and analyzed by NTA analysis. In all cases, the effluents and resultants after bead removal underwent NTA analysis for verification.

5.4.8 Ultracentrifugation of NK cell-derived exosome

Ultracentrifugation was used for two reasons: **1)** Characterization of exosome secretion from cells in each well plate and **2)** ExoBead device characterization. In both cases, we used a Sorvall ultracentrifuge (ThermoFisher, USA). For comparison study, the same volume of initial plasma sample was used but diluted into 1mL of PBS. Blood samples were first centrifuged at 2000g for 15 minutes, and then 12000g for 20 minutes. After initial ultracentrifugation at 100,000g for 90 minutes, we aspirated the supernatant and injected another 38mL of PBS for a 2^{nd} round of ultracentrifugation at the same conditions. The pellet after the 2^{nd} UC was gently spiked into 500µl or 200µl, for well-plate samples and ExoBead characterization samples, respectively.

5.4.9 Field emission scanning electron microscopy (FE-SEM)

The capture and release of exosomes by ExoBeads was examined by FEI Nova 200 Nanolab Dualbeam FIB scanning electron microscope under beam energies (2.0-5.0kV) at the Michigan Center for Materials Characterization at University of Michigan. Right after capture and release experiments, ExoBeads were immobilized on clean carbon tape and the specimen was naturally dehydrated. The dehydrated specimen was then mounted on an SEM stub and coated

with gold by sputtering. The images from SEM were saved and processed using the desired SEM image analysis software.

5.4.10 Nanoparticle tracking analysis

Evaluation of exosome concentration and size distribution was analyzed by nanoparticle tracking analysis (NTA) using NanoSight NS300 (Marven Instruments, UK). 30 µl of the prepared solution was applied to the jig of the system, and laser module was mounted inside the main instrument housing. NTA visualizes the scattered lights from the particles of interest based on their Brownian motion. This movement was monitored through a video sequence for 20 seconds in triplicate. All data acquisition and processing were performed using NanoSight NS300 control software, and concentration of particles in exosome size range was used for calculating capture and release efficiencies of the present platform.

5.4.11 Protein extraction and western blot analysis

RIPA buffer with 1% protease inhibitor was prepared for lysis of captured exosomes. 30 µl of the prepared buffer solution was injected to post-capture ExoBeads and incubated for 20 minutes. After incubation, the protein lysate was aspirated and stored separately. Total amount of proteins in the lysate from the ExoBeads was measured by standard micro bicinchoninic acid (BCA) analysis according to the manufacturer's instructions. Western blot analysis was performed on a precast 4-20% SDS gel (BioRad, USA). The samples were prepared in 4x Laemelli buffer with 2-mercaptoethanol and heated to 90°C for 6 minutes before loading onto the gel. The gel was run at 120V for 50 minutes before transferring at 120V for 1 hour on ice. Blocking was performed in 5% non-fat milk in TBST for 90 minutes. Primary antibody incubated overnight on a rocker at 4°C at a concentration of 1:1000 in 3% non-fat milk in TBST. Thorough rinsing was performed,

and then secondary antibody was incubated for 90 minutes at room temperature at 1:1500 in 3% non-fat milk in TBST.

5.4.12 Isolation of circulating tumor cells from NSCLC patients using label-free microfluidic device

Briefly, 18 mL of blood was collected in EDTA tubes and processed through the Labyrinth within 2 hours of collection[11]. Prior to processing in the Labyrinth, RBCs in the blood samples were removed using Ficoll-Paque™ PLUS Media (GE Healthcare, USA) following the company's protocol. The supernatant (plasma and buffy coat layers), which included all whole blood components except RBCs, was carefully removed and diluted with PBS (1:5). The diluted samples were then processed through the Labyrinth at a flow rate of 2500 μL/min. The pass-through product from outlet was collected after stabilization.

5.4.13 NK exosome uptake and cytotoxicity experiment

NK-92®MI derived exosomes were prepared using UC of cell culture media. For uptake experiments, the exosomes were fluorescently labeled using PKH dye (Sigma-Aldrich, USA) The exosomes were then added into 96 well plates where patient-derived expanded CTC line were seeded 24hr before. After 3hr of incubation, cancer cells were then fixed using 4% PFA for 10 minutes. Within the well plate, the cells were stained with Cellmask (ThermoFisher, USA) and DAPI for 10 minutes. The well was then imaged under a fluorescent microscope.

5.4.14 NK exosome cytotoxicity experiment using clinical sample-derived NK exosomes

In-house patient-derived expanded CTC line were used for NK exosome cytotoxicity experiments. Briefly, CTCs from an EGFR mutant NSCLC (encoded R022-V8) were isolated using Labyrinth, then they were expanded in vitro successfully[241]. Given that in-house patient-

derived expanded CTC line might resemble cancer cells in circulation than conventional cancer cell lines, this patient-derived expanded CTCs were used for evaluating cytotoxic potential of NK Exos. The cells were seeded into 384 well plate at a density of 100 cells per well and incubated for 24 hours before the event of NK-Exo treatment. In order to prevent further contaminations from biotin and magnetic beads residues, recovered NK-Exos from ExoBeads were ultracentrifuged and resuspended into serum free RPMI media. 1-2.3x $x10^7$ of NK-Exos were seeded into the wells containing pre-seeded cancer cells. After 72 hours of incubation, a live/dead kit-based assay was performed under manufacture's instruction (L3324, ThermoFisher, USA), followed by entire well scanning using a fluorescent microscope (Nikon, Ti2). The images were then counted using auto-recognition of ROIs in the Nikon software.

5.4.15 Statistical Analysis

All results are presented as mean ± standard deviation. Statistical analyses were demonstrated using Graphpad Prism 9. Unpaired t-tests (two-tailed) were used to compare the differences between live cell count between NK exosome treated (n = 4) versus control (n = 4). Statistical significance was defined as $p < 0.05$.

5.5 Results

5.5.1 Viable NK cell isolation using a NK-GO microfluidic chip

The high surface area and biocompatibility of GO nanosheet facilitates sensitive and efficient NK cell isolation and on-chip short-term culture for NK-exo biogenesis. The ability of the NK-GO chip (Figure 5-2) to isolate NK cells was initially examined using spiked cell experiments with two different conditions: **1)** NK cell line (NK-92MI) spiked in Phosphate-buffered saline (PBS) buffer and **2)** NK cell line spiked in whole blood. NK cell capturing

performance of NK-GO chip was first compared with control device without antibody conjugation and showed that the current device isolates more than 95% NK cells spiked in buffer, which implies that anti-CD56 and its functionalization on the GO chip is capable of NK cell isolation (Figure 5-2b). Based on previous studies[279,280], we found that the frequency of NK cells are usually in the range of ~10^5 cells/ 1 mL of peripheral blood, thus we examined our NK-GO chip's NK cell capturing performance at two different concentrations, 10^3 cells/mL and 10^5 cells/mL. The pre-labeled NK cells at two different concentrations were spiked into each of the two different model samples and the number of the captured cells were enumerated using a fluorescence microscope. Capture efficiencies at four different conditions are shown in Figure 5-2c. In each case, capture efficiencies of NK cells spiked in blood were considerably lower (30%) than that of buffer. This is expected due to the presence of NK cells in blood, leading to competition for capture at binding site on the NK-GO chip; reported capture efficiencies are calculated based only on the number of pre-labeled NK-92®MI cells. Linearity plot was also prepared based on NK cell recovered compared to NK cell spiked (Figure 5-2d). In addition, the viability of NK cells was evaluated to ensure that the isolated NK cells are viable and hence can exosomes during the post-capture incubation. Using the live/dead staining assay post-capture, we found that over 70% of the isolated NK cells remained viable before and after short-term incubation (Figure 5-2e).

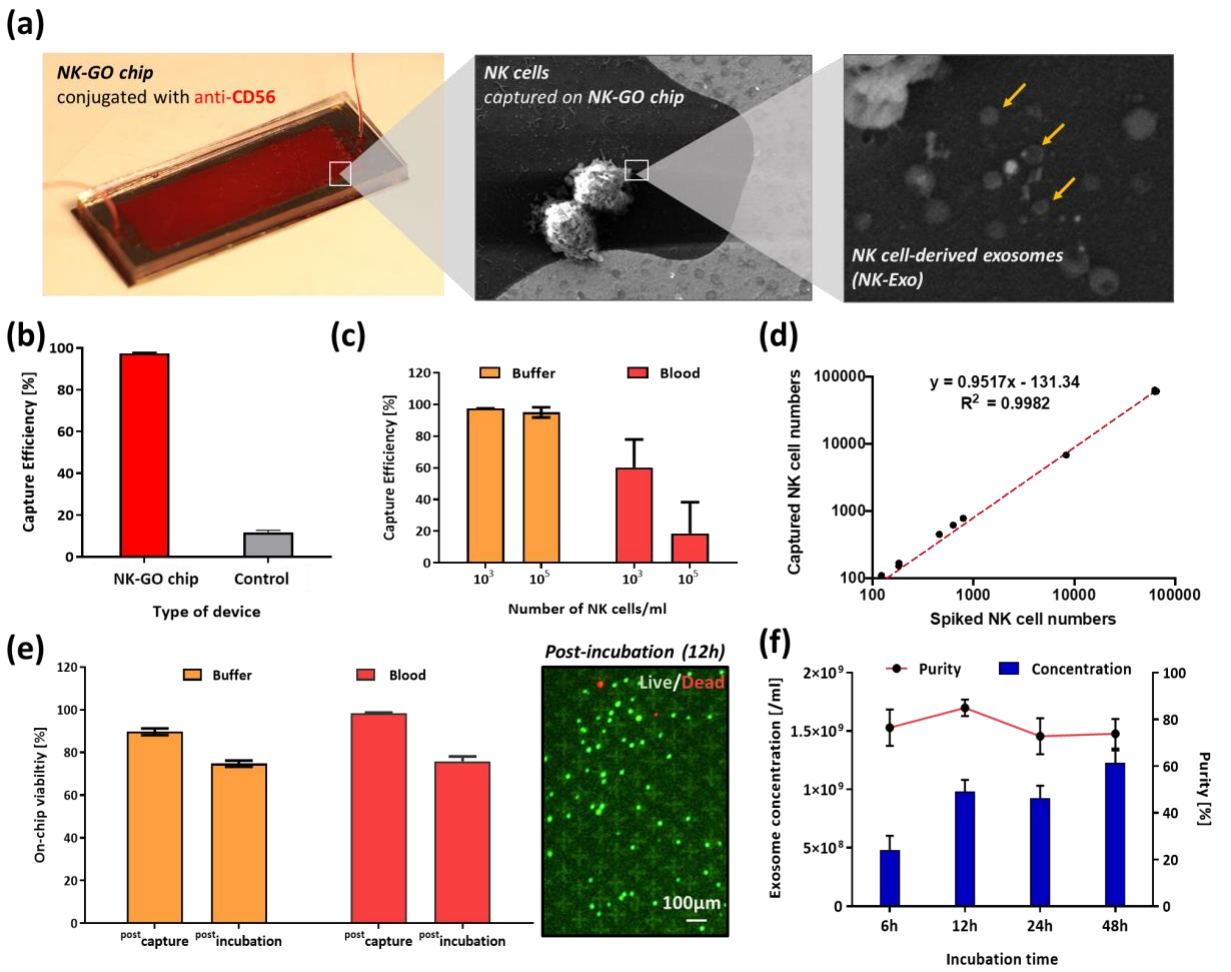

Figure 5-2 On-chip NK cell isolation and in situ exosome biogenesis and harvesting from the isolated NK cells: a) in situ exosome biogenesis from isolated NK cells on NK-GO chip; b) NK cell capturing performance of NK-GO chip compared to control device without antibody conjugation; c) Capture efficiency of the NK-GO chip for different concentrations of NK cells spiked in buffer and blood samples. d) Captured NK cells depending on spiked NK cells in buffer solution. The red dashed line is a linear fit to the data; e) Viability of the isolated NK cells at different time points and conditions (left) and live/dead staining of isolated NK cells on chip after 12-hour incubation; f) Exosome secretion from NK cells depending on incubation times.

5.5.2 On-chip NK exosome biogenesis and harvesting using ExoBead

To evaluate the exosome biogenesis rate from NK cells, we spiked 5,000 NK-92®MI cells into a six-well plate and incubated them for 6, 12, 24, and 48 hours. After incubation, we collected the supernatant from each well and centrifuged them at 300g for 10 minutes to remove cells or cellular debris. The supernatant was then ultracentrifuged using an Airfuge (Beckman, USA) at 100,000xg for 30 minutes to collect NK-Exos. Exosome concentration was determined by

nanoparticle tracking analysis (NTA) and exosome secretion rates showed an increasing trend with increased incubation time (Figure 5-2f). However, exosomal purity, the fraction of exosome sized vesicles out of all vesicles in the sample, was highest at 12 hours of incubation. It is possible that the longer incubations led to cell death and secretion of apoptotic bodies and microvesicles[281–283]. Considering the low O_2 concentration in on-chip conditions compared to cell culture flasks, combined with the goal of establishing a rapid assay, we implemented the protocol of incubating for 12 hours for on-chip NK exosome biogenesis and then NK exosome harvesting.

Using the supernatant from the NK cells isolated on NK-GO chips, we further isolated the exosomes selectively using our ExoBeads (Figure 5-3). Beads without an antibody (anti-CD63) conjugation were prepared as a control (control beads). In order to initially evaluate the exosomal recovery performance, we prepared three different conditions: **(a)** ExoBeads with on-chip NK cell supernatant sample, **(b)** control beads with on-chip NK cell supernatant sample, and **(c)** control beads without supernatant sample. Using these conditions, we isolated and released the bound vesicles from beads and evaluated their concentration by nanoparticle tracking analysis (NTA). As a result, we verified that only the sample prepared with ExoBeads **(a)** had any detectable amount of exosomal vesicles, with more than 83% of purity (Figure 5-3b). Sample from condition **(b)** had the highest purity but its exosomal concentration was considerably lower than that from condition **(a)**. After this quantitative study, we imaged the ExoBeads after capturing exosomes from the on-chip NK cell supernatant samples using scanning electron microscope (SEM). The SEM images of the ExoBeads clearly showed that the beads isolated exosomal vesicles. The sizes of these vesicles ranged 80-130nm (Figure 5-3a). Given the specific antibody used for exosome capture and the size criteria we applied to the resultant, we concluded that our ExoBeads are capable of

isolating exosome-like vesicles from heterogeneous samples containing other subtypes of extracellular vesicles, such as microvesicles and apoptotic bodies.

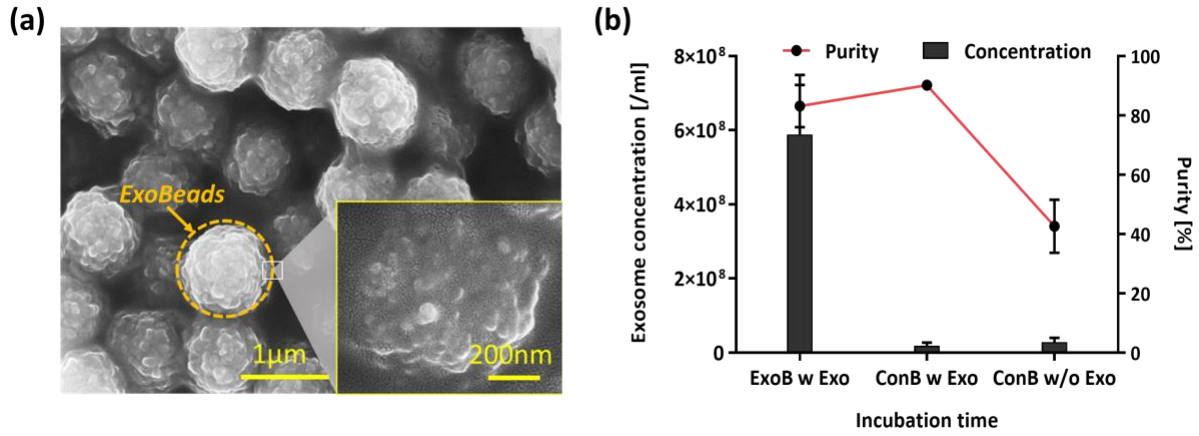

Figure 5-3 ExoBead-based NK exosome isolation and release for therapeutic use: a) Scanning electron microscope image of the isolated exosomal vesicles on ExoBeads with supernatant from NK-GO chip after 12 hours incubation; b) Concentration and purity of exosomal vesicles recovered from NK-92®MI culture supernatant under three different conditions using ExoBeads (ExoB) and control beads (ConB) non-conjugated with antibodies.

5.5.3 Molecular characterization and cytotoxic capabilities of NK cells and NK-Exos using the present microsystem

In order to demonstrate a streamlined microfluidic approach to harvest NK-Exos from clinical samples, we first optimized our platform using NK cell model sample having NK cells spiked in blood (Figure 5-4a). The NK cell model samples were processed until the PBS wash step following our optimized conditions. After PBS wash and application of 300 µL of serum free culture media, the devices were then transferred into 37°C, 5% CO_2 incubator for exosome secretion. After short-term incubation, on-chip supernatant was collected for exosome isolation by flowing serum free media into the device. Following exosome harvesting, we ran 4% PFA or RIPA buffer through the device to fix or lyse captured cells on chip, respectively. Immunofluorescence and western blot were performed to characterize the NK cells captured on chip, while NK exosomes were characterized by western blot. In addition, NK exosomes were investigated for

cellular uptake and potential cancer cell cytotoxicity. On chip staining of captured cells after fixation was conducted using our optimized NK staining panel including CD56 and NCR1. This staining panel was used thoroughly to identify and enumerate NK cell number from limited number of T cell contamination.

A direct comparison of CD56 and FLOT1 expression between captured cell lysate and ExoBead lysate was evaluated by western blot analysis (Figure 5-4b) using a NK-92®MI spike sample. Previously, exosomes derived from NK cells were shown to express NK cell signature protein (CD56)[257], exosomal protein (ALIX, CD63)[137] and lytic protein (FasL and Perforin)[284]. We chose two protein markers, CD56 and FLOT1, for western blot analysis. From our study, CD56 is expressed in both cell lysate and ExoBead lysate, with higher expression in our ExoBead lysate. Furthermore, FLOT1, an exosomal marker, is expressed in isolated ExoBead lysate sample but not cell lysate, which is in alignment with previous studies.

In order to further evaluate NK-Exo uptake by cancer cells, we prepared cancer cells from our in-house patient-derived expanded CTC line[241] and exosomes from NK-92®MI cells. The prepared cells and exosomes were stained using Cellmask and DiO, respectively, and incubated together for 3 hours. After 3 hours, NK cell derived exosomes showed co-localization with cancer cells and within cancer cell membrane (Figure 5-4c). Furthermore, we evaluated the potential cytotoxicity of NK-92®MI derived exosomes. Live/dead assay was conducted at 24 hr, 48 hr, and 72 hr individually, then live cells (stained green) were enumerated. A comparison between the control and NK-Exo treatment wells was shown by immunofluorescence scanning of the whole well (Figure 5-4d), with green fluorescence indicating live cells. In all cases, cell number in control wells increased due to cell proliferation, whereas in the NK exosome treated well, the cancer cells showed a peak number at 48hr but subsequently decreased and dead after 72 hours (Figure 5-4e).

Thus, 72 hours incubation time was applied for preclinical cytotoxicity experiments using NK-Exos from patients.

From this model sample experiment, we identified NK cells on chip using a DAPI+/CD56+/NCR1+ NK cell panel, showed that the recovered NK-Exos from NK cells express CD56 and FLOT1, and that they are able to be taken up by cancer cells and result in cytotoxic cell death of the cancer cells.

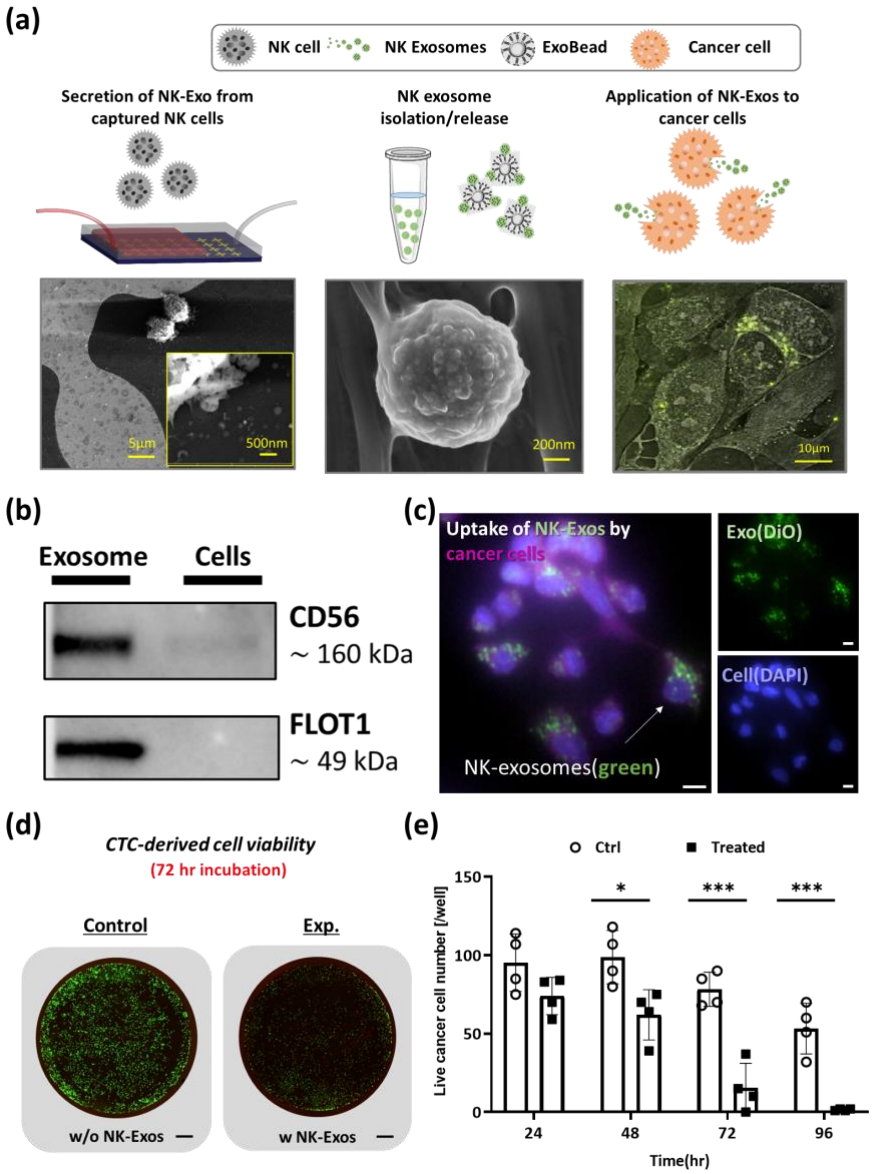

Figure 5-4 Cytotoxicity of NK cell-derived exosomes: a) NK cells (left) and NK exosomes (center) recovered from current platform and theranostic use of NK exosomes with cancer cells (right); b) Western blots

showing the positive expression of CD56 and FLOT1 in exosome lysate using a NK-92®MI spike in buffer sample for on-chip exosome biogenesis. The cell lysate from the same device also shows positive expression for CD56; c) Uptake of NK-92®MI exosomes by in-house CTC-derived cell line. Exosomes are fluorescently labeled in green (FITC) channel, and cell membrane is labeled in violet (Cy5). (Scale bar=10μm); d) Cytotoxicity comparison between control well and NK exosome treated well at 72hr. (Scale bar=800μm); e) In-vitro cytotoxicity experiment using exosomes derived from NK-92®MI. Live cells were quantified through a live/dead assay that was performed 24hours, 48hours, and 72hours after treating cancer cells with or without NK exosomes. Unpaired t-tests (two-tailed) were used to compare the differences between live cell count between NK exosome treated (n = 4) versus control (n = 4). Asterisks denote one of three levels of statistical significance ($p \leq 0.05$; ** $p \leq 0.01$; *** $p \leq 0.001$)*

5.5.4 Preclinical study of NK cell/exosome using clinical specimens

Following experiments with model samples, we validated our approach with whole blood samples collected from non-small cell lung cancer (NSCLC) patients (n=5) and healthy donors (n=2). We used 1-2 mL whole blood sample for each experiment. Whole blood samples were processed through NK-GO chip thoroughly and NK-Exos were harvested from the isolated NK cells. Figure 5-5a shows NK cells from two NSCLC cancer patients stained by the predefined NK staining panel.

Using 4 clinical samples including cancer and healthy donors, we analyzed the exosomal protein expression in NK-cell derived exosomes. The clinical samples, both healthy and patient, indicate sufficiently high levels of FLOT1 and HLA-C after isolation using anti-CD63 magnetic beads (ExoBeads) (Figure 5-5b). In combination, these bands indicate the presence of EVs isolated from our target NK cells.

The cells captured by NK-GO chip expressed CD56 and NCR1 dominantly. The number of NK cells, NK cell-exosome quantity, and their cytotoxicity were evaluated using fluorescent staining, NTA and in-vitro cytotoxicity test, respectively. Cancer patients showed a higher number and concentration of NK cells and NK exosomes, respectively, compared to two healthy donors. (Figure 5-5c). Cancer patients showed higher proportion of NK exosomes among total EV concentration as well (Figure 5-5d). Thus far, various studies showed no significant difference in

overall NK cell concentration in peripheral blood of patients with various forms of cancers and healthy controls. Also, NK cell activity has shown to be decreased in cancer patients, as this may be indicator of susceptibility to disease[285–287]. However, the patients we processed had undergone various cancer treatments, such as immunotherapy and anticancer treatment, results here might differ from previous studies mostly examining an initial state of cancer. The increase in concentration in NK derived EVs shown here may be linked to NK cell activation. Through various signaling pathways, such as dendritic cell activation, the presence of tumors in the body leads to an increase in NK cell activation[288]. While some previous investigations have displayed no noticeable increase in NK cells[285–287] or NK-Exos[284,289] in cancer patients, these studies isolated bulk exosomes in samples, using less-sensitive methods such as ultracentrifugation. In this study, we specifically isolate NK cells, and utilized secreted NK-Exos for following studies. Thus, we believe that the exosomes recovered are NK cell-derived and thus can more accurately define the specific concentration in patients compared to healthy donors. These results are supported by other lymphocytes, such as T cells, which demonstrate significant increases in exosome release once converted from resting to active states[290]. While little investigation has been done into the cause of increased exosome release in activated NK cells or NK cells exposed to cancer, it is likely the correlation between cell activation and exosome release follows that of T cells. Thus, the higher incidence of NK cell activation in the NSCLC patients examined in this study likely leads to the increase in extracellular vesicle concentration in these patients compared to healthy donors, as seen in Figure 5-5d. The NK-Exo secretion rate normalized by the number of NK cells captured on chip also confirmed that NK cells from lung cancer patients secrete more exosomes compared to that of healthy donors (Figure 5-5e).

We also examined the cytotoxic potential of NK-Exos from clinical samples on cancer cells. Same number of NK-Exos from NSCLC cancer patients and healthy donors were applied to in-house patient derived expanded CTC line and incubated for 72 hours. Following incubation, the cells underwent live/dead fluorescent staining and microscopy scanning to identify live cells. As shown in Figure 5-5f, in-house patient-derived expanded CTC line were mostly killed by patient (*LC4*)-derived NK-Exos (center) compared to that without NK-Exos (left) after 72 hours. At the same time, the cancer cells were completely killed by NK-Exos from *HD2* (right). Live cell number per well between control groups (without NK-Exos) and NK-Exo treated groups was significantly different ($p < 0.0001$).

We then compared NK-Exo's cytotoxic capabilities between NSCLC patients and healthy donors (Figure 5-5g). At the same conditions, NK-Exos from healthy donors show higher average specific lysis percentage (98.1%) than that of cancer patients (82.4%). This difference between two groups is significant (p=0.0024). This implies that single NK exosomes from healthy donors have greater cytotoxic potentials; however, as previously noted, the NSCLC patients tested contained significantly more bloodborne NK exosomes than the healthy donors per mL of blood.

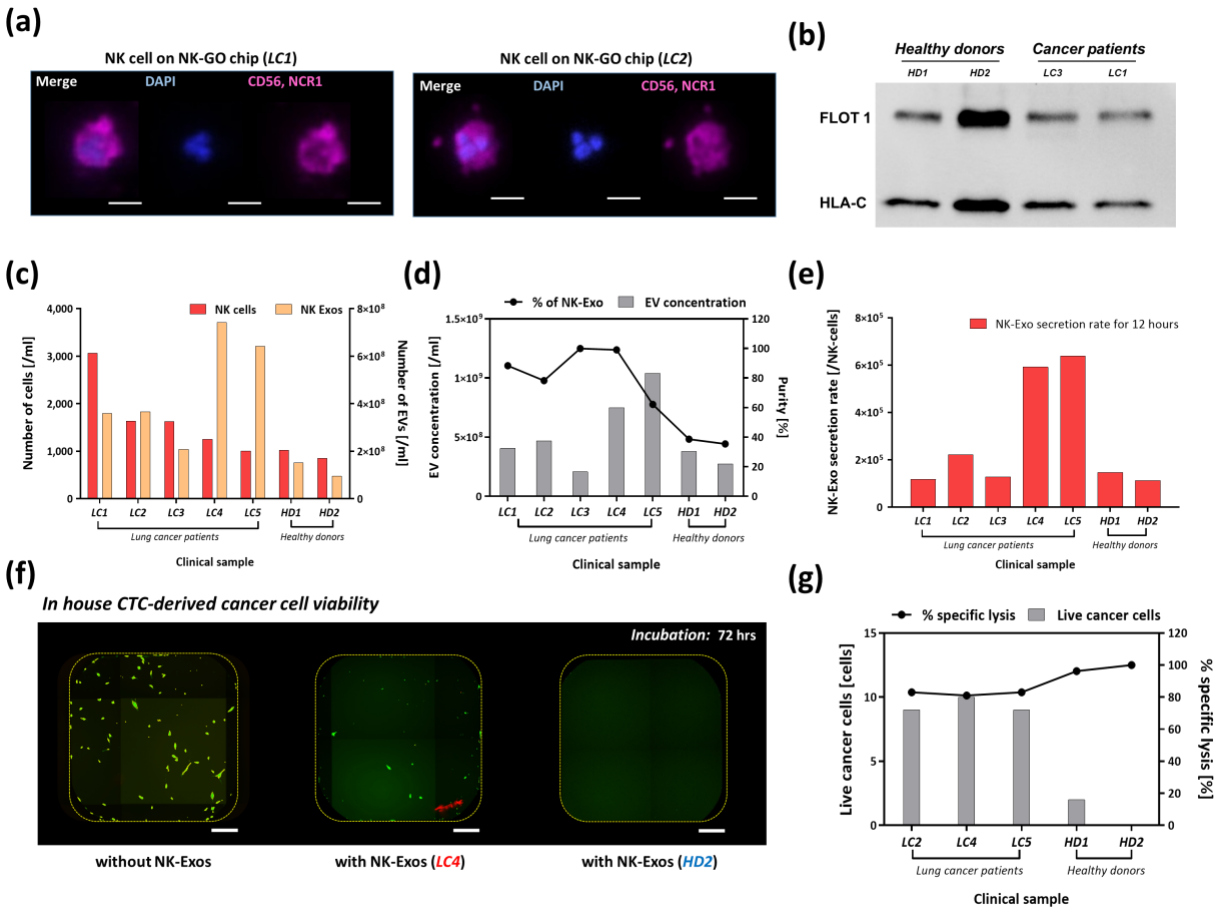

Figure 5-5 Analysis of clinical samples from NSCLC patients using NK-GO microfluidic platform: a) Immunofluorescence image examples of CD56/NCR1 + NK cells captured on NK-GO chip. (Scale bar=20μm); b) Western blot analysis for showing the positive expression of FLOT1 and HLA-C in exosomes from clinical samples; c) Profiling in quantity of NK cells and NK cell-derived exosomes among different patients and healthy individuals observed after 12 hour on-chip incubation; d) Total extracellular vesicle concentration and percentage of exosomes among patient samples and healthy control samples; e) Biogenesis of exosomes quantified as secretion rate of exosomes per captured NK cells for 12 hours; f) Live cancer cell number after 72 hours incubation and percentage of specific lysis between samples from cancer patients and healthy donors (Scale bar=20μm); g) Cytotoxicity of clinical sample driven NK-Exos to CTC-derived cells after 72 hours incubation.

5.5.5 Correlation study between NK cell/exosome and circulating tumor cell using clinical samples

Five peripheral blood samples enrolled in clinical studies of NK cell/exosome were processed through our label-free circulating tumor cell isolation platform to evaluate correlation between CTC numbers and NK cell/exosome concentrations (Figure 5-6). These 5 patients were with metastatic, stage IV NSCLC patients. Among these 5 patients, there were patients with EGFR

mutations (n=3), ROS1 rearrangements (n=1), and ALK fusion (n = 1). After CTC isolation, the pass-through samples from outlet #2 was analyzed for CTCs as described previously[11]. Overall CTC numbers for 5 patients is described in Figure 5-6a. CTCs were detected by immunofluorescence (IF) staining. CTCs were defined and enumerated if they were PanCK+/CD45-/DAPI+. Furthermore, heterogeneous CTC populations, including CTCs expressing epithelial (EpCAM), mesenchymal (Vimentin) or both markers were detected. Figure 5-6b illustrates IF staining of some isolated single/cluster CTCs stained positive for PanCK (red), EpCAM (orange), and Vimentin (Pink), and negative for CD45 (green) to distinguish CTCs from WBCs. We determined that all 5 patients had detectable CTCs with an average of 212 ± 194 total CTCs/mL (Figure 5-6a). Of the captured CTCs among all the patient samples (n=5), 49 ± 54 were CTCs/mL, 10 ± 15 were EpCAM+ CTCs, 88 ± 123 were Vimentin+ CTCs, and 65 ± 91 were double positive CTCs/mL.

After this identification of CTCs, we compared CTC numbers to NK cells detected (Figure 5-6d) and NK Exo concentration (Figure 5-6e). From this correlation study, we discovered a negative correlation (r = - 0.580, P-value = 0.305) between NK cell number and CTC number (Figure 5-6f). This negative correlation between CTC number and NK number has previously been shown in a variety of cancers including NSCLC, breast, colorectal, and prostate cancer[119,120]. It is believed that a decrease in the presence of lymphocytes, including NK cells, provides limited immune response which enables tumor cell growth and allows for an increase in CTC concentration in blood. A relatively strong positive correlation (r = 0.732, P-value = 0.159) was observed between NK-Exo concentration and CTC number. To our knowledge, this finding has not been previously reported. This positive correlation could be a consequence of an increased presence of bloodborne CTCs leading to more circulating NK cells becoming stressed, which

coupled with the proper environment, may induce the stressed NK cells to actively release more exosomes. This concept has been demonstrated with other immune cells, such as T cells, which release increased amounts of exosomes upon stress induced activation brought on by the presence of cancer[291]. Larger investigations need to be done to have significant results. To evaluate individual samples' NK Exo cytotoxicity with consideration of both NK Exo concentration and each NK Exo's cancer cell lysis performance, we prepared relative NK Exo cytotoxicity for 3 samples enrolled in the cytotoxicity study. This relative cytotoxicity value shows close correlation with CTC numbers in blood (Figure 5-6g). This result suggests that, while NK cell number in blood may not in itself affect the total cytotoxicity, the increase of NK-Exos in bloodborne concentration brought about by NK activation with abundant CTCs greatly increases its anti-tumor capabilities.

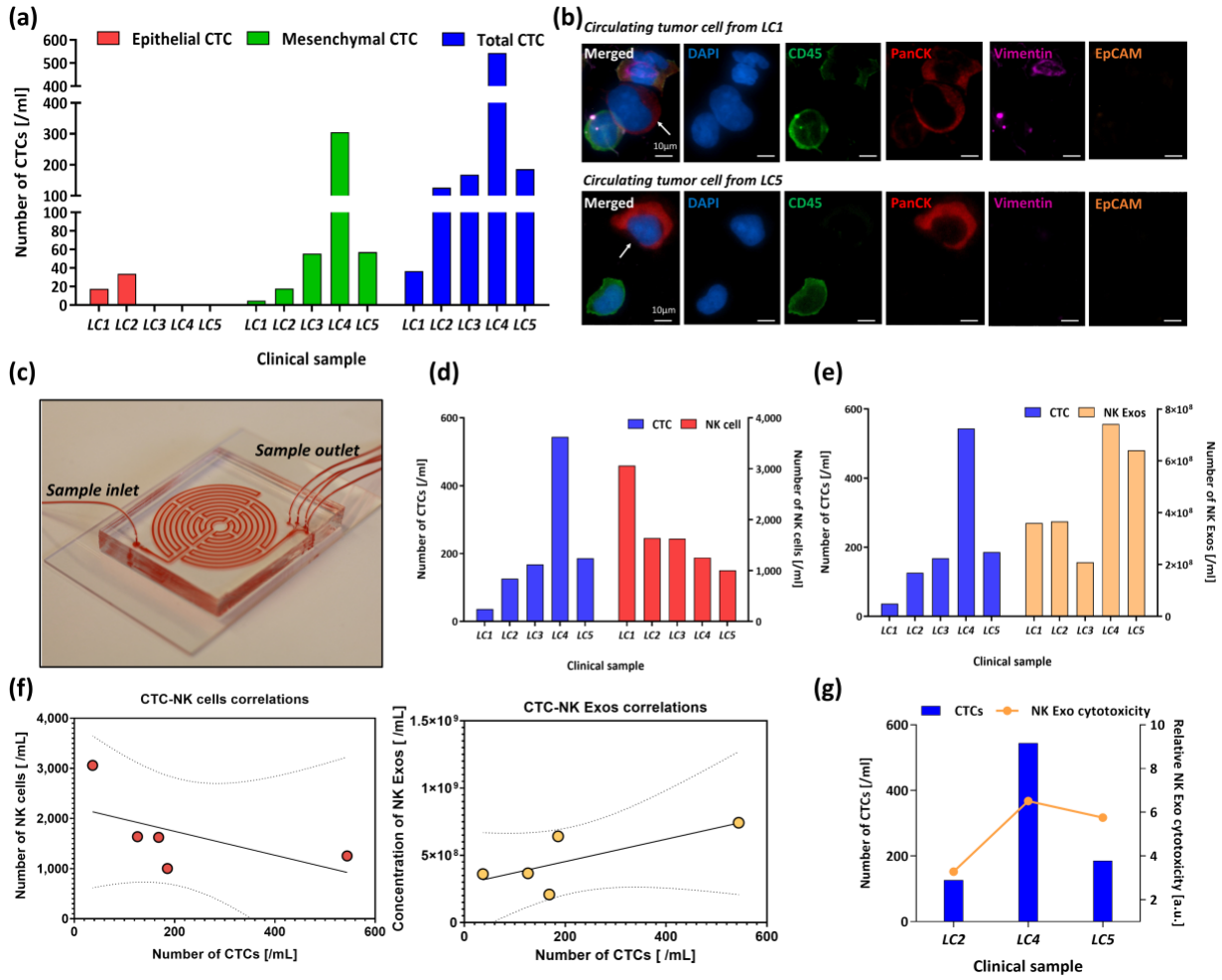

Figure 5-6 Profiling of circulating tumor cell (CTC) populations in non-small cell lung cancer (NSCLC) patients and correlation with NK cells and NK cell-derived exosomes: a) Profiling in quantity of epithelial-, mesenchymal-, and total CTCs between NSCLC patients; b) Representative images of CTCs recovered from the patients; c) Image of label free CTC isolation platform; d) Comparison between total CTC and NK cell number; e) Comparison between total CTC and NK exosome concentration; f) Correlation between CTC-NK cell (left, r = - 0.580, P-value = 0.305) or CTC-NK Exo (right, r = 0.732, P-value = 0.159); g) Correlation between relative total cytotoxicity of NK Exos and total CTC number in samples.

5.6 Discussion

As a proof of concept, here we have demonstrated the possibility of a streamlined microfluidic approach to on-chip biogenesis and harvest of natural killer cell-derived exosomes through comprehensive studies using NK cell lines and clinical samples from lung cancer patients. In the future, NK cell-derived exosomes may find a complementary use as both diagnosis and therapeutic tools for patients with cancer. Given the burgeoning interest in this field, it is important

to fill the technical gaps pertaining to exosome isolation, harvest and expansion. We hereby present a highly sensitive method to isolate NK exosomes derived from viable NK cells using our NK-GO chip. Using the NK-GO chip, we showed that patients with non-small cell lung cancer presented with high numbers of NK and NK cell-derived exosomes compared with healthy donors. These concentrations were further correlated with numbers of bloodborne circulating tumor cell in each sample, and we found that a sample having a higher number of CTCs shows lower NK cells but may lead to a greater secretion of NK cell-derived exosomes. Furthermore, we were able to demonstrate functional relevance of NK cell-derived exosomes as shown by their cytotoxic effects against in-house patient derived expanded CTC line. The immediate future studies can focus on doing the similar analysis with large cohort of patient samples as well as healthy donors to make more robust comparisons. Future studies will be needed to further validate our initial observations and how best to use this to inform clinical needs. Given the critical diagnostic value of CTCs in cancer, immune phenotyping associated immune cells such as NKs may complement and enhance their predictive potential of patient prognosis. Moreover, such a precise isolation of cells may also help us investigate interactions between CTCs and immune cells in circulation, enabling the understanding of potential metastasis-specific immune surveillance mechanisms. We expect that our versatile microfluidic platform can provide a foundation to be used for hitherto undiscovered roles of exosomes in cancer and other disease states.

Chapter 6 Conclusions

6.1 Research summary

This thesis can help advance research in the field by answering the two questions. First, how can CTC metrics help inform clinical treatment studies? I examined this question in depth using the GO chip-based platform in Chapters 2 and 3 regarding bladder, lung, and liver cancer translational studies. Second, how can we target cancer metastasis through CTCs? In Chapters 4 and 5, I hypothesized the critical role of NK cells in eliminating CTCs based on existing literature, and I presented workflows to investigate the CTC–NK interaction and develop new NK-based therapies. My findings strongly demonstrate the value of CTCs as biomarkers and therapeutic targets in clinical cancer management, especially in bladder, lung, and liver cancer.

6.1.1 CTC profiling using the GO platform in metastatic bladder cancer

CellSearch^{TM} technology is mainly used to detect CTCs in bladder cancer. But it has a low detection rate and limited molecular profiling applications. Based on previous studies using the GO platform from our lab[20,292], I optimized the GO platform for bladder cancer and presented a protein and RNA co-analysis workflow. I first successfully identified CTCs using protein immunofluorescent staining from a cohort of 16 bladder-cancer-patient blood samples. I found that the CTC concentrations in patients with metastatic disease were significantly higher than those in healthy controls and in patients with no evidence of disease at the time of blood draw. Patients who had higher CTC counts/mL (> 3 CTCs/mL) potentially had shorter survival times. This result is consistent with those of studies that used other technologies[179]. I also used multiplex

immunofluorescent staining to investigate the expression of EGFR, HER-2, CD31, and ADAM15 on isolated CTCs. I observed positive staining for all of these invasive markers in a subset of CTCs. When correlating these expressions to survival data, patients who had positive staining for most of these markers had shorter overall survival rates.

On the RNA level, I showed for the first time the feasibility of profiling GO chip-isolated CTCs using bulk amplicon-based targeted transcriptome sequencing. I then developed a customized bioinformatics pipeline to perform differential gene-expression analysis while removing variance in contaminated WBCs. By comparing patients with and without disease at the time of blood draw, I observed the upregulation of many well-studied metastasis-related signatures, such as KRT5, KRT10, MMP-2, MMP-13, AKR1C2, GATM, SYTL1, and CAPN1, in patients with metastatic disease. This demonstrates the ability of the GO chip and targeted sequencing workflow to capture the metastatic signatures of bladder cancer. Although these findings will need to be further confirmed in a larger cohort, this study showcases the potential of the GO chip and bioinformatics pipeline.

6.1.2 CTC profiling in longitudinal clinical studies in NSCLC and HCC

Analyzing CTCs in longitudinal studies could provide unique treatment-monitoring insights and enable early prediction of patient outcomes. In the current GO chip workflow, there is an unmet need to develop an analytical workflow to handle data sets with time-point information. In Chapter 3, I presented the customized analytical pipeline to correlate CTC count metrics and RNA microarray data with patient progression-free survival. I first demonstrated this pipeline in locally advanced (stage III) NSCLC patients treated with chemoradiation and immunotherapy.

First, I tested multiple CTC metrics as biomarkers to predict progression-free survival. I found that CTC counts at single time points did not correlate with progression-free survival time.

For patients who received durvalumab immunotherapy, a high PD-L1+ CTC subpopulation percentage at single time points may be associated with shorter PFS. Importantly, I observed a significant correlation (P value = 0.0076) with longer PFS in patients who had a large decrease in CTC percentage (> 75%) after 4 weeks of chemoradiation.

Second, I developed custom bioinformatic workflows using open-source packages for microarray data analysis. Through the differential gene-expression analyses, I observed significantly upregulated genes between pre-TX and week 4 that corresponded to phenotypes that were invasive, proliferative, and potentially immune-evasive. I also identified genes whose expressions at single points significantly predicted PFS. From these predictive genes, I calculated principal components to showcase the predictive power of these genes.

Lastly, I applied this workflow analysis to other clinical studies in HCC and established a workflow to remove contaminated WBC signals in microarray data. I found 85 significantly downregulated genes in the HCC study, comparing CTC samples from after the first cycle of chemoradiation to pretreatment samples. Twenty-one of these downregulated genes were found to relate to liver function, which could indicate the decrease in CTCs and liver function during treatment.

In summary, the findings in Chapter 2 and 3 showcase the prognostic value of CTC counts and gene expression profiles. The presence of and increase in CTC counts during treatment are signs of minimal residual disease and predict worse patient outcome. The GO platform-based CTC isolation and clinical and RNA analysis workflow developed in these first 2 chapters could be applied to future CTC clinical studies at large.

6.1.3 CTCs' sensitivity to NK cells

The study of therapeutic targeting and the immune interaction of CTCs is still an underdeveloped field. Based on the existing literature on NK cells' role in controlling metastasis, I hypothesize that CTCs would present a NK-sensitive phenotype. In Chapter 4, I presented a series of methods to evaluate and quantify the NK sensitivity in patient-derived CTCs on a single-cell level. I observed NK–CTC cytotoxicity through live-cell imaging and quantified this cytotoxicity through dose-response model fitting. For in-house derived CTC lines, CTC-Lu1 and CTC-Lu2, over 80% of cancer cells were killed through NK-mediated cytotoxicity. These two cell lines also had the highest sensitivity compared to the other 5 lung cancer cell lines tested.

To further investigate the molecular basis of the NK–CTC interaction, I profiled fresh and expanded patient-derived CTCs for NK-related ligands using quantitative immunofluorescence and bulk and single-cell RNA sequencing. I presented a novel method to calculate NK and EMT scores to represent cancer-cell molecular profiles, and I found a strong correlation between these 2 scores in my data set, including the CTC lines and data from 80 other CCLE lung cell lines. This indicates that patient-derived CTCs, especially those with mesenchymal phenotypes, could be highly sensitive to NK-mediated killing and that patients could benefit from NK-cell-based therapies to control metastasis. Additionally, I established a single-cell analysis workflow to identify epithelial and mesenchymal CTC populations utilizing the EMT score. This workflow could be applied to future single-cell profiling CTC studies to further investigate the NK–CTC interaction on a single-cell level. Taken together, this study demonstrated CTCs' NK sensitivity from multiple different angles and developed widely applicable assays and analysis workflows.

6.1.4 Development of NK exosome biogenesis workflow and their cytotoxicity against CTCs

Thus far, over 150 NK-cell-based immunotherapy clinical trials have been performed and applied to various cancers, including ovarian, breast[293], and non-small-cell lung cancer[294].

However, NK-cell-based therapies struggle with the ability to deliver adequate numbers of NK cells to tumors due to limited infiltration capabilities. To overcome this, I proposed the use of NK-cell-derived exosomes as therapeutic agents instead. In Chapter 5, I presented an integrated and rapid workflow to harvest NK-cell-derived exosomes using the GO platform and ExoBeads. I isolated viable NK cells and harvested NK exosomes from model samples, 5 NSCLC patients, and 2 healthy donors. Through the co-analysis of CTCs from the same blood samples, I found that NSCLC patients had high numbers of NK cells and NK exosomes compared to healthy donors, and these concentrations negatively and positively correlated with CTC numbers, respectively. I also demonstrated that the NK exosomes harvested from the NK-GO chip had a cytotoxic effect on CTCs, and I observed over 80% cell death compared to controls after 72 hours of incubation. This versatile system can be used for patient-specific NK-based immunotherapies along with CTCs for potential prognostic and diagnostic applications.

6.2 Limitation and future directions

6.2.1 The improvement and application of microfluidics-based CTC workflow

In chapters 2 and 3 of this thesis I drew upon multiple clinical studies to discuss the prognostic and treatment-monitoring values of CTCs using the versatile GO platform. These studies, however, were limited by their small patient sizes and need to be validated in larger cohorts. To achieve this, as I discuss below, there are several aspects in the profiling workflow that can be improved.

6.2.1.1 Pre-analytical considerations and study design

Because of the unstable and apoptotic nature of CTCs[295,296], it is generally recommended that blood samples using K2EDTA tubes for CTC analysis should be processed within 4 hours after blood draw[297]. This limits most CTC studies to single-center cohorts, resulting in limited and

undiversified patient pools. In this thesis, most studies were conducted within the Michigan medicine system, except for one multicenter study in Chapter 3, in which NSCLC patients went through pembrolizumab in combination with platinum-based doublet chemotherapy. The samples were shipped in K2EDTA tubes and on ice, and the clustering and bursting of WBCs caused device leak and sample loss in some cases. There are cell-preserving blood tubes currently available on the market, such as CellSave tubes (Veridex) and BCT tubes (Streck). However, these tubes contain fixatives for cellular proteins, and the RNA materials and viability are not preserved. Thus, development of efficient preservation solutions for CTCs is urgently needed to conduct larger studies and advance CTC-based liquid biopsy tests in the clinic[298].

In addition, 2 major aspects need to be considered when choosing an appropriate isolation technology: clinical study design and downstream applications. A thorough literature review is needed to determine the expected size distribution and cell-surface-marker expression level. Farace et al. performed a direct comparison on the same cohort of metastatic breast, prostate, and lung cancer patients using CellSearch and ISET[299]. CTC counts were higher using CellSearch™ for metastatic breast cancer patients; they were higher using the ISET assay for metastatic lung and prostate cancer patients. In another comparison using epithelial and mesenchymal cell-line-derived mock samples, the Parsortix™ system showed superior capture of mesenchymal cells compared to the CellSearch™ system[34]. There was no significant difference in epithelial cell capture between the 2 technologies.

The second consideration is whether the device is compatible with downstream assays. Most immunoaffinity-based devices immobilize captured CTCs so that molecular materials will have to be extracted from bulk samples. The physical property-based technologies often have cells in solution, which makes single-cell partitioning and single-cell analysis possible. The GO chip

workflow developed in Chapters 2 and 3 does not currently have the capability to release captured cells; thus, it is compatible only with bulk isolation and analysis of the RNA materials.

6.2.1.2 Incorporating artificial intelligence in CTC identification

At the end of the GO platform workflow, CTCs are manually identified using immunofluorescent staining, specifically the positive staining of cytokeratin and negative staining of CD45. This process is time-consuming, prone to error, and could be easily influenced by environmental conditions like computer screen brightness and room lighting. Recent studies have been leveraging AI to improve this counting process[300,301]. Zeune et al. developed an open-source CTC scoring tool to help researchers reach consensus in CTC counting[300]. The tool is based on scoring from 15 independent reviewers from 6 different institutes. They also used a deep-learning approach to automate the whole process. Another interesting tool to separate morphologically similar cell types using machine learning was developed by Ota et al[301]. Cells were labeled with single-color fluorophore and classified based on cytoplasm morphology. The researchers successfully identified different cell populations from a mixture of 2 breast cancer cell lines and cancer cell lines with PBMCs. For future CTC studies, the advancements in computer-aided biomedical image analysis and CTC identification will not only enable efficient workflow and larger multicenter studies, but also drive the standardization of CTC-based liquid biopsy assays.

In addition, one of the challenges in developing automated machine learning tools is the lack of large high-resolution and high-quality data sets for algorithm training. Increasing the accessibility and transparency of raw CTC images and data sets could be highly beneficial. Moreover, standardizing the definition of CTCs and cutoffs in clinical analysis between different institutions is also an important future step. Some discussions and efforts have been initiated. For

example, Zhao et al. constructed an easy-to-use database for mRNA and lncRNA expression data from CTCs in 7 cancer types and 320 studies[302].

6.2.2 Further investigation of the NK–CTC interaction and NK-based therapeutic potentials

In chapters 4 and 5 I showed preliminary evidence for the potential use of NK-cell-based therapeutics against CTCs and cancer metastasis. However, there is still a long way to go. These findings need to be translated to a clinical setting to advance the clinical utilization of NK therapies. In the following sections, I discuss some aspects that could be further explored to uncover the full picture of NK–CTC interaction and improve NK-based therapies.

6.2.2.1 Co-isolation and analysis of the blood microenvironment

In Chapter 4, I demonstrated the NK sensitivity of CTCs through in vitro experiments with an NK leukemia cell line, NK92-MI. Based on my findings, one of the next logical research questions to ask is, why are a patient's existing NK cells not eliminating CTCs already? To better understand the immune evasion mechanism and find new drug targets, future studies need to be comprehensively conducted in the metastatic blood microenvironment. Several immune evasion mechanisms have been hypothesized for CTCs[303]. For example, one of the most-studied mechanisms involves platelet–CTC adhesion. Platelets can confer NK-inhibitory signals like MHC class I molecules onto CTCs to prevent NK-mediated killing[304]. In addition, platelets can secrete TGF-β, which downregulates the NK receptor NKG2D to impair NK cell function[305]. Discussions and developments on antiplatelet therapies are currently ongoing[306].

6.2.2.2 Improvement of NK sensitivity prediction score: Incorporating NK receptor expressions

Since CTC-evading mechanisms are highly heterogenous among patients, it is critical to develop predictive biomarkers through assessing a patient's blood microenvironment, including CTCs. Another exciting finding in Chapter 4 was enabled by calculating a predicted NK-sensitivity

score using NK-related ligands on cancer-cell lines. As expected, the cells with NK-sensitive phenotypes showed a higher prediction score; however, NK-based cytotoxicity does not solely depend on the ligand expressions of cancer cells. The NK-cell population in cancer patients has been often reported as decreased or impaired. Thus, co-profiling the receptors on NK cells in the same patients or from the adoptive transfer products and incorporating those expressions in the NK-score calculation will provide a better biomarker metric. The development of single-cell profiling technologies, such as the 10X Chromium system, makes it highly possible to profile multiple cell populations on the transcriptomic and genomic levels. I explored this technology's use in Chapter 4; however, more research is needed to draw meaningful conclusions.

6.2.2.3 Improving NK exosome-based therapies: Study of exosome homing effect

The NK exosomes derived in Chapter 5 showed a promising a cytotoxicity effect against our in-house derived CTC lines. This was again tested only in ex vivo cell-line models. When applying these exosome-based therapies to in vivo models or human patients, optimizing the biological distribution and achieving a high enough concentration of the target cancer cells are the inevitable next steps. Excitingly, recent studies have found that exosomes exert organotropism properties[307]. In other words, exosomes can be preferentially uptaken by specific organs in the body.

To test this phenomenon in lung cancer, I administered fluorescently labeled exosomes derived from the lung cancer cell line, H1650, into breast cancer cells (MCF7) and bladder cancer cells (UC-5). The concentrations of exosomes and cells between different cell lines are normalized to same exosome concentrations per cell. After 18 to 20 hours of incubation (same time between different conditions), the cells were washed and assessed for fluorescence. Shown in Figure 6-1, I observed the highest fluorescent intensity in the H1650 cells, indicating a potential preferential

uptake by exosome parental cells. The investigation of the molecular mechanisms of such exosomal tropisms is still ongoing and could potentially enable the engineering of exosomes, especially NK exosomes, to specifically target cancer cells.

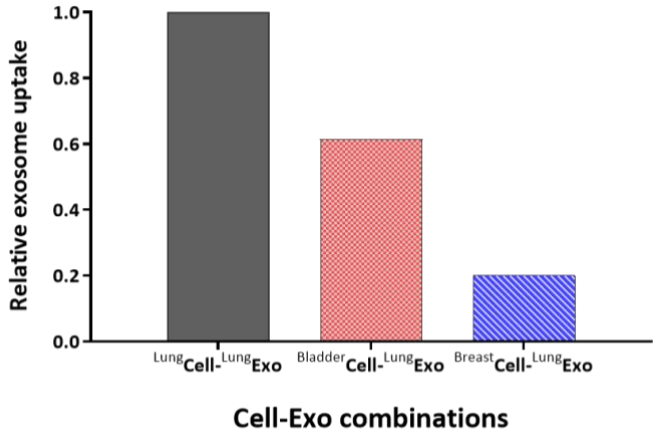

Figure 6-1 Specific uptake of lung cancer exosomes by 3 different cells from different organs.

6.3 Conclusions

My thesis work demonstrated the translational potential of CTCs in liquid biopsy as a biomarker and a therapeutic target for cancer metastasis. I developed microfluidic characterization and analysis workflows on protein and RNA level for CTCs isolated from single time point bladder cancer patient cohorts (Chapter 2), and multi-time point lung cancer patient cohorts (Chapter 3). I then investigated the interaction between NK cells and CTCs and developed single-cell based workflows to characterize NK-related ligands on patient-derived CTCs (Chapter 4). Lastly, I explored NK cell derived exosomes as potential therapeutic reagents to target CTCs (Chapter 5). Taken together, CTCs can be used as part of liquid biopsy to monitor and predict cancer patient disease status and outcome and can be potentially a therapeutic target for NK based therapies.

Appendix

Appendix A. Gene lists found in the RDART study (Chapter 3)

Table 8 Genes that predict progression-free survival at a single time point in the RDART study

pre-TX genes					
CD248	FEZF2	GALNT9	SLC7A9	GASK1A	IDH2
LRRC75B	FAM86B2	CSPG4P1Y	C12orf56	GAREM2	NPM1
PHLDA1	DMRTA1	C11orf24	KIF17	TDRP	PDHB
ST6GALNAC5	PDGFB	OR6C76	STAR	KRBOX4	DNAJB6
LRRC14	SELENOO	TCF21	CYP1A2	RMI2	ZNF439
MBD1	SLC47A2	ENDOV	SURF2	MAS1	SYT11
NKX2.3	ZNF433	CD1E	FZD7	OR2Z1	SDHA
CHGB	EXO1	SPON1	UNC5B	BRINP1	MRPL32
UPK3A	GTF2H4	IL36A	PIP4K2B	C7orf25	PPIAP30
CDC37L1	LRRTM4	ZNF469	RPP25L	SERPINB12	GORASP1
C7orf69	MYT1	FLJ33534	PKD2L2	DUOXA2	ERLEC1
DAZL	KIFC2	ATP10B	BRINP2	C1S	RNASEH2A
NUDT15	CAPS	PIF1	PACC1	CCDC68	ICOS
IL13	SPOCK3	VCX2	RAB38	RNASE9	PTCD3
C1orf35	ASPHD1	CLEC14A	IHO1	SLC27A3	UBE2J2
CTRB1	ZNF205	MAP3K13	INSRR	PCCA	FANCF
MST1R	TIGD6	ERVV.1	ARIH2	GDPGP1	TSHR
SYT14	ZNF517	FAM71C	HCP5	TCEAL2	HMGN5
ITPRIPL2	LINC00482	SLIT1	TEX33	PPM1A	WFDC9
PTTG1	SPEGNB	CPN1	WDR38	PSMA3.AS1	H3.5
TUSC2	ALDH7A1	DTX1	CHD5	VPS37A	LIN7B
KRTAP20.4	MUTYH	PTPRT	SLC2A1	CRYL1	
TMEM179	ARHGEF4	TMEM150B	NCKIPSD	MAPK8	
PTRH1	KCNB1	TAGLN	ACOX2	MPC1	
MYH13	BMPER	KBTBD11	PAEP	C1orf43	
Week 4 genes					
GPT	LIMK1	VSTM4	THNSL2	OR1S2	RPP21
HTRA4	BCS1L	ELMO1	SMG7	TLR7	CDT1
BPIFB6	SGCZ	NCBP3	CCL23	SWT1	EVI5L
FYB1	BANF2	WNT11	OR5A1	TBC1D23	KIF21A
HROB	TMEM132E	CTPS2	ASAP3	RFX5	S1PR5
VPS37D	PSG6	GOLGA6L1	TAAR5	MPDU1	DMRT1
VTCN1	AQP11	PPIP5K1	GPAT2	ANKRD52	CELA2A
DPYSL3	PITX2	CDON	KYAT1	PRKCI	FAM162B
CD1B	CLDN10	PROSER3	RGS9	SLC25A26	TMEM175

CES1	LMO1	QRFPR	IL2RG	PTPRCAP	RHOF
GOLGA6L9	OR6B3	ADORA1	ZBTB49	PHC3	TAS2R4
AMPD3	F2RL1	KCNS2	SLC25A35	TAPBPL	TCEAL3
CEACAM6	SLC25A45	PTTG2	SERPINA11	PLCXD1	ZNF615
CNTNAP2	JPH3	BAMBI	ZKSCAN1	SLC39A10	FOXR2
CCDC174	COLCA2	SNX33	ZNF224	LRATD2	SKA2
APPBP2	CCSAP	LY6G5C	CHN1	SCD	ZNF627
GCKR	SPATA31A1	WDR53	MANSC1	ELAC2	RWDD2A
FCGR2A	ADSS1	UBE2O	PSMD11	ZNF827	MYL1
DMAC2	SDCBP	LINC00654	SIAE	RBM48	AKR1C4
TMEM98	SYT6	ZNF773	ERMAP	SEPSECS	LINC02877
GEMIN5	HJURP	KLLN	ANKRD55	ZNF84	SPOCK2
H3C13	POMGNT2	EFEMP1	DDX11	DOCK9	ENOX2
GOLGA8R	CREB5	HEPHL1	OR10C1	MRPL54	PDGFD
NPY4R	RABGGTA	NDC80	ZNF346	SARM1	BEX2
OR52J3					
Week 10 genes					
PAFAH2	TP53	ACBD3	CREB3	GNPNAT1	NUP58
ELFN2	CD40	HEATR3	ANXA4	RNF6	DHX34
SALL3	INTS9	FH	LOC100130691	ZNF121	SCAMP2
TRIM41	P2RY10	TBCD	DYNC1I2	ANKMY2	SOGA1
ANP32E	PPIB	JDP2	SLC25A43	TTN	TM9SF3
JAKMIP3	BNIP1	ALG14	CASP6	GALNT7	PCBP1
TRIM26	EIF5AL1	ZNF3	AGMO	RIOK1	TNF
CORO1B	NFKB1	AZU1	BCL7A	OSBPL1A	ATP1B1
WDR24	BPNT1	WDR7	ZNF268	UCHL5	LRRC3C
MTOR	ZDHHC4	ACSF2	NAA30	OR4P4	ALPK2
TSTD3	LRRC40	HYLS1	ZNF25	NKTR	GABRA4
TMEM150B	ASNSD1	GDPD1	RTCB	THUMPD1	POF1B

Bibliography

1. Hosseini H, Obradović MMS, Hoffmann M, et al. Early dissemination seeds metastasis in breast cancer. *Nature*. 2016;540(7634):552-558. doi:10.1038/nature20785

2. Hu Z, Curtis C. Looking backward in time to define the chronology of metastasis. *Nat Commun*. 2020;11(1):3213. doi:10.1038/s41467-020-16995-y

3. Massagué J, Obenauf AC. Metastatic colonization by circulating tumour cells. *Nature*. 2016;529(7586):298-306. doi:10.1038/nature17038

4. Luzzi KJ, MacDonald IC, Schmidt EE, et al. Multistep nature of metastatic inefficiency: dormancy of solitary cells after successful extravasation and limited survival of early micrometastases. *Am J Pathol*. 1998;153(3):865-873. doi:10.1016/S0002-9440(10)65628-3

5. Faltas B. Cornering metastases: therapeutic targeting of circulating tumor cells and stem cells . *Front Oncol* . 2012;2. https://www.frontiersin.org/articles/10.3389/fonc.2012.00068

6. Chambers AF, MacDonald IC, Schmidt EE, Morris VL, Groom ACBTA in CR. Clinical targets for anti-metastasis therapy. In: Vol 79. Academic Press; 2000:91-121. doi:https://doi.org/10.1016/S0065-230X(00)79003-8

7. Steeg PS, Theodorescu D. Metastasis: a therapeutic target for cancer. *Nat Clin Pract Oncol*. 2008;5(4):206-219. doi:10.1038/ncponc1066

8. Rolfo C, Russo A. Liquid biopsy for early stage lung cancer moves ever closer. *Nat Rev Clin Oncol*. 2020;17(9):523-524. doi:10.1038/s41571-020-0393-z

9. Ashworth TR. A case of cancer in which cells similar to those in the tumours were seen in the blood after death. *Aust Med J*. 1869;14:146.

10. Shishido SN, Carlsson A, Nieva J, et al. Circulating tumor cells as a response monitor in stage IV non-small cell lung cancer. *J Transl Med*. 2019;17(1):1-14. doi:10.1186/s12967-019-2035-8

11. Zeinali M, Lee M, Nadhan A, et al. High-Throughput Label-Free Isolation of Heterogeneous Circulating Tumor Cells and CTC Clusters from Non-Small-Cell Lung Cancer Patients. *Cancers* . 2020;12(1):1-17. doi:10.3390/cancers12010127

12. Mendelaar PAJ, Kraan J, Van M, et al. Defining the dimensions of circulating tumor cells

in a large series of breast, prostate, colon, and bladder cancer patients. *Mol Oncol*. 2021;15(1):116-125. doi:https://doi.org/10.1002/1878-0261.12802

13. Hodgkinson CL, Morrow CJ, Li Y, et al. Tumorigenicity and genetic profiling of circulating tumor cells in small-cell lung cancer. *Nat Med*. 2014;20(8):897-903. doi:10.1038/nm.3600

14. Miller MC, Doyle G V, Terstappen LWMM. Significance of circulating tumor cells detected by the CellSearch system in patients with metastatic breast colorectal and prostate cancer. *J Oncol*. 2010;2010.

15. Hayes DF, Cristofanilli M, Budd GT, et al. Circulating Tumor Cells at Each Follow-up Time Point during Therapy of Metastatic Breast Cancer Patients Predict Progression-Free and Overall Survival. *Clin Cancer Res*. 2006;12(14):4218-4224. doi:10.1158/1078-0432.CCR-05-2821

16. Wang L, Balasubramanian P, Chen AP, Kummar S, Evrard YA, Kinders RJ. Promise and limits of the CellSearch platform for evaluating pharmacodynamics in circulating tumor cells. *Semin Oncol*. 2016;43(4):464-475. doi:https://doi.org/10.1053/j.seminoncol.2016.06.004

17. Andree KC, van Dalum G, Terstappen LWMM. Challenges in circulating tumor cell detection by the CellSearch system. *Mol Oncol*. 2016;10(3):395-407. doi:https://doi.org/10.1016/j.molonc.2015.12.002

18. Nagrath S, Sequist L V, Maheswaran S, et al. Isolation of rare circulating tumour cells in cancer patients by microchip technology. *Nature*. 2007;450(7173):1235-1239. doi:10.1038/nature06385

19. Pecot C V, Bischoff FZ, Mayer JA, et al. A Novel Platform for Detection of CK+ and CK− CTCs. *Cancer Discov*. 2011;1(7):580-586. doi:10.1158/2159-8290.CD-11-0215

20. Yoon HJ, Kim TH, Zhang Z, et al. Sensitive capture of circulating tumour cells by functionalized graphene oxide nanosheets. *Nat Nanotechnol*. 2013;8(10):735-741. doi:10.1038/nnano.2013.194

21. Kim TH, Yoon HJ, Fouladdel S, et al. Characterizing circulating tumor cells isolated from metastatic breast cancer patients using graphene oxide based microfluidic assay. *Adv Biosyst*. 2019;3(2):1800278.

22. Kozminsky M, Fouladdel S, Chung J, et al. Detection of CTC clusters and a dedifferentiated RNA-expression survival signature in prostate cancer. *Adv Sci*. 2019;6(2):1801254.

23. Wang Y, Kim TH, Fouladdel S, et al. PD-L1 Expression in Circulating Tumor Cells Increases during Radio(chemo)therapy and Indicates Poor Prognosis in Non-small Cell Lung Cancer. *Sci Rep*. 2019;9(1):566. doi:10.1038/s41598-018-36096-7

24. Vona G, Sabile A, Louha M, et al. Isolation by Size of Epithelial Tumor Cells: A New Method for the Immunomorphological and Molecular Characterization of Circulating

Tumor Cells. *Am J Pathol*. 2000;156(1):57-63. doi:https://doi.org/10.1016/S0002-9440(10)64706-2

25. Vona G, Estepa L, Béroud C, et al. Impact of cytomorphological detection of circulating tumor cells in patients with liver cancer. *Hepatology*. 2004;39(3):792-797. doi:https://doi.org/10.1002/hep.20091

26. ANGLE plc. ANGLE ACHIEVES WORLD FIRST WITH FDA CLEARANCE FOR ITS PARSORTIX SYSTEM [Press release]. Published 2022. Accessed July 5, 2022. https://polaris.brighterir.com/public/angle_plc/news/rns/story/w1ygp3w

27. Xu L, Mao X, Imrali A, et al. Optimization and evaluation of a novel size based circulating tumor cell isolation system. *PLoS One*. 2015;10(9):1-23. doi:10.1371/journal.pone.0138032

28. Xu L, Mao X, Guo T, et al. The Novel Association of Circulating Tumor Cells and Circulating Megakaryocytes with Prostate Cancer Prognosis. *Clin Cancer Res*. 2017;23(17):5112-5122. doi:10.1158/1078-0432.CCR-16-3081

29. Ring A, Campo D, Porras TB, et al. Circulating Tumor Cell Transcriptomics as Biopsy Surrogates in Metastatic Breast Cancer. *Ann Surg Oncol*. 2022;29(5):2882-2894. doi:10.1245/s10434-021-11135-2

30. Szczerba BM, Castro-Giner F, Vetter M, et al. Neutrophils escort circulating tumour cells to enable cell cycle progression. *Nature*. 2019;566(7745):553-557. doi:10.1038/s41586-019-0915-y

31. Acheampong E, Abed A, Morici M, et al. Evaluation of PD-L1 expression on circulating tumour cells in small-cell lung cancer. *Transl Lung Cancer Res*. 2022;11(3):440-451. doi:10.21037/tlcr-21-819

32. Manuelli V, Cahill F, Wylie H, et al. Invadopodia play a role in prostate cancer progression. *BMC Cancer*. 2022;22(1):1-9. doi:10.1186/s12885-022-09424-4

33. Asante DBB, Morici M, Mohan GRKAKA, et al. Multi-Marker Immunofluorescent Staining and PD-L1 Detection on Circulating Tumour Cells from Ovarian Cancer Patients. *Cancers* . 2021;13(24):1-17. doi:10.3390/cancers13246225

34. Kitz J, Goodale D, Postenka C, Lowes LE, Allan AL. EMT-independent detection of circulating tumor cells in human blood samples and pre-clinical mouse models of metastasis. *Clin Exp Metastasis*. 2021;38(1):97-108. doi:10.1007/s10585-020-10070-y

35. Emre O, M. SA, C. CJ, et al. Inertial Focusing for Tumor Antigen–Dependent and –Independent Sorting of Rare Circulating Tumor Cells. *Sci Transl Med*. 2013;5(179):179ra47-179ra47. doi:10.1126/scitranslmed.3005616

36. Kalinich M, Bhan I, Kwan TT, et al. An RNA-based signature enables high specificity detection of circulating tumor cells in hepatocellular carcinoma. *Proc Natl Acad Sci U S A*.

2017;114(5):1123-1128. doi:10.1073/pnas.1617032114

37. Cho HY, Choi JH, Lim J, Lee SN, Choi JW. Microfluidic chip-based cancer diagnosis and prediction of relapse by detecting circulating tumor cells and circulating cancer stem cells. *Cancers (Basel)*. 2021;13(6):1-17. doi:10.3390/cancers13061385

38. Zhou J, Zhu X, Wu S, et al. Epithelial-mesenchymal transition status of circulating tumor cells in breast cancer and its clinical relevance. *Cancer Biol Med*. 2020;17(1):169-180. doi:10.20892/j.issn.2095-3941.2019.0118

39. Mazel M, Jacot W, Pantel K, et al. Frequent expression of PD-L1 on circulating breast cancer cells. *Mol Oncol*. 2015;9(9):1773-1782. doi:https://doi.org/10.1016/j.molonc.2015.05.009

40. Nicolazzo C, Raimondi C, Mancini M, et al. Monitoring PD-L1 positive circulating tumor cells in non-small cell lung cancer patients treated with the PD-1 inhibitor Nivolumab. *Sci Rep*. 2016;6(1):31726. doi:10.1038/srep31726

41. Strati A, Nikolaou M, Georgoulias V, Lianidou ES. Prognostic Significance of TWIST1, CD24, CD44, and ALDH1 Transcript Quantification in EpCAM-Positive Circulating Tumor Cells from Early Stage Breast Cancer Patients. *Cells* . 2019;8(7). doi:10.3390/cells8070652

42. Alix-Panabières C, Pantel K. Characterization of single circulating tumor cells. *FEBS Lett*. 2017;591(15):2241-2250. doi:10.1002/1873-3468.12662

43. Sinkala E, Sollier-Christen E, Renier C, et al. Profiling protein expression in circulating tumour cells using microfluidic western blotting. *Nat Commun*. 2017;8(1):14622. doi:10.1038/ncomms14622

44. Abouleila Y, Onidani K, Ali A, et al. Live single cell mass spectrometry reveals cancer-specific metabolic profiles of circulating tumor cells. *Cancer Sci*. 2019;110(2):697-706. doi:https://doi.org/10.1111/cas.13915

45. Reza KK, Dey S, Wuethrich A, et al. In Situ Single Cell Proteomics Reveals Circulating Tumor Cell Heterogeneity during Treatment. *ACS Nano*. 2021;15(7):11231-11243. doi:10.1021/acsnano.0c10008

46. Eremina OE, Czaja AT, Fernando A, Aron A, Eremin DB, Zavaleta C. Expanding the Multiplexing Capabilities of Raman Imaging to Reveal Highly Specific Molecular Expression and Enable Spatial Profiling. *ACS Nano*. Published online June 8, 2022. doi:10.1021/acsnano.2c00353

47. Strati A, Markou A, Parisi C, et al. Gene expression profile of circulating tumor cells in breast cancer by RT-qPCR. *BMC Cancer*. 2011;11(1):422. doi:10.1186/1471-2407-11-422

48. De Albuquerque A, Kubisch I, Breier G, et al. Multimarker gene analysis of circulating tumor cells in pancreatic cancer patients: a feasibility study. *Oncology*. 2012;82(1):3-10.

49. Hoshimoto S, Shingai T, Morton DL, et al. Association between circulating tumor cells and prognosis in patients with stage III melanoma with sentinel lymph node metastasis in a phase III international multicenter trial. *J Clin Oncol*. 2012;30(31):3819.

50. Devriese LA, Bosma AJ, van de Heuvel MM, Heemsbergen W, Voest EE, Schellens JHM. Circulating tumor cell detection in advanced non-small cell lung cancer patients by multi-marker QPCR analysis. *Lung Cancer*. 2012;75(2):242-247. doi:https://doi.org/10.1016/j.lungcan.2011.07.003

51. Smirnov DA, Zweitzig DR, Foulk BW, et al. Global Gene Expression Profiling of Circulating Tumor Cells. *Cancer Res*. 2005;65(12):4993-4997. doi:10.1158/0008-5472.CAN-04-4330

52. Lang JE, Ring A, Porras T, et al. RNA-Seq of Circulating Tumor Cells in Stage II–III Breast Cancer. *Ann Surg Oncol*. 2018;25(8):2261-2270. doi:10.1245/s10434-018-6540-4

53. D'Avola D, Villacorta-Martin C, Martins-Filho SN, et al. High-density single cell mRNA sequencing to characterize circulating tumor cells in hepatocellular carcinoma. *Sci Rep*. 2018;8(1):1-7. doi:10.1038/s41598-018-30047-y

54. Vismara M, Reduzzi C, Silvestri M, et al. Single-Cell Phenotypic and Molecular Characterization of Circulating Tumor Cells Isolated from Cryopreserved Peripheral Blood Mononuclear Cells of Patients with Lung Cancer and Sarcoma. *Clin Chem*. 2022;68(5):691-701. doi:10.1093/clinchem/hvac019

55. Cappelletti V, Verzoni E, Ratta R, et al. Analysis of Single Circulating Tumor Cells in Renal Cell Carcinoma Reveals Phenotypic Heterogeneity and Genomic Alterations Related to Progression. *Int J Mol Sci* . 2020;21(4). doi:10.3390/ijms21041475

56. Newman AM, Liu CL, Green MR, et al. Robust enumeration of cell subsets from tissue expression profiles. *Nat Methods*. 2015;12(5):453-457. doi:10.1038/nmeth.3337

57. Poonia S, Goel A, Chawla S, et al. Marker-free characterization of single live circulating tumor cell full-length transcriptomes. *bioRxiv*. Published online January 1, 2021:2021.11.16.468747. doi:10.1101/2021.11.16.468747

58. Lin D, Shen L, Luo M, et al. Circulating tumor cells: biology and clinical significance. *Signal Transduct Target Ther*. 2021;6(1). doi:10.1038/s41392-021-00817-8

59. Janni WJ, Rack B, Terstappen LWMM, et al. Pooled Analysis of the Prognostic Relevance of Circulating Tumor Cells in Primary Breast Cancer. *Clin Cancer Res*. 2016;22(10):2583-2593. doi:10.1158/1078-0432.CCR-15-1603

60. Fu L, Liu F, Fu H, et al. Circulating Tumor Cells Correlate with Recurrence in Stage III Small-cell Lung Cancer after Systemic Chemoradiotherapy and Prophylactic Cranial Irradiation. *Jpn J Clin Oncol*. 2014;44(10):948-955. doi:10.1093/jjco/hyu109

61. Li Y, Tian X, Gao L, et al. Clinical significance of circulating tumor cells and tumor markers

in the diagnosis of lung cancer. *Cancer Med*. 2019;8(8):3782-3792. doi:https://doi.org/10.1002/cam4.2286

62. Lucci A, Hall CS, Patel SP, et al. Circulating Tumor Cells and Early Relapse in Node-positive Melanoma. *Clin Cancer Res*. 2020;26(8):1886-1895. doi:10.1158/1078-0432.CCR-19-2670

63. Raimondi C, Gradilone A, Gazzaniga P. Circulating tumor cells in early bladder cancer: insight into micrometastatic disease. *Expert Rev Mol Diagn*. 2014;14(4):407-409. doi:10.1586/14737159.2014.908119

64. Broncy L, Paterlini-Bréchot P. Clinical Impact of Circulating Tumor Cells in Patients with Localized Prostate Cancer. *Cells* . 2019;8(7). doi:10.3390/cells8070676

65. Lorente D, Olmos D, Mateo J, et al. Decline in Circulating Tumor Cell Count and Treatment Outcome in Advanced Prostate Cancer. *Eur Urol*. 2016;70(6):985-992. doi:https://doi.org/10.1016/j.eururo.2016.05.023

66. Abreu M, Abalo A, Lago-lest M, Rafael L. Analysis of a Real-World Cohort of Metastatic Breast Cancer Patients Shows Circulating Tumor Cell. Published online 2020.

67. Su PW, Lai W, Liu L, et al. Mesenchymal and Phosphatase of Regenerating Liver-3 Status in Circulating Tumor Cells May Serve as a Crucial Prognostic Marker for Assessing Relapse or Metastasis in Postoperative Patients With Colorectal Cancer. *Clin Transl Gastroenterol*. 2020;11(12):e00265. doi:10.14309/ctg.0000000000000265

68. Papadaki MA, Stoupis G, Theodoropoulos PA, Mavroudis D, Georgoulias V, Agelaki S. Circulating tumor cells with stemness and epithelial-to-mesenchymal transition features are chemoresistant and predictive of poor outcome in metastatic breast cancer. *Mol Cancer Ther*. 2019;18(2):437-447. doi:10.1158/1535-7163.MCT-18-0584

69. Nagrath S, Sequist L V., Maheswaran S, et al. Isolation of rare circulating tumour cells in cancer patients by microchip technology. *Nature*. 2007;450(7173):1235-1239. doi:10.1038/nature06385

70. Thery L, Meddis A, Cabel L, et al. Circulating Tumor Cells in Early Breast Cancer. *JNCI Cancer Spectr*. 2019;3(2):pkz026. doi:10.1093/jncics/pkz026

71. Ignatiadis M, Litière S, Rothe F, et al. Trastuzumab versus observation for HER2 nonamplified early breast cancer with circulating tumor cells (EORTC 90091-10093, BIG 1-12, Treat CTC): a randomized phase II trial. *Ann Oncol*. 2018;29(8):1777-1783. doi:https://doi.org/10.1093/annonc/mdy211

72. Marchetti A, Del Grammastro M, Felicioni L, et al. Assessment of EGFR Mutations in Circulating Tumor Cell Preparations from NSCLC Patients by Next Generation Sequencing: Toward a Real-Time Liquid Biopsy for Treatment. *PLoS One*. 2014;9(8):e103883. https://doi.org/10.1371/journal.pone.0103883

73. Paoletti C, Cani AK, Larios JM, et al. Comprehensive Mutation and Copy Number Profiling in Archived Circulating Breast Cancer Tumor Cells Documents Heterogeneous Resistance Mechanisms. *Cancer Res*. 2018;78(4):1110-1122. doi:10.1158/0008-5472.CAN-17-2686

74. Fehm T, Müller V, Aktas B, et al. HER2 status of circulating tumor cells in patients with metastatic breast cancer: a prospective, multicenter trial. *Breast Cancer Res Treat*. 2010;124(2):403-412.

75. Munzone E, Nolé F, Goldhirsch A, et al. Changes of HER2 status in circulating tumor cells compared with the primary tumor during treatment for advanced breast cancer. *Clin Breast Cancer*. 2010;10(5):392-397.

76. Aktas B, Kasimir-Bauer S, Müller V, et al. Comparison of the HER2, estrogen and progesterone receptor expression profile of primary tumor, metastases and circulating tumor cells in metastatic breast cancer patients. *BMC Cancer*. 2016;16(1):1-8.

77. Jordan NV, Bardia A, Wittner BS, et al. HER2 expression identifies dynamic functional states within circulating breast cancer cells. *Nature*. 2016;537(7618):102-106.

78. Wang C, Mu Z, Ye Z, et al. Prognostic value of HER2 status on circulating tumor cells in advanced-stage breast cancer patients with HER2-negative tumors. *Breast Cancer Res Treat*. 2020;181(3):679-689. doi:10.1007/s10549-020-05662-x

79. Kwan TT, Bardia A, Spring LM, et al. A Digital RNA Signature of Circulating Tumor Cells Predicting Early Therapeutic Response in Localized and Metastatic Breast Cancer. *Cancer Discov*. 2018;8(10):1286-1299. doi:10.1158/2159-8290.CD-18-0432

80. Smit DJ, Pantel K, Jücker M. Circulating tumor cells as a promising target for individualized drug susceptibility tests in cancer therapy. *Biochem Pharmacol*. 2021;188(March):114589. doi:10.1016/j.bcp.2021.114589

81. Min Y, Aditya B, Nicola A, et al. Ex vivo culture of circulating breast tumor cells for individualized testing of drug susceptibility. *Science (80-)*. 2014;345(6193):216-220. doi:10.1126/science.1253533

82. Lee HLL, Chiou JFF, Wang PYY, et al. Ex vivo expansion and drug sensitivity profiling of circulating tumor cells from patients with small cell lung cancer. *Cancers (Basel)*. 2020;12(11):1-17. doi:10.3390/cancers12113394

83. Vaddepally RK, Kharel P, Pandey R, Garje R, Chandra AB. Review of indications of FDA-approved immune checkpoint inhibitors per NCCN guidelines with the level of evidence. *Cancers (Basel)*. 2020;12(3):1-19. doi:10.3390/cancers12030738

84. Khunger M, Hernandez A V, Pasupuleti V, et al. Programmed Cell Death 1 (PD-1) Ligand (PD-L1) Expression in Solid Tumors As a Predictive Biomarker of Benefit From PD-1/PD-L1 Axis Inhibitors: A Systematic Review and Meta-Analysis. *JCO Precis Oncol*. 2017;(1):1-15. doi:10.1200/PO.16.00030

85. Zhong X, Zhang H, Zhu Y, et al. Circulating tumor cells in cancer patients: Developments and clinical applications for immunotherapy. *Mol Cancer*. 2020;19(1):1-12. doi:10.1186/s12943-020-1141-9

86. Yue C, Jiang Y, Li P, et al. Dynamic change of PD-L1 expression on circulating tumor cells in advanced solid tumor patients undergoing PD-1 blockade therapy. *Oncoimmunology*. 2018;7(7):1-12. doi:10.1080/2162402X.2018.1438111

87. Guibert N, Delaunay M, Lusque A, et al. PD-L1 expression in circulating tumor cells of advanced non-small cell lung cancer patients treated with nivolumab. *Lung Cancer*. 2018;120(February):108-112. doi:10.1016/j.lungcan.2018.04.001

88. Manjunath Y, Upparahalli S V, Avella DM, et al. PD-L1 Expression with Epithelial Mesenchymal Transition of Circulating Tumor Cells Is Associated with Poor Survival in Curatively Resected Non-Small Cell Lung Cancer. *Cancers* . 2019;11(6). doi:10.3390/cancers11060806

89. Papadaki MA, Koutsopoulos A V, Tsoulfas PG, et al. Clinical Relevance of Immune Checkpoints on Circulating Tumor Cells in Breast Cancer. *Cancers* . 2020;12(2). doi:10.3390/cancers12020376

90. Jaiswal S, Jamieson CHM, Pang WW, et al. CD47 Is Upregulated on Circulating Hematopoietic Stem Cells and Leukemia Cells to Avoid Phagocytosis. *Cell*. 2009;138(2):271-285. doi:https://doi.org/10.1016/j.cell.2009.05.046

91. Weber GF. Why does cancer therapy lack effective anti-metastasis drugs? *Cancer Lett*. 2013;328(2):207-211. doi:https://doi.org/10.1016/j.canlet.2012.09.025

92. Rana K, Liesveld JL, King MR. Delivery of apoptotic signal to rolling cancer cells: A novel biomimetic technique using immobilized TRAIL and E-Selectin. *Biotechnol Bioeng*. 2009;102(6):1692-1702. doi:10.1002/bit.22204

93. Mitchell MJ, Wayne E, Rana K, Schaffer CB, King MR. Trail-coated leukocytes that kill cancer cells in the circulation. *Proc Natl Acad Sci U S A*. 2014;111(3):930-935. doi:10.1073/pnas.1316312111

94. Ortiz-Otero N, Marshall JR, Glenn A, et al. TRAIL-coated leukocytes to kill circulating tumor cells in the flowing blood from prostate cancer patients. *BMC Cancer*. 2021;21(1):898. doi:10.1186/s12885-021-08589-8

95. Li J, Ai Y, Wang L, et al. Targeted drug delivery to circulating tumor cells via platelet membrane-functionalized particles. *Biomaterials*. 2016;76:52-65. doi:https://doi.org/10.1016/j.biomaterials.2015.10.046

96. Lian S, Xie R, Ye Y, et al. Dual blockage of both PD-L1 and CD47 enhances immunotherapy against circulating tumor cells. *Sci Rep*. 2019;9(1):4532. doi:10.1038/s41598-019-40241-1

97. Dianat-Moghadam H, Mahari A, Heidarifard M, et al. NK cells-directed therapies target circulating tumor cells and metastasis. *Cancer Lett*. 2021;497(July 2020):41-53. doi:10.1016/j.canlet.2020.09.021

98. Lorenzo-Herrero S, López-Soto A, Sordo-Bahamonde C, Gonzalez-Rodriguez AP, Vitale M, Gonzalez S. *NK Cell-Based Immunotherapy in Cancer Metastasis*. Vol 11.; 2019:29. doi:10.3390/cancers11010029

99. López-Soto A, Gonzalez S, Smyth MJ, Galluzzi L. Control of Metastasis by NK Cells. *Cancer Cell*. 2017;32(2):135-154. doi:https://doi.org/10.1016/j.ccell.2017.06.009

100. R&D systems. Natural Killer Cell Receptors: Human Target Cell – NK Cell Ligand-Receptor Interactions. Accessed July 2, 2021. https://www.rndsystems.com/pathways/natural-killer-cell-receptors-human-target-cell-nk-cell-ligand-receptor-interactions-pathway

101. Lanier LL. NK cell recognition. *Annu Rev Immunol*. 2005;23(1):225-274.

102. McQueen KL, Parham P. Variable receptors controlling activation and inhibition of NK cells. *Curr Opin Immunol*. 2002;14(5):615-621. doi:https://doi.org/10.1016/S0952-7915(02)00380-1

103. Morvan MG, Lanier LL. NK cells and cancer: You can teach innate cells new tricks. *Nat Rev Cancer*. 2016;16(1):7-19. doi:10.1038/nrc.2015.5

104. Korkolopoulou P, Kaklamanis L, Pezzella F, Harris AL, Gatter KC. Loss of antigen-presenting molecules (MHC class I and TAP-1) in lung cancer. *Br J Cancer*. 1996;73(2):148-153. doi:10.1038/bjc.1996.28

105. Garrido F, Algarra I. MHC antigens and tumor escape from immune surveillance. Published online 2001.

106. Pantel K, Schlimok G, Kutter D, et al. Frequent Down-Regulation of Major Histocompatibility Class I Antigen Expression on Individual Micrometastatic Carcinoma Cells. *Cancer Res*. 1991;51(17):4712-4715. Accessed June 16, 2019. http://cancerres.aacrjournals.org.proxy.lib.umich.edu/content/canres/51/17/4712.full.pdf

107. Diefenbach A, Jensen ER, Jamieson AM, Raulet DH. Rae1 and H60 ligands of the NKG2D receptor stimulate tumour immunity. *Nature*. 2001;413(6852):165-171. doi:10.1038/35093109

108. Malladi S, Macalinao DG, Jin X, et al. Metastatic Latency and Immune Evasion through Autocrine Inhibition of WNT. *Cell*. 2016;165(1):45-60. doi:https://doi.org/10.1016/j.cell.2016.02.025

109. Street SEAA, Cretney E, Smyth MJ. Perforin and interferon-γ activities independently control tumor initiation, growth, and metastasis. *Blood*. 2001;97(1):192-197. doi:10.1182/blood.V97.1.192

110. Takeda K, Hayakawa Y, Smyth MJ, et al. Involvement of tumor necrosis factor-related apoptosis-inducing ligand in surveillance of tumor metastasis by liver natural killer cells. *Nat Med*. 2001;7(1):94-100. doi:10.1038/83416

111. Werneck MBF, Lugo-Villarino G, Hwang ES, Cantor H, Glimcher LH. T-Bet Plays a Key Role in NK-Mediated Control of Melanoma Metastatic Disease. *J Immunol*. 2008;180(12):8004 LP - 8010. doi:10.4049/jimmunol.180.12.8004

112. Ghandi M, Huang FW, Jané-Valbuena J, et al. Next-generation characterization of the Cancer Cell Line Encyclopedia. *Nature*. 2019;569(7757):503-508. doi:10.1038/s41586-019-1186-3

113. Ruggeri L, Mancusi A, Burchielli E, et al. NK cell alloreactivity and allogeneic hematopoietic stem cell transplantation. *Blood Cells, Mol Dis*. 2008;40(1):84-90. doi:https://doi.org/10.1016/j.bcmd.2007.06.029

114. Hansrivijit P, Gale RP, Barrett J, Ciurea SO. Cellular therapy for acute myeloid Leukemia – Current status and future prospects. *Blood Rev*. 2019;37:100578. doi:https://doi.org/10.1016/j.blre.2019.05.002

115. Habif G, Crinier A, André P, Vivier E, Narni-Mancinelli E. Targeting natural killer cells in solid tumors. *Cell Mol Immunol*. 2019;16(5):415-422. doi:10.1038/s41423-019-0224-2

116. Klingemann H. Challenges of cancer therapy with natural killer cells. *Cytotherapy*. 2015;17(3):245-249.

117. Qin Z, Chen J, Zeng J, et al. Effect of NK cell immunotherapy on immune function in patients with hepatic carcinoma: A preliminary clinical study. *Cancer Biol Ther*. 2017;18(5):323-330. doi:10.1080/15384047.2017.1310346

118. Lin M, Liang SZZ, Shi J, et al. Circulating tumor cell as a biomarker for evaluating allogenic NK cell immunotherapy on stage IV non-small cell lung cancer. *Immunol Lett*. 2017;191(September):10-15. doi:10.1016/j.imlet.2017.09.004

119. Santos MF, Mannam VKRR, Craft BS, et al. Comparative analysis of innate immune system function in metastatic breast, colorectal, and prostate cancer patients with circulating tumor cells. *Exp Mol Pathol*. 2014;96(3):367-374. doi:10.1016/j.yexmp.2014.04.001

120. Ye L, Zhang F, Li H, et al. Circulating Tumor Cells Were Associated with the Number of T Lymphocyte Subsets and NK Cells in Peripheral Blood in Advanced Non-Small-Cell Lung Cancer. González A, ed. *Dis Markers*. 2017;2017:5727815. doi:10.1155/2017/5727815

121. Kang YT, Niu Z, Hadlock T, et al. On-Chip Biogenesis of Circulating NK Cell-Derived Exosomes in Non-Small Cell Lung Cancer Exhibits Antitumoral Activity. *Adv Sci*. 2021;8(6):1-13. doi:10.1002/advs.202003747

122. Chockley PJ, Chen J, Chen G, Beer DG, Standiford TJ, Keshamouni VG. Epithelial-

mesenchymal transition leads to NK cell-mediated metastasis-specific immunosurveillance in lung cancer. *J Clin Invest*. 2018;128(4):1384-1396. doi:10.1172/JCI97611

123. Sheffer M, Lowry E, Beelen N, et al. Genome-scale screens identify factors regulating tumor cell responses to natural killer cells. *Nat Genet*. 2021;53(August). doi:10.1038/s41588-021-00889-w

124. Lo HC, Xu Z, Kim IS, et al. Resistance to natural killer cell immunosurveillance confers a selective advantage to polyclonal metastasis. *Nat Cancer*. 2020;1(7):709-722. doi:10.1038/s43018-020-0068-9

125. Huaman J, Naidoo M, Zang X, Ogunwobi OO. Fibronectin Regulation of Integrin B1 and SLUG in Circulating Tumor Cells. *Cells*. 2019;8(6):618. doi:10.3390/cells8060618

126. Ramsköld D, Luo S, Wang YCC, et al. Full-length mRNA-Seq from single-cell levels of RNA and individual circulating tumor cells. *Nat Biotechnol*. 2012;30(8):777-782. doi:10.1038/nbt.2282

127. Morotti M, Albukhari A, Alsaadi A, et al. Promises and challenges of adoptive T-cell therapies for solid tumours. *Br J Cancer*. 2021;124(11):1759-1776. doi:10.1038/s41416-021-01353-6

128. Vitale M, Cantoni C, Pietra G, Mingari MC, Moretta L. Effect of tumor cells and tumor microenvironment on NK-cell function. *Eur J Immunol*. 2014;44(6):1582-1592. doi:https://doi.org/10.1002/eji.201344272

129. Parkhurst MR, Riley JP, Dudley ME, Rosenberg SA. Adoptive transfer of autologous natural killer cells leads to high levels of circulating natural killer cells but does not mediate tumor regression. *Clin Cancer Res*. 2011;17(19):6287-6297. doi:10.1158/1078-0432.CCR-11-1347

130. Nayyar G, Chu Y, Cairo MS. Overcoming Resistance to Natural Killer Cell Based Immunotherapies for Solid Tumors . *Front Oncol* . 2019;9:51. doi:10.3389/fonc.2019.00051

131. Kooijmans SAA, Fliervoet LAL, van der Meel R, et al. PEGylated and targeted extracellular vesicles display enhanced cell specificity and circulation time. *J Control Release*. 2016;224:77-85. doi:https://doi.org/10.1016/j.jconrel.2016.01.009

132. Gao D, Jiang L. Exosomes in cancer therapy: a novel experimental strategy. *Am J Cancer Res*. 2018;8(11):2165-2175. http://www.ncbi.nlm.nih.gov/pubmed/30555736%0Ahttp://www.pubmedcentral.nih.gov/articlerender.fcgi?artid=PMC6291654

133. Murphy DE, de Jong OG, Brouwer M, et al. Extracellular vesicle-based therapeutics: natural versus engineered targeting and trafficking. *Exp Mol Med*. 2019;51(3):1-12. doi:10.1038/s12276-019-0223-5

134. Di Pace AL, Tumino N, Besi F, et al. Characterization of Human NK Cell-Derived Exosomes: Role of DNAM1 Receptor in Exosome-Mediated Cytotoxicity against Tumor. *Cancers* . 2020;12(3). doi:10.3390/cancers12030661

135. Wu CH, Li J, Li L, et al. Extracellular vesicles derived from natural killer cells use multiple cytotoxic proteins and killing mechanisms to target cancer cells. *J Extracell Vesicles*. 2019;8(1):1588538. doi:10.1080/20013078.2019.1588538

136. Boyiadzis M, Hong CS, Whiteside TL. Natural Killer Cell Derived Exosomes As a Novel Therapeutic for Acute Myeloid Leukemia. *Blood*. 2018;132:5226. doi:https://doi.org/10.1182/blood-2018-99-115385

137. Zhu L, Kalimuthu S, Gangadaran P, et al. Exosomes derived from natural killer cells exert therapeutic effect in melanoma. *Theranostics*. 2017;7(10):2732. doi:10.7150/thno.18752

138. Institute NC. Surveillance, Epidemiology, and End Results (SEER) Program SEER*Stat Database: Cancer Stat Facts: Bladder Cancer. Published 2022. www.seer.cancer.gov

139. Witjes JA, Bruins HM, Cathomas R, et al. European Association of Urology Guidelines on Muscle-invasive and Metastatic Bladder Cancer: Summary of the 2020 Guidelines. *Eur Urol*. 2021;79(1):82-104. doi:10.1016/j.eururo.2020.03.055

140. Meeks JJ, Al-Ahmadie H, Faltas BM, et al. Genomic heterogeneity in bladder cancer: challenges and possible solutions to improve outcomes. *Nat Rev Urol*. 2020;17(5):259-270.

141. Robertson AG, Kim J, Al-Ahmadie H, et al. Comprehensive Molecular Characterization of Muscle-Invasive Bladder Cancer. *Cell*. 2017;171(3):540-556.e25. doi:https://doi.org/10.1016/j.cell.2017.09.007

142. Pang S, Li H, Xu S, et al. Circulating tumour cells at baseline and late phase of treatment provide prognostic value in breast cancer. *Sci Rep*. 2021;11(1):13441. doi:10.1038/s41598-021-92876-8

143. Cieślikowski WA, Antczak A, Nowicki M, Zabel M, Budna-Tukan J. Clinical Relevance of Circulating Tumor Cells in Prostate Cancer Management. *Biomed* . 2021;9(9). doi:10.3390/biomedicines9091179

144. Gazzaniga P, Gradilone A, De berardinis E, et al. Prognostic value of circulating tumor cellsin nonmuscle invasive bladder cancer: Acellsearch analysis. *Ann Oncol*. 2012;23(9):2352-2356. doi:10.1093/annonc/mdr619

145. Fina E, Necchi A, Giannatempo P, et al. Clinical significance of early changes in circulating tumor cells from patients receiving first-line cisplatin-based chemotherapy for metastatic urothelial carcinoma. *Bl Cancer*. 2016;2(4):395-403. doi:10.3233/BLC-160069

146. Rupp B, Ball H, Wuchu F, Nagrath D, Nagrath S. Circulating tumor cells in precision medicine: challenges and opportunities. *Trends Pharmacol Sci*. 2022;43(5):378-391. doi:https://doi.org/10.1016/j.tips.2022.02.005

147. Cheng SJ, Hsieh KY, Chen SL, et al. Microfluidics and Nanomaterial-based Technologies for Circulating Tumor Cell Isolation and Detection. *Sensors* . 2020;20(7). doi:10.3390/s20071875

148. Rink M, Chun FK, Dahlem R, et al. Prognostic Role and HER2 Expression of Circulating Tumor Cells in Peripheral Blood of Patients Prior to Radical Cystectomy: A Prospective Study. *Eur Urol*. 2012;61(4):810-817. doi:https://doi.org/10.1016/j.eururo.2012.01.017

149. Anantharaman A, Friedlander T, Lu D, et al. Programmed death-ligand 1 (PD-L1) characterization of circulating tumor cells (CTCs) in muscle invasive and metastatic bladder cancer patients. *BMC Cancer*. 2016;16(1):744. doi:10.1186/s12885-016-2758-3

150. Lorenzatti Hiles G, Bucheit A, Rubin JR, et al. ADAM15 is functionally associated with the metastatic progression of human bladder cancer. *PLoS One*. 2016;11(3):e0150138.

151. Najy AJ, Day KC, Day ML. ADAM15 supports prostate cancer metastasis by modulating tumor cell–endothelial cell interaction. *Cancer Res*. 2008;68(4):1092-1099.

152. Lin PP. Aneuploid Circulating Tumor-Derived Endothelial Cell (CTEC): A Novel Versatile Player in Tumor Neovascularization and Cancer Metastasis. *Cells* . 2020;9(6). doi:10.3390/cells9061539

153. Gast CE, Silk AD, Zarour L, et al. Cell fusion potentiates tumor heterogeneity and reveals circulating hybrid cells that correlate with stage and survival. *Sci Adv*. 2018;4(9):eaat7828-eaat7828. doi:10.1126/sciadv.aat7828

154. Day KC, Hiles GL, Kozminsky M, et al. HER2 and EGFR Overexpression Support Metastatic Progression of Prostate Cancer to Bone. *Cancer Res*. 2017;77(1):74-85. doi:10.1158/0008-5472.CAN-16-1656

155. Li W, Wang Y, Tan S, et al. Overexpression of Epidermal Growth Factor Receptor (EGFR) and HER-2 in Bladder Carcinoma and Its Association with Patients' Clinical Features. *Med Sci Monit*. 2018;24:7178-7185. doi:10.12659/MSM.911640

156. Awadalla A, Abol-Enein H, Gabr MM, Hamam ET, Shokeir AA. Prediction of recurrence and progression in patients with T1G3 bladder cancer by gene expression of circulating tumor cells. *Urol Oncol Semin Orig Investig*. 2020;38(4):278-285. doi:https://doi.org/10.1016/j.urolonc.2019.12.002

157. Gazzaniga P, Nofroni I, Gandini O, et al. Tenascin C and epidermal growth factor receptor as markers of circulating tumoral cells in bladder and colon cancer. *Oncol Rep*. 2005;14(5):1199-1202.

158. Osman I, Bajorin DF, Sun TT, et al. Novel Blood Biomarkers of Human Urinary Bladder Cancer. *Clin Cancer Res*. 2006;12(11):3374-3380. doi:10.1158/1078-0432.CCR-05-2081

159. Hovelson DH, Udager AM, McDaniel AS, et al. Targeted DNA and RNA Sequencing of Paired Urothelial and Squamous Bladder Cancers Reveals Discordant Genomic and

Transcriptomic Events and Unique Therapeutic Implications. *Eur Urol*. 2018;74(6):741-753. doi:https://doi.org/10.1016/j.eururo.2018.06.047

160. Risso D, Ngai J, Speed TP, Dudoit S. Normalization of RNA-seq data using factor analysis of control genes or samples. *Nat Biotechnol*. 2014;32(9):896-902. doi:10.1038/nbt.2931

161. Risso D, Schwartz K, Sherlock G, Dudoit S. GC-Content Normalization for RNA-Seq Data. *BMC Bioinformatics*. 2011;12(1):480. doi:10.1186/1471-2105-12-480

162. Bullard JH, Purdom E, Hansen KD, Dudoit S. Evaluation of statistical methods for normalization and differential expression in mRNA-Seq experiments. *BMC Bioinformatics*. 2010;11(1):94. doi:10.1186/1471-2105-11-94

163. Palmer C, Diehn M, Alizadeh AA, Brown PO. Cell-type specific gene expression profiles of leukocytes in human peripheral blood. *BMC Genomics*. 2006;7(1):115. doi:10.1186/1471-2164-7-115

164. Xie X, Liu M, Zhang Y, et al. Single-cell transcriptomic landscape of human blood cells. *Natl Sci Rev*. 2021;8(3):nwaa180.

165. Gagnon-Bartsch JA, Speed TP. Using control genes to correct for unwanted variation in microarray data. *Biostatistics*. 2012;13(3):539-552.

166. Yu G, Wang LG, Yan GR, He QY. DOSE: an R/Bioconductor package for disease ontology semantic and enrichment analysis. *Bioinformatics*. 2015;31(4):608-609. doi:10.1093/bioinformatics/btu684

167. Yu G, Wang LG, Han Y, He QY. clusterProfiler: an R Package for Comparing Biological Themes Among Gene Clusters. *Omi A J Integr Biol*. 2012;16(5):284-287. doi:10.1089/omi.2011.0118

168. Sato K, Sasaki R, Ogura Y, et al. Expression of vascular endothelial growth factor gene and its receptor (flt-1) gene in urinary bladder cancer. *Tohoku J Exp Med*. 1998;185(3):173-184. doi:10.1620/tjem.185.173

169. Tauro M, Lynch CC. Cutting to the chase: How matrix metalloproteinase-2 activity controls breast-cancer-to-bone metastasis. *Cancers (Basel)*. 2018;10(6). doi:10.3390/cancers10060185

170. Tai HL, Lin TS, Huang HH, et al. Overexpression of aldo-keto reductase 1C2 as a high-risk factor in bladder cancer. *Oncol Rep*. 2007;17(2):305-311.

171. Shirato A, Kikugawa T, Miura N, et al. Cisplatin resistance by induction of aldo-keto reductase family 1 member C2 in human bladder cancer cells. *Oncol Lett*. 2014;7(3):674-678. doi:10.3892/ol.2013.1768

172. McNamara KM, Guestini F, Sauer T, et al. In breast cancer subtypes steroid sulfatase (STS) is associated with less aggressive tumour characteristics. *Br J Cancer*. 2018;118(9):1208-

1216. doi:10.1038/s41416-018-0034-9

173. Shimizu Y, Tamada S, Kato M, et al. Steroid sulfatase promotes invasion through epithelial-mesenchymal transition and predicts the progression of bladder cancer. *Exp Ther Med*. 2018;16(6):4463-4470.

174. Choi W, Czerniak B, Ochoa A, et al. Intrinsic basal and luminal subtypes of muscle-invasive bladder cancer. *Nat Rev Urol*. 2014;11(7):400-410. doi:10.1038/nrurol.2014.129

175. Zhang L, Zhu Z, Yan H, et al. Creatine promotes cancer metastasis through activation of Smad2/3. *Cell Metab*. 2021;33(6):1111-1123.e4. doi:https://doi.org/10.1016/j.cmet.2021.03.009

176. Xu X, Wang Y, Zhang S, Zhu Y, Wang J. Exploration of Prognostic Biomarkers of Muscle-Invasive Bladder Cancer (MIBC) by Bioinformatics. *Evol Bioinforma*. 2021;17:11769343211049270.

177. Nian H, Ma B. Calpain-calpastatin system and cancer progression. *Biol Rev Camb Philos Soc*. 2021;96(3):961-975. doi:10.1111/brv.12686

178. Aoki T, Weber G. Carbamoyl phosphate synthetase (glutamine-hydrolyzing): increased activity in cancer cells. *Science (80-)*. 1981;212(4493):463-465.

179. Jiang H, Gu X, Zuo Z, Tian G, Liu J. Prognostic value of circulating tumor cells in patients with bladder cancer: A meta-analysis. *PLoS One*. 2021;16(7 July):1-12. doi:10.1371/journal.pone.0254433

180. Owen S, Lo TW, Fouladdel S, et al. Simultaneous Single Cell Gene Expression and EGFR Mutation Analysis of Circulating Tumor Cells Reveals Distinct Phenotypes in NSCLC. *Adv Biosyst*. 2020;2000110:1-11. doi:10.1002/adbi.202000110

181. Kapeleris J, Kulasinghe A, Warkiani ME, et al. The prognostic role of circulating tumor cells (CTCs) in lung cancer. *Front Oncol*. 2018;8(AUG):311. doi:10.3389/fonc.2018.00311

182. Bertolini G, Roz L, Perego P, et al. Highly tumorigenic lung cancer CD133+ cells display stem-like features and are spared by cisplatin treatment. *Proc Natl Acad Sci*. 2009;106(38):16281-16286. doi:10.1073/pnas.0905653106

183. Carvalho BS, Irizarry RA. A framework for oligonucleotide microarray preprocessing. *Bioinformatics*. 2010;26(19):2363-2367. doi:10.1093/bioinformatics/btq431

184. Irizarry RA, Hobbs B, Collin F, et al. Exploration, normalization, and summaries of high density oligonucleotide array probe level data. *Biostatistics*. 2003;4(2):249-264. doi:10.1093/biostatistics/4.2.249

185. Ritchie ME, Phipson B, Wu D, et al. Limma powers differential expression analyses for RNA-sequencing and microarray studies. *Nucleic Acids Res*. 2015;43(7):e47. doi:10.1093/nar/gkv007

186. Lin E, Rivera-Báez L, Fouladdel S, et al. High-Throughput Microfluidic Labyrinth for the Label-free Isolation of Circulating Tumor Cells. *Cell Syst*. 2017;5(3):295-304.e4. doi:10.1016/j.cels.2017.08.012

187. Wan S, Kim TH, Smith KJ, et al. New Labyrinth Microfluidic Device Detects Circulating Tumor Cells Expressing Cancer Stem Cell Marker and Circulating Tumor Microemboli in Hepatocellular Carcinoma. *Sci Rep*. 2019;9(1):18575. doi:10.1038/s41598-019-54960-y

188. Kulasinghe A, Kapeleris J, Kimberley R, et al. The prognostic significance of circulating tumor cells in head and neck and non-small-cell lung cancer. *Cancer Med*. 2018;7(12):5910-5919. doi:10.1002/cam4.1832

189. Naz S, Bashir M, Ranganathan P, Bodapati P, Santosh V, Kondaiah P. Protumorigenic actions of S100A2 involve regulation of PI3/Akt signaling and functional interaction with Smad3. *Carcinogenesis*. 2014;35(1):14-23. doi:10.1093/carcin/bgt287

190. Wang Y, Fu D, Chen Y, et al. G3BP1 promotes tumor progression and metastasis through IL-6/G3BP1/STAT3 signaling axis in renal cell carcinomas article. *Cell Death Dis*. 2018;9(5). doi:10.1038/s41419-018-0504-2

191. Tuo Z, Zheng X, Zong Y, et al. HK3 is correlated with immune infiltrates and predicts response to immunotherapy in non-small cell lung cancer. *Clin Transl Med*. 2020;10(1):319-330. doi:10.1002/ctm2.6

192. Liu Q, Li H, Yang M, et al. Suppression of tumor growth and metastasis in Shkbp1 knockout mice. *Cancer Gene Ther*. Published online 2021. doi:10.1038/s41417-021-00349-x

193. US Food and Drug Administration. FDA approves atezolizumab as adjuvant treatment for non-small cell lung cancer [Press release]. Published 2021. https://www.fda.gov/drugs/resources-information-approved-drugs/fda-approves-atezolizumab-adjuvant-treatment-non-small-cell-lung-cancer

194. Felip E, Altorki N, Zhou C, et al. Adjuvant atezolizumab after adjuvant chemotherapy in resected stage IB–IIIA non-small-cell lung cancer (IMpower010): a randomised, multicentre, open-label, phase 3 trial. *Lancet*. 2021;398(10308):1344-1357. doi:https://doi.org/10.1016/S0140-6736(21)02098-5

195. Faivre-Finn C, Vicente D, Kurata T, et al. Four-Year Survival With Durvalumab After Chemoradiotherapy in Stage III NSCLC—an Update From the PACIFIC Trial. *J Thorac Oncol*. 2021;16(5):860-867. doi:https://doi.org/10.1016/j.jtho.2020.12.015

196. Gray JE, Villegas A, Daniel D, et al. Three-Year Overall Survival with Durvalumab after Chemoradiotherapy in Stage III NSCLC—Update from PACIFIC. *J Thorac Oncol*. 2020;15(2):288-293. doi:10.1016/j.jtho.2019.10.002

197. Walsh RJ, Soo RA. Resistance to immune checkpoint inhibitors in non-small cell lung cancer: biomarkers and therapeutic strategies. *Ther Adv Med Oncol*. 2020;12:1758835920937902-1758835920937902. doi:10.1177/1758835920937902

198. Perea F, Sánchez-Palencia A, Gómez-Morales M, et al. HLA class I loss and PD-L1 expression in lung cancer: impact on T-cell infiltration and immune escape. *Oncotarget*. 2017;9(3):4120-4133. doi:10.18632/oncotarget.23469

199. Morvan MG, Lanier LL. NK cells and cancer: You can teach innate cells new tricks. *Nat Rev Cancer*. 2016;16(1):7-19. doi:10.1038/nrc.2015.5

200. Street SEA, Cretney E, Smyth MJ. Perforin and interferon-γ activities independently control tumor initiation, growth, and metastasis. *Blood*. 2001;97(1):192-197. doi:10.1182/blood.V97.1.192

201. Best SA, Hess JB, Souza-Fonseca-Guimaraes F, et al. Harnessing Natural Killer Immunity in Metastatic SCLC. *J Thorac Oncol*. 2020;15(9):1507-1521. doi:10.1016/j.jtho.2020.05.008

202. Merzoug L Ben, Marie S, Satoh-Takayama N, et al. Conditional ablation of NKp46+ cells using a novel Ncr1greenCre mouse strain: NK cells are essential for protection against pulmonary B16 metastases. *Eur J Immunol*. 2014;44(11):3380-3391. doi:10.1002/eji.201444643

203. Ichise H, Tsukamoto S, Hirashima T, et al. Functional visualization of NK cell-mediated killing of metastatic single tumor cells. *Elife*. 2022;11:1-28. doi:10.7554/ELIFE.76269

204. Zhang Z, Ramnath N, Nagrath S. Current status of CTCs as liquid biopsy in lung cancer and future directions. *Front Oncol*. 2015;5:209.

205. Francart ME, Lambert J, Vanwynsberghe AM, et al. Epithelial–mesenchymal plasticity and circulating tumor cells: Travel companions to metastases. *Dev Dyn*. 2018;247(3):432-450. doi:https://doi.org/10.1002/dvdy.24506

206. Ha Y, Kim TH, Shim JE, et al. Circulating tumor cells are associated with poor outcomes in early-stage hepatocellular carcinoma: a prospective study. *Hepatol Int*. 2019;13(6):726-735. doi:10.1007/s12072-019-09994-9

207. Zeinali M, Lee M, Nadhan A, et al. High-throughput label-free isolation of heterogeneous circulating tumor cells and CTC clusters from non-small-cell lung cancer patients. *Cancers (Basel)*. 2020;12(1):1-17. doi:10.3390/cancers12010127

208. Wang C, Mu Z, Chervoneva I, et al. Longitudinally collected CTCs and CTC-clusters and clinical outcomes of metastatic breast cancer. *Breast Cancer Res Treat*. 2017;161(1):83-94. doi:10.1007/s10549-016-4026-2

209. Santos MF, Mannam VKR, Craft BS, et al. Comparative analysis of innate immune system function in metastatic breast, colorectal, and prostate cancer patients with circulating tumor cells. *Exp Mol Pathol*. 2014;96(3):367-374. doi:10.1016/j.yexmp.2014.04.001

210. Green TL, Cruse JM, Lewis RE. Circulating tumor cells (CTCs) from metastatic breast cancer patients linked to decreased immune function and response to treatment. *Exp Mol*

Pathol. 2013;95(2):174-179. doi:https://doi.org/10.1016/j.yexmp.2013.06.013

211. Brodbeck T, Nehmann N, Bethge A, Wedemann G, Schumacher U. Perforin-dependent direct cytotoxicity in natural killer cells induces considerable knockdown of spontaneous lung metastases and computer modelling-proven tumor cell dormancy in a HT29 human colon cancer xenograft mouse model. *Mol Cancer*. 2014;13(1):1-11. doi:10.1186/1476-4598-13-244

212. Loh CY, Chai JY, Tang TF, et al. The E-Cadherin and N-Cadherin Switch in Epithelial-to-Mesenchymal Transition: Signaling, Therapeutic Implications, and Challenges. *Cells*. 2019;8(10). doi:10.3390/cells8101118

213. Pantel K, Schaller G, Kutter D, Genz T, Riethmüller G. Frequent Down-Regulation of Major Histocompatibility Class I Antigen Expression on Individual Micrometastatic Carcinoma Cells. *Cancer Res*. 1991;51(17):4712-4715.

214. Ramsköld D, Luo S, Wang YC, et al. Full-length mRNA-Seq from single-cell levels of RNA and individual circulating tumor cells. *Nat Biotechnol*. 2012;30(8):777-782. doi:10.1038/nbt.2282

215. Kozminsky M, Nagrath S. Circulating tumor cells, cancer stem cells, and emerging microfluidic detection technologies with clinical applications. *Cancer Stem Cells; Elsevier Amsterdam, Netherlands*. Published online 2016:473-497.

216. Rivera-Báez L, Lohse I, Lin E, et al. Expansion of Circulating Tumor Cells from Patients with Locally Advanced Pancreatic Cancer Enable Patient Derived Xenografts and Functional Studies for Personalized Medicine. *Cancers* . 2020;12(4). doi:10.3390/cancers12041011

217. Zhang Z, Shiratsuchi H, Lin J, et al. Expansion of CTCs from early stage lung cancer patients using a microfluidic co-culture model. *Oncotarget*. 2014;5(23):12383-12397. doi:10.18632/oncotarget.2592

218. Zhu Z, Achreja A, Meurs N, et al. Tumour-reprogrammed stromal BCAT1 fuels branched-chain ketoacid dependency in stromal-rich PDAC tumours. *Nat Metab*. 2020;2(8):775-792.

219. Miyamoto DT, Zheng Y, Wittner BS, et al. RNA-Seq of single prostate CTCs implicates noncanonical Wnt signaling in antiandrogen resistance. *Science (80-)*. 2015;349(6254):1351-1356. doi:10.1126/science.aab0917

220. Köster J, Rahmann S. Snakemake—a scalable bioinformatics workflow engine. *Bioinformatics*. 2012;28(19):2520-2522. doi:10.1093/bioinformatics/bts480

221. Martin M. Cutadapt removes adapter sequences from high-throughput sequencing reads. *EMBnet J*. 2011;17(1):10-12.

222. Andrews S. FastQC: a quality control tool for high throughput sequence data. Published online 2010.

223. Dobin A, Davis CA, Schlesinger F, et al. STAR: ultrafast universal RNA-seq aligner. *Bioinformatics*. 2013;29(1):15-21.

224. Li B, Dewey CN. RSEM: accurate transcript quantification from RNA-Seq data with or without a reference genome. *BMC Bioinformatics*. 2011;12(1):1-16.

225. Ewels P, Magnusson M, Lundin S, Käller M. MultiQC: summarize analysis results for multiple tools and samples in a single report. *Bioinformatics*. 2016;32(19):3047-3048.

226. Zhang Y, Parmigiani G, Johnson WE. ComBat-seq: batch effect adjustment for RNA-seq count data. *NAR genomics Bioinforma*. 2020;2(3):lqaa078.

227. Love MI, Huber W, Anders S. Moderated estimation of fold change and dispersion for RNA-seq data with DESeq2. *Genome Biol*. 2014;15(12):1-21.

228. Taube JH, Herschkowitz JI, Komurov K, et al. Erratum: Core epithelial-to-mesenchymal transition interactome gene-expression signature is associated with claudinlow and metaplastic breast cancer subtypes (Proceedings of the National Academy of Sciences of the United States of America (2010) 107:35 (1. *Proc Natl Acad Sci U S A*. 2010;107(44):19132. doi:10.1073/pnas.1015095107

229. Pegram HJ, Andrews DM, Smyth MJ, Darcy PK, Kershaw MH. Activating and inhibitory receptors of natural killer cells. *Immunol Cell Biol*. 2011;89(2):216-224.

230. Ito M, Maruyama T, Saito N, Koganei S, Yamamoto K, Matsumoto N. Killer cell lectin-like receptor G1 binds three members of the classical cadherin family to inhibit NK cell cytotoxicity. *J Exp Med*. 2006;203(2):289-295.

231. Hosomi S, Grootjans J, Huang YH, Kaser A, Blumberg RS. New Insights Into the Regulation of Natural-Killer Group 2 Member D (NKG2D) and NKG2D-Ligands: Endoplasmic Reticulum Stress and CEA-Related Cell Adhesion Molecule 1 . *Front Immunol* . 2018;9. https://www.frontiersin.org/article/10.3389/fimmu.2018.01324

232. Garg A, Barnes PF, Porgador A, et al. Vimentin expressed on Mycobacterium tuberculosis-infected human monocytes is involved in binding to the NKp46 receptor. *J Immunol*. 2006;177(9):6192-6198.

233. Pende D, Sivori S, Accame L, et al. HLA-G recognition by human natural killer cells. Involvement of CD94 both as inhibitory and as activating receptor complex. *Eur J Immunol*. 1997;27(8):1875-1880. doi:10.1002/eji.1830270809

234. Stuart T, Butler A, Hoffman P, et al. Comprehensive Integration of Single-Cell Data. *Cell*. 2019;177(7):1888-1902.e21. doi:10.1016/j.cell.2019.05.031

235. Siemaszko J, Marzec-Przyszlak A, Bogunia-Kubik K. NKG2D Natural Killer Cell Receptor—A Short Description and Potential Clinical Applications. *Cells* . 2021;10(6). doi:10.3390/cells10061420

236. Boles KS, Barchet W, Diacovo T, Cella M, Colonna M. The tumor suppressor TSLC1/NECL-2 triggers NK-cell and CD8+ T-cell responses through the cell-surface receptor CRTAM. *Blood*. 2005;106(3):779-786.

237. Tamara T, Henry EJ, C. CÂ, L. SJ. The HLA-G cycle provides for both NK tolerance and immunity at the maternal–fetal interface. *Proc Natl Acad Sci*. 2015;112(43):13312-13317. doi:10.1073/pnas.1517724112

238. Gay LJ, Felding-Habermann B. Contribution of platelets to tumour metastasis. *Nat Rev Cancer*. 2011;11(2):123-134. doi:10.1038/nrc3004

239. Yu X, Pan XY, Zhang SQ, et al. Identification of Gene Signatures and Expression Patterns During Epithelial-to-Mesenchymal Transition From Single-Cell Expression Atlas. *Front Genet*. 2021;11(January):1-11. doi:10.3389/fgene.2020.605012

240. Tayoun T, Faugeroux V, Oulhen M, Aberlenc A, Pawlikowska P, Farace F. CTC-Derived Models: A Window into the Seeding Capacity of Circulating Tumor Cells (CTCs). *Cells*. 2019;8(10). doi:10.3390/cells8101145

241. Zeinali M. *Isolation, Characterization, and Expansion of Heterogeneous Circulating Tumor Cell (CTC) Populations from Cancer Patients Using Microfluidic Technologies*. University of Heidelberg; 2019.

242. Guo T, Wang CS, Wang W, Lu Y. Culture of Circulating Tumor Cells - Holy Grail and Big Challenge. *Int J Cancer Clin Res*. 2016;3(4). doi:10.23937/2378-3419/3/4/1065

243. Ebright RY, Lee S, Wittner BS, et al. Deregulation of ribosomal protein expression and translation promotes breast cancer metastasis. *Science (80-)*. 2020;367(6485):1468-1473. doi:10.1126/science.aay0939

244. Elhamamsy AR, Metge BJ, Alsheikh HA, Shevde LA, Samant RS. Ribosome biogenesis: A central player in cancer metastasis and therapeutic resistance. *Cancer Res*. Published online 2022.

245. Dermit M, Dodel M, Lee FCY, et al. Subcellular mRNA Localization Regulates Ribosome Biogenesis in Migrating Cells. *Dev Cell*. 2020;55(3):298-313.e10. doi:https://doi.org/10.1016/j.devcel.2020.10.006

246. Davis ID. An overview of cancer immunotherapy. *Immunol Cell Biol*. 2000;78(3):179-195. doi:https://doi.org/10.1046/j.1440-1711.2000.00906.x

247. June CH. Adoptive T cell therapy for cancer in the clinic. *J Clin Invest*. 2007;117(6):1466-1476. doi:10.1172/JCI32446

248. Dine J, Gordon R, Shames Y, Kasler MK, Barton-Burke M. Immune checkpoint inhibitors: An innovation in immunotherapy for the treatment and management of patients with cancer. *Asia-Pacific J Oncol Nurs*. 2017;4(2):127-135. doi:https://doi.org/10.4103/apjon.apjon_4_17

249. Barbee MS, Ogunniyi A, Horvat TZ, Dang TO. Current status and future directions of the immune checkpoint inhibitors ipilimumab, pembrolizumab, and nivolumab in oncology. *Ann Pharmacother*. 2015;49(8):907-937.

250. Algarra I, García-Lora A, Cabrera T, Ruiz-Cabello F, Garrido F. The selection of tumor variants with altered expression of classical and nonclassical MHC class I molecules: implications for tumor immune escape. *Cancer Immunol Immunother*. 2004;53(10):904-910.

251. Kiessling R, Klein E, Wigzell H. „Natural" killer cells in the mouse. I. Cytotoxic cells with specificity for mouse Moloney leukemia cells. Specificity and distribution according to genotype. *Eur J Immunol*. 1975;5(2):112-117. doi:https://doi.org/10.1002/eji.1830050208

252. Lotzová E, McCredie KB. Natural killer cells in mice and man and their possible biological significance. *Cancer Immunol Immunother*. 1978;4(4):215-221.

253. Hanna N. Role of natural killer cells in control of cancer metastasis. *Cancer Metastasis Rev*. 1982;1(1):45-64.

254. Matosevic S. Viral and nonviral engineering of natural killer cells as emerging adoptive cancer immunotherapies. *J Immunol Res*. 2018;2018.

255. Tiwary S, Morales JE, Kwiatkowski SC, Lang FF, Rao G, McCarty JH. Metastatic brain tumors disrupt the blood-brain barrier and alter lipid metabolism by inhibiting expression of the endothelial cell fatty acid transporter Mfsd2a. *Sci Rep*. 2018;8(1):1-13.

256. Arvanitis CD, Ferraro GB, Jain RK. The blood–brain barrier and blood–tumour barrier in brain tumours and metastases. *Nat Rev Cancer*. 2020;20(1):26-41.

257. Jong AY, Wu CHH, Li J, et al. Large-scale isolation and cytotoxicity of extracellular vesicles derived from activated human natural killer cells. *J Extracell Vesicles*. 2017;6(1):1294368. doi:10.1080/20013078.2017.1294368

258. Edgar JR. Q&A: What are exosomes, exactly? *BMC Biol*. 2016;14(1):1-7.

259. Vader P, Mol EA, Pasterkamp G, Schiffelers RM. Extracellular vesicles for drug delivery. *Adv Drug Deliv Rev*. 2016;106:148-156.

260. Kim OY, Lee J, Gho YS. Extracellular vesicle mimetics: novel alternatives to extracellular vesicle-based theranostics, drug delivery, and vaccines. In: *Seminars in Cell & Developmental Biology*. Vol 67. Elsevier; 2017:74-82.

261. Zhu Q, Heon M, Zhao Z, He M. Microfluidic engineering of exosomes: Editing cellular messages for precision therapeutics. *Lab Chip*. 2018;18(12):1690-1703. doi:10.1039/c8lc00246k

262. Yong T, Zhang X, Bie N, et al. Tumor exosome-based nanoparticles are efficient drug carriers for chemotherapy. *Nat Commun*. 2019;10(1):1-16.

263. Golán I, Rodríguez de la Fuente L, Costoya JA. NK cell-based glioblastoma immunotherapy. *Cancers (Basel)*. 2018;10(12):522.

264. Chen H, Cao B, Chen H, Lin YS, Zhang J. Combination of antibody-coated, physical-based microfluidic chip with wave-shaped arrays for isolating circulating tumor cells. *Biomed Microdevices*. 2017;19(3):1-9.

265. Chen H. Capturing and clinical applications of circulating tumor cells with wave microfluidic chip. *Appl Biochem Biotechnol*. 2020;190(4):1470-1483.

266. Varillas JI, Zhang J, Chen K, et al. Microfluidic isolation of circulating tumor cells and cancer stem-like cells from patients with pancreatic ductal adenocarcinoma. *Theranostics*. 2019;9(5):1417.

267. Kang YT, Kim YJ, Bu J, Cho YH, Han SW, Moon BI. High-purity capture and release of circulating exosomes using an exosome-specific dual-patterned immunofiltration (ExoDIF) device. *Nanoscale*. 2017;9(36):13495-13505.

268. Kanwar SS, Dunlay CJ, Simeone DM, Nagrath S. Microfluidic device (ExoChip) for on-chip isolation, quantification and characterization of circulating exosomes. *Lab Chip*. 2014;14(11):1891-1900.

269. Kang Y, Purcell E, Palacios-Rolston C, et al. Isolation and profiling of circulating tumor-associated exosomes using extracellular vesicular lipid–protein binding affinity based microfluidic device. *Small*. 2019;15(47):1903600.

270. Guo SC, Tao SC, Dawn H. Microfluidics-based on-a-chip systems for isolating and analysing extracellular vesicles. *J Extracell vesicles*. 2018;7(1):1508271.

271. Dong J, Jan YJ, Cheng J, et al. Covalent chemistry on nanostructured substrates enables noninvasive quantification of gene rearrangements in circulating tumor cells. *Sci Adv*. 2019;5(7):eaav9186.

272. Kang YT, Hadlock T, Jolly S, Nagrath S. Extracellular vesicles on demand (EVOD) chip for screening and quantification of cancer-associated extracellular vesicles. *Biosens Bioelectron*. 2020;168:112535. doi:https://doi.org/10.1016/j.bios.2020.112535

273. Yoon HJ, Shanker A, Wang Y, et al. Tunable Thermal-Sensitive Polymer–Graphene Oxide Composite for Efficient Capture and Release of Viable Circulating Tumor Cells. *Adv Mater*. Published online 2016:4891-4897. doi:10.1002/adma.201600658

274. Wan Y, Cheng G, Liu X, et al. Rapid magnetic isolation of extracellular vesicles via lipid-based nanoprobes. *Nat Biomed Eng*. 2017;1(4):58. doi:10.1038/s41551-017-0058

275. Ying LQ, Branchaud BP. Design of a reversible biotin analog and applications in protein labeling, detection, and isolation. *Chem Commun*. 2011;47(30):8593-8595.

276. Lambert CR, Nijsure D, Huynh V, Wylie RG. Hydrogels with reversible chemical

environments for in vitro cell culture. *Biomed Mater*. 2018;13(4):45002.

277. Hirsch JD, Eslamizar L, Filanoski BJ, et al. Easily reversible desthiobiotin binding to streptavidin, avidin, and other biotin-binding proteins: uses for protein labeling, detection, and isolation. *Anal Biochem*. 2002;308(2):343-357. doi:https://doi.org/10.1016/S0003-2697(02)00201-4

278. Lo TW, Zhu Z, Purcell E, et al. Microfluidic device for high-throughput affinity-based isolation of extracellular vesicles. *Lab Chip*. 2020;20(10):1762-1770.

279. Toner M, Irimia D. Blood-on-a-chip. *Annu Rev Biomed Eng*. 2005;7:77.

280. Smyth MJ, Hayakawa Y, Takeda K, Yagita H. New aspects of natural-killer-cell surveillance and therapy of cancer. *Nat Rev Cancer*. 2002;2(11):850-861.

281. Atkin-Smith GK, Poon IKH. Disassembly of the dying: mechanisms and functions. *Trends Cell Biol*. 2017;27(2):151-162.

282. Ståhl A lie, Johansson K, Mossberg M, Kahn R, Karpman D. Exosomes and microvesicles in normal physiology, pathophysiology, and renal diseases. *Pediatr Nephrol*. 2019;34(1):11-30.

283. Caruso S, Poon IKH. Apoptotic cell-derived extracellular vesicles: more than just debris. *Front Immunol*. 2018;9:1486.

284. Lugini L, Cecchetti S, Huber V, et al. Immune surveillance properties of human NK cell-derived exosomes. *J Immunol*. 2012;189(6):2833-2842.

285. LeFever A V, Funahashi A. Phenotype and function of natural killer cells in patients with bronchogenic carcinoma. *Cancer Res*. 1991;51(20):5596-5601.

286. Sibbitt WLJ, Bankhurst AD, Jumonville AJ, Saiki JH, Saiers JH, Doberneck RC. Defects in natural killer cell activity and interferon response in human lung carcinoma and malignant melanoma. *Cancer Res*. 1984;44(2):852-856.

287. Brittenden J, Heys SD, Ross J, Eremin O. Natural killer cells and cancer. *Cancer*. 1996;77(7):1226-1243. doi:https://doi.org/10.1002/(SICI)1097-0142(19960401)77:7<1226::AID-CNCR2>3.0.CO;2-G

288. Waldhauer I, Steinle A. NK cells and cancer immunosurveillance. *Oncogene*. 2008;27(45):5932-5943. doi:10.1038/onc.2008.267

289. Fais S. NK cell-released exosomes: natural nanobullets against tumors. *Oncoimmunology*. 2013;2(1):e22337.

290. Fomina AF, Deerinck TJ, Ellisman MH, Cahalan MD. Regulation of membrane trafficking and subcellular organization of endocytic compartments revealed with FM1-43 in resting and activated human T cells. *Exp Cell Res*. 2003;291(1):150-166.

doi:https://doi.org/10.1016/S0014-4827(03)00372-0

291. Van der Vlist EJ, Arkesteijn GJA, van de Lest CHA, Stoorvogel W, Nolte-'t Hoen ENM, Wauben MHM. CD4+ T cell activation promotes the differential release of distinct populations of nanosized vesicles. *J Extracell Vesicles*. 2012;1(1):18364.

292. Kozminsky M. *Isolation and Analysis of Circulating Tumor Cells in Genitourinary Cancers*. University of Michigan; 2017.

293. Geller MA, Cooley S, Judson PL, et al. A phase II study of allogeneic natural killer cell therapy to treat patients with recurrent ovarian and breast cancer. *Cytotherapy*. 2011;13(1):98-107. doi:10.3109/14653249.2010.515582

294. Iliopoulou EG, Kountourakis P, Michalis •, et al. A phase I trial of adoptive transfer of allogeneic natural killer cells in patients with advanced non-small cell lung cancer. doi:10.1007/s00262-010-0904-3

295. Qin J, Alt JR, Hunsley BA, Williams TL, Fernando MR. Stabilization of circulating tumor cells in blood using a collection device with a preservative reagent. *Cancer Cell Int*. 2014;14(1):23. doi:10.1186/1475-2867-14-23

296. Larson CJ, Moreno JG, Pienta KJ, et al. Apoptosis of circulating tumor cells in prostate cancer patients. *Cytom Part A*. 2004;62A(1):46-53. doi:https://doi.org/10.1002/cyto.a.20073

297. Jiang CY, Niu Z, Green MD, et al. It's not "just a tube of blood": principles of protocol development, sample collection, staffing and budget considerations for blood-based biomarkers in immunotherapy studies. *J Immunother cancer*. 2021;9(7). doi:10.1136/jitc-2021-003212

298. Ignatiadis M, Sledge GW, Jeffrey SS. Liquid biopsy enters the clinic — implementation issues and future challenges. *Nat Rev Clin Oncol*. 2021;18(5):297-312. doi:10.1038/s41571-020-00457-x

299. Farace F, Massard C, Vimond N, et al. A direct comparison of CellSearch and ISET for circulating tumour-cell detection in patients with metastatic carcinomas. *Br J Cancer*. 2011;105(6):847-853. doi:10.1038/bjc.2011.294

300. Zeune LL, de Wit S, Berghuis AMS, IJzerman MJ, Terstappen LWMM, Brune C. How to Agree on a CTC: Evaluating the Consensus in Circulating Tumor Cell Scoring. *Cytom Part A*. 2018;93(12):1202-1206. doi:https://doi.org/10.1002/cyto.a.23576

301. Ota S, Horisaki R, Kawamura Y, et al. Ghost cytometry. *Science (80-)*. 2018;360(6394):1246-1251. doi:10.1126/science.aan0096

302. Zhao L, Wu X, Li T, Luo J, Dong D. ctcRbase: the gene expression database of circulating tumor cells and microemboli. *Database*. 2020;2020:baaa020. doi:10.1093/database/baaa020

303. Wang WC, Zhang XF, Peng J, et al. Survival Mechanisms and Influence Factors of Circulating Tumor Cells. *Biomed Res Int*. 2018;2018:6304701. doi:10.1155/2018/6304701

304. Placke T, Orgel M€, Schaller M, et al. Platelet-Derived MHC Class I Confers a Pseudonormal Phenotype to Cancer Cells That Subverts the Antitumor Reactivity of Natural Killer Immune Cells. Published online 2012. doi:10.1158/0008-5472.CAN-11-1872

305. Guo SW, Du Y, Liu X. Platelet-derived TGF-β1 mediates the down-modulation of NKG2D expression and may be responsible for impaired natural killer (NK) cytotoxicity in women with endometriosis. *Hum Reprod*. 2016;31(7):1462-1474.

306. Elaskalani O, Berndt MC, Falasca M, Metharom P. Targeting Platelets for the Treatment of Cancer. *Cancers* . 2017;9(7). doi:10.3390/cancers9070094

307. Hoshino A, Costa-Silva B, Shen TL, et al. Tumour exosome integrins determine organotropic metastasis. *Nature*. 2015;527(7578):329-335. doi:10.1038/nature15756